CRCLEME
Cooperative Research Centre for
Landscape Evolution & Mineral Exploration

OPEN FILE
REPORT
SERIES

CSIRO
EXPLORATION
AND MINING

AMIRA
Australian Mineral Industries Research Association Limited ACN 004 448 266

THE PETROGRAPHY, MINERALOGY AND GEOCHEMISTRY OF A FELSIC, MAFIC, ULTRAMAFIC AND METASEDIMENTARY WEATHERED PROFILE AT RAND PIT, REEDY MINE - CUE, WESTERN AUSTRALIA

Volume 1

I.D.M. Robertson, M.A. Chaffee and G.F. Taylor

CRC LEME OPEN FILE REPORT 39

September 1998

(CSIRO Division of Exploration Geoscience Report 102R, 1990.
Second impression 1998)

AMIRA
Australian Mineral Industries Research Association Limited ACN 004 448 266

CRCLEME
Cooperative Research Centre for
Landscape Evolution & Mineral Exploration

CSIRO
EXPLORATION
AND MINING

THE PETROGRAPHY, MINERALOGY AND GEOCHEMISTRY OF A FELSIC, MAFIC, ULTRAMAFIC AND METASEDIMENTARY WEATHERED PROFILE AT RAND PIT, REEDY MINE - CUE, WA

Volume 1

I.D.M. Robertson, M.A. Chaffee and G.F. Taylor

CRC LEME OPEN FILE REPORT 39

September 1998

(CSIRO Division of Exploration Geoscience Report 102R, 1990.
Second impression 1998)

CRC LEME is an unincorporated joint venture between The Australian National University, University of Canberra, Australian Geological Survey Organisation and CSIRO Exploration and Mining
Headquarters: CRC LEME c/o CSIRO Exploration and Mining, Private Bag, PO Wembley, Western Australia, 6014

RESEARCH ARISING FROM CSIRO/AMIRA REGOLITH GEOCHEMISTRY PROJECTS 1987-1993

In 1987, CSIRO commenced a series of multi-client research projects in regolith geology and geochemistry which were sponsored by companies in the Australian mining industry, through the Australian Mineral Industries Research Association Limited (AMIRA). The initial research program, "Exploration for concealed gold deposits, Yilgarn Block, Western Australia" (1987-1993) had the aim of developing improved geological, geochemical and geophysical methods for mineral exploration that would facilitate the location of blind, buried or deeply weathered gold deposits. The program included the following projects:

P240: Laterite geochemistry for detecting concealed mineral deposits (1987-1991). Leader: Dr R.E. Smith.
Its scope was development of methods for sampling and interpretation of multi-element laterite geochemistry data and application of multi-element techniques to gold and polymetallic mineral exploration in weathered terrain. The project emphasised viewing laterite geochemical dispersion patterns in their regolith-landform context at local and district scales. It was supported by 30 companies.

P241: Gold and associated elements in the regolith - dispersion processes and implications for exploration (1987-1991). Leader: Dr C.R.M. Butt.
The project investigated the distribution of ore and indicator elements in the regolith. It included studies of the mineralogical and geochemical characteristics of weathered ore deposits and wall rocks, and the chemical controls on element dispersion and concentration during regolith evolution. This was to increase the effectiveness of geochemical exploration in weathered terrain through improved understanding of weathering processes. It was supported by 26 companies.

These projects represented "an opportunity for the mineral industry to participate in a multi-disciplinary program of geoscience research aimed at developing new geological, geochemical and geophysical methods for exploration in deeply weathered Archaean terrains". This initiative recognised the unique opportunities, created by exploration and open-cut mining, to conduct detailed studies of the weathered zone, with particular emphasis on the near-surface expression of gold mineralisation. The skills of existing and specially recruited research staff from the Floreat Park and North Ryde laboratories (of the then Divisions of Minerals and Geochemistry, and Mineral Physics and Mineralogy, subsequently Exploration Geoscience and later Exploration and Mining) were integrated to form a task force with expertise in geology, mineralogy, geochemistry and geophysics. Several staff participated in more than one project. Following completion of the original projects, two continuation projects were developed.

P240A: Geochemical exploration in complex lateritic environments of the Yilgarn Craton, Western Australia (1991-1993). Leaders: Drs R.E. Smith and R.R. Anand.
The approach of viewing geochemical dispersion within a well-controlled and well-understood regolith-landform and bedrock framework at detailed and district scales continued. In this extension, focus was particularly on areas of transported cover and on more complex lateritic environments typified by the Kalgoorlie regional study. This was supported by 17 companies.

P241A: Gold and associated elements in the regolith - dispersion processes and implications for exploration. Leader: Dr. C.R.M. Butt.
The significance of gold mobilisation under present-day conditions, particularly the important relationship with pedogenic carbonate, was investigated further. In addition, attention was focussed on the recognition of primary lithologies from their weathered equivalents. This project was supported by 14 companies.

Although the confidentiality periods of the research reports have expired, the last in December 1994, they have not been made public until now. Publishing the reports through the CRC LEME Report Series is seen as an appropriate means of doing this. By making available the results of the research and the authors' interpretations, it is hoped that the reports will provide source data for future research and be useful for teaching. CRC LEME acknowledges the Australian Mineral Industries Research Association and CSIRO Division of Exploration and Mining for authorisation to publish these reports. It is intended that publication of the reports will be a substantial additional factor in transferring technology to aid the Australian Mineral Industry.

This report (CRC LEME Open File Report 39) is a first revision of CSIRO, Division of Exploration Geoscience Restricted Report 102R, first issued in 1990, which formed part of the CSIRO/AMIRA Project P241.

Copies of this publication can be obtained from:
The Publication Officer, CRC LEME, CSIRO Exploration and Mining, PMB, Wembley, WA 6014, Australia. Information on other publications in this series may be obtained from the above or from http://leme.anu.edu.au/
Bibliographic reference:
This publication should be referred to as Robertson, I.D.M., Chaffee, M.A. and Taylor, G.F., 1998. The petrography, mineralogy and geochemistry of a felsic, mafic, ultramafic and metasedimentary weathered profile at Rand Pit, Reedy Mine - Cue, WA. Open File Report 39, Cooperative Research Centre for Landscape Evolution and Mineral Exploration, Perth, Australia.
Cataloguing-in-Publication:
Robertson, I.D.M.
The petrography, mineralogy and geochemistry of a felsic, mafic, ultramafic and metasedimentary weathered profile at Rand Pit, Reedy Mine - Cue, WA
ISBN v1: 0 642 28287 0 v2: 0 642 28288 9 set: 0 642 28289 7
1. Mineralogy 2. Weathering 3. Geochemistry - Western Aistralia.
I. Chaffee, M.A. II. Taylor, G.F. III. Title
CRC LEME Open File Report 39.
ISSN 1329-4768

FRONTISPIECE

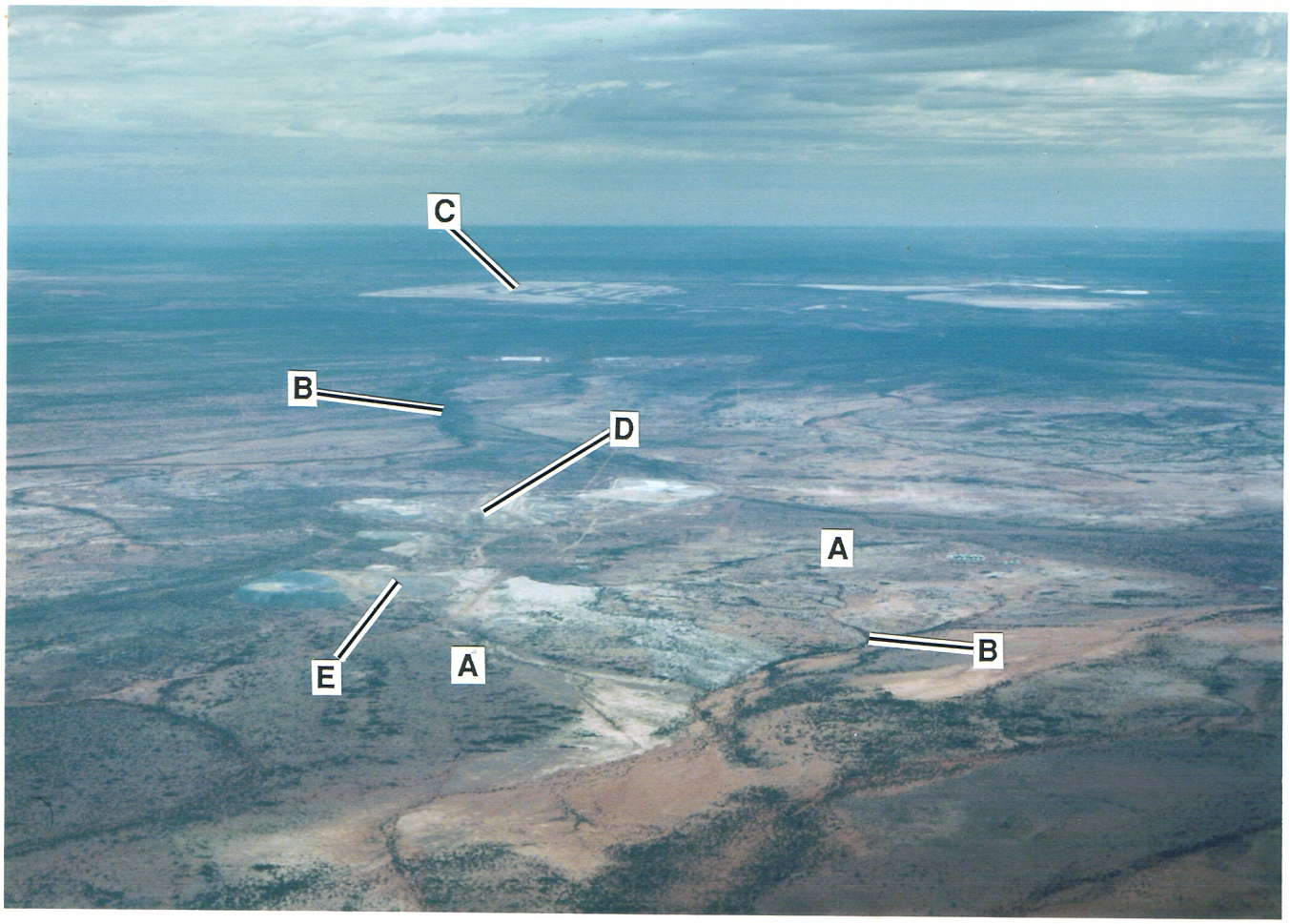

An oblique aerial view looking north, along the line of lode, showing the Reedy Mines on a low divide (A) between ephemeral streams (B) draining a low gradient erosional plain towards the playas (C) of lake Annean. The Rand Pit is located at D and the South Emu pit at E. For further details see Figure 2.

PREFACE

The CSIRO - AMIRA project "Exploration for Concealed Gold Deposits, Yilgarn Block, Western Australia" has, as its overall aim, the development of improved geological, geochemical and geophysical methods for mineral exploration that will facilitate the location of blind, concealed or deeply weathered Au deposits.

This report presents results of research conducted as part of Module 2 of this project (AMIRA Project 241): "Gold and Associated Elements in the Regolith - Dispersion Processes and Implications for Exploration". The objectives of this Module are, *inter alia* to obtain a better understanding of the nature and genesis of the lateritic regolith and of the supergene Au deposits within it and to provide data applicable for exploration for other commodities in and beneath the regolith.

Recent open cut mining has provided the opportunity to study complete weathering profiles over individual, specific lithological units, in particular to determine the principal changes in the fabric, mineralogy and geochemistry that take place as weathering progresses. This report describes such a study from the Rand Pit at Reedy near Cue. A limited suite of lithologies mafic and ultramafic komatiites, mica schists, carbonaceous shales and felsic rocks are exposed and accessible at different levels in the weathering profile and the alteration of each has been examined in detail. As well as providing background data on the processes of rock weathering, the study was designed to assist with rock identification, particularly from drill cuttings.

C.R.M. Butt
Project Leader

December,1990.

TABLE OF CONTENTS

LIST OF FIGURES

LIST OF TABLES

1.0 ABSTRACT

A near vertical sequence of variably-deformed, alternating, mafic and ultramafic metavolcanic rocks, interleaved with mica schists and black shales and intruded by porphyry pods, is exposed on the south face of the Rand Pit at Reedy to a depth of 75 m. The face has been mapped and each lithology sampled at approximately 20 m intervals from the base to the top. The samples have been studied mineralogically and petrographically to illustrate the mineral and fabric changes caused by weathering. Each sample has been analysed for 55 (major and trace) elements and the drying losses, ignition losses and densities were measured in order to understand further the geochemical changes due to weathering and to find ways of distinguishing the rock types on a geochemical basis despite their weathering state.

Where fresh, the ultramafic rocks are talc-chlorite±tremolite schists and the mafic rocks are schists of granular quartz and albite with muscovite, chlorite and talc. Initially weathering solutions have penetrated the margins of quartz veins and some cleavage planes. Sulphides are among the first minerals to weather and, in the mafic rocks, these are closely followed by plagioclase which is almost completely altered at 70 m depth. At a depth of 50 m, needles of tremolite in the ultramafic rocks have largely dissolved, leaving voids, some of which have been filled by goethite. Chlorite in all rocks becomes progressively more turbid, Fe-stained and altered to smectite, and both sphene and ilmenite alter to anatase. Above 30 m depth, and particularly in the top 10 m, kaolinite becomes very abundant where it is an alteration product of talc, muscovite, feldspar, chlorite and smectite. It forms secondary fine-grained mats, coarser-grained stumpy stacks and accordion structures which progressively destroy the schistose saprolite fabric. The rocks become pockmarked with vesicles and solution channels which are in part filled with secondary clays. Muscovite and talc, in the mica schists and ultramafic rocks respectively, are relatively stable minerals which persist to close to the surface where both are partly altered to kaolinite.

The regolith exposed at Rand may be divided into a shallow zone (0-15 m), marked by rocks of low density (<2.0) in which there has been extensive leaching and element dispersion, and a more dense deep zone, extending to saprock and relatively fresh rock. In the deep zone some elements (As, Au, Cu, Pb, Sb, Sn, W, Zn and, to a lesser extent, Ag, Mo, Se, Te and Tl) appear to be ore-related and many show an exponential relationship of their maximum concentrations to their distance from the main ore shoots. Of the remaining lithologically related elements, Cr differentiates the mafic from the ultramafic suite, Al and Ga separate the mafic rocks from the mica schists, low Fe concentrations mark the mica schists, black shales and porphyries, and abundant Ba characterises the mica schists and porphyries.

The number of useful pathfinder elements (As, Au, Cu, Se and W) is less in the low density shallow zone of the regolith where Al, B, Ba, Fe, Ga, Nb, Si, Sr, Ta, Th and V have been enriched but Ag, Al, Ca, Cd, Ce, Co, Eu, Fe, Ge, La, Li, Lu, Mg, Mn, Na, Ni, Sm, Y and Zn have been leached. Chromium, Ti, K, Cs, Rb, Zr and Hf are relatively unaffected by weathering; K, Rb and Cs are probably sited in residual micas and Zr and Hf in stable zircon.

Discriminant analysis has been used to separate the five lithologies at Rand. Effective discrimination (better than 94%) may be achieved by using power transformed Cr, Nb, Co, Sc, Lu, Hf, Ba, Eu and Zr data and using curved boundaries on canonical plots. Log transformed data is almost as successful. Discrimination may well be improved if samples below 10-15 m depth are used as, above this level, the geochemical and fabric changes are most severe.

2.0 INTRODUCTION

The Reedy Mine lies 50 km to the north-east of Cue and 4.3 km south-east of Cullculli (Figure 1) and mining has occurred intermittently since the discovery of Au there by Tom Reedy in 1901. The Rand Pit is located at 118° 16' 11" E and 27° 07' 12" S, where a resource of 650,000 tonnes at 4.5 g/t Au has been outlined. The climate is semi-arid, with an average rainfall of 215 mm. Most of the rain falls around March and is derived from convective storms, with subsidiary rainfall centred around January and May. The months September through to November are largely dry. Although the mean maximum temperature reaches 38°C in January to December with a mean minimum of 7°C in June and July, there are marked diurnal and seasonal temperatrure fluctuations. Evaporation greatly exceeds precipitation with annual evaporation rates of 2280-2790 mm and this becomes extreme in summer (Arnold, 1963).

2.1 Regional Geological Setting

The Reedy Mine is situated on the eastern edge of the Meekatharra-Mt. Magnet greenstone belt which forms part of the Murchison Province of the Yilgarn Block (Figure 1). The Rand Gold Mine lies on a north striking line of lode (Frontispiece, Figure 2), together with the North Rand, North Triton, Triton and South Emu open pit mines, which follow the contact between magnesian amphibole-chlorite-talc schists to the east and metabasaltic units to the west (Watkins *et al.*, 1987). These greenstones have been intruded by both late, post-tectonic, equigranular, biotite granite plutons and earlier, porphyritic, recrystallised biotite granites. The biotite granites have foliated margins and massive cores, containing gneissic enclaves. The nearest known post-tectonic granite contact is about 1.0 km to the west of the Rand Pit. The greenstones are also cut by several north-northeast striking faults and shears.

2.2 Local Geology

The stratigraphy in the immediate vicinity of the mines, from west to east, consists of interlaminated mafic schists and banded iron formations, followed by interlayered chlorite, tremolite and talc schists, post-tectonic porphyry pods and layers of carbonaceous schists of the ore zone, passing into actinolite schists. Further to the east lie mafic and felsic pyroclastics and shales. Intruded into all these are metadolerites. All the rocks are schistose, with one strong schistosity and, in places, a kinking in the rocks suggests a second schistosity. Although no definitive lava flow structures were found, some features, suggesting flattened and deformed pillow structures (Figure 3A) were seen on the lower-mid bench at the south-east corner of the Rand Pit. Although these could also be interpreted as intersecting fractures, a pillow structure origin is preferred. These rocks comprise Unit 3 of Watkins *et al.*, (1987) which comprises high-Mg and tholeiitic basalts and ultramafic and mafic sheet intrusions with felsic volcanics and volcanogenic sediments. The depositional environment has been interpreted as a submarine sequence of mafic and ultramafic volcanics with argillaceous and chemical interflow sediments. Henderson and Hill (1988) considered that dolerite intrusion occurred prior to folding but some of the doleritic rocks could equally well have been thick flows. Intrusion of granitoid porphyries, which are located close to the Au-bearing lodes, occurred after folding, possibly during granite emplacement and during or prior to major shearing.

2.3 Gold Lodes

The Au-bearing lodes (Henderson and Hill, 1988), which lie along a considerable but discontinuous strike length of 3.5 km, are situated on the eastern limb of a southerly plunging syncline. They dip

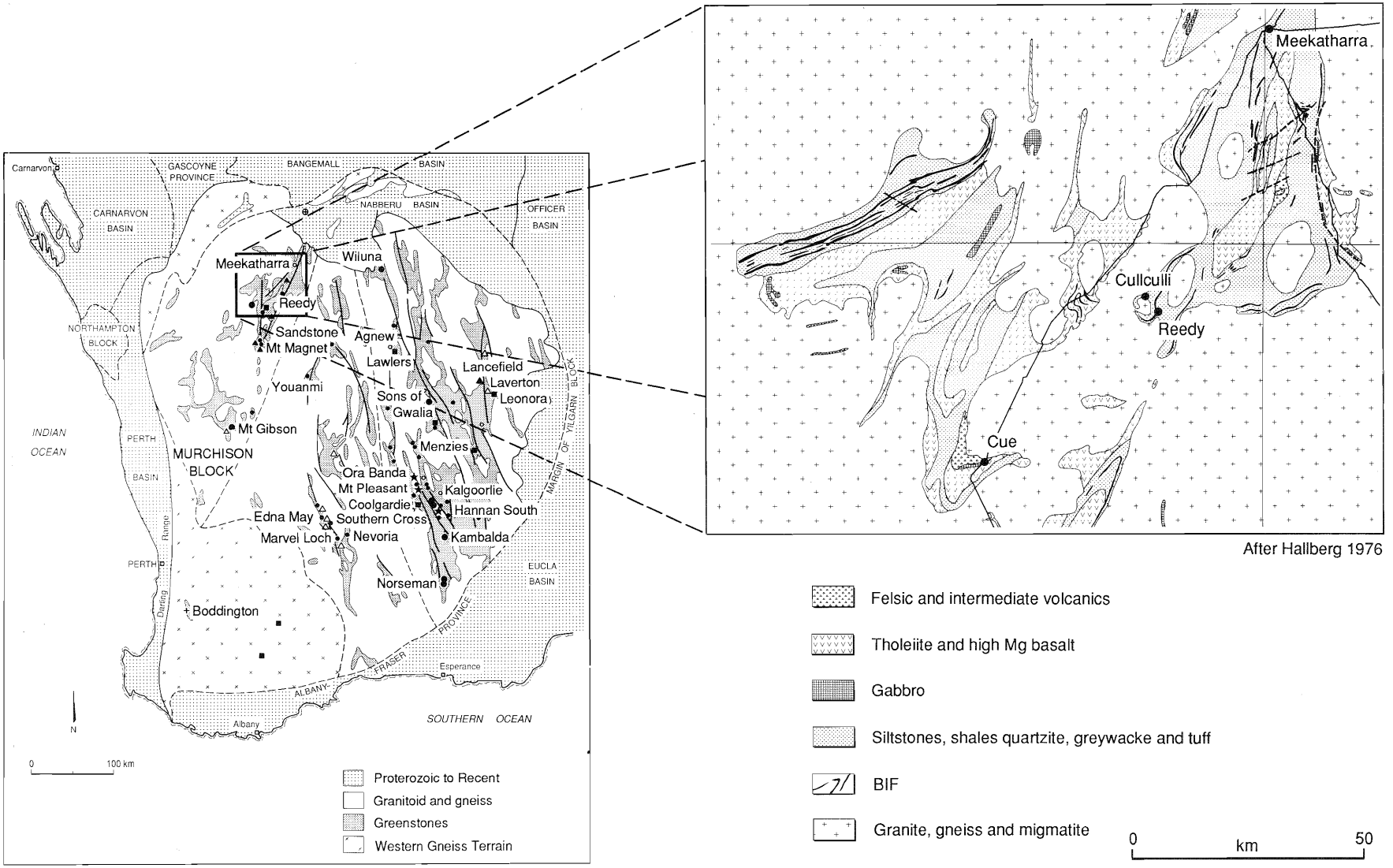

Figure 1. Location map showing geology

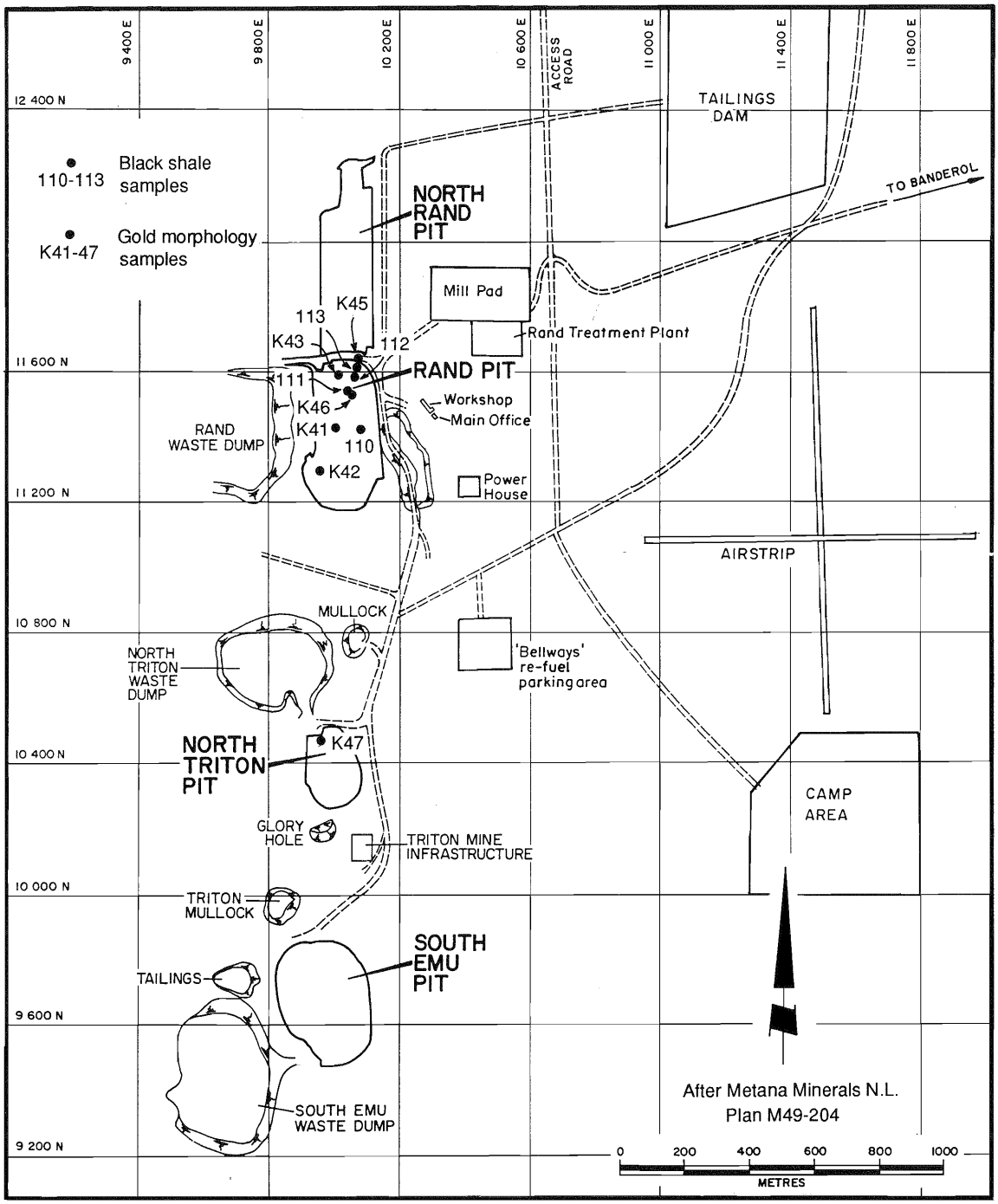

Figure 2. Details of the mines and open pits at Reedy, showing the locations of samples taken for Au morphology study (K41-47) and the black shale samples (RE110-113; see also Figure 4).

FIGURE 3

Figure 3A. Probable deformed pillows in mafic schists of band M1, near the location of Specimen RE33. The degree of deformation of the pillow structures varies considerably.

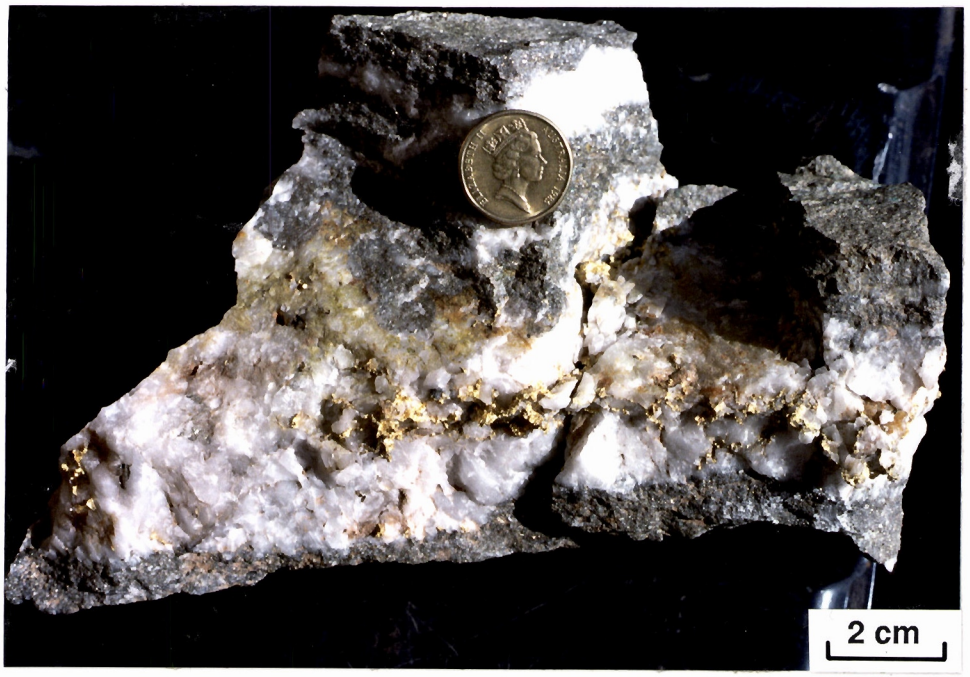

Figure 3B. Specimen primary Au in quartz from the floor of the Rand Pit (see Figure 4A)

steeply west, with sporadic dip reversals due to faulting and flexing. They are generally associated with porphyry, have a southerly plunge and are fine-grained biotite-pyrite-quartz-chlorite-feldspar schists, with a Au grade of about 4 g/t. Although most of the Au has a 20 μm grain size, some very coarse Au is found on the margins of quartz veins and some very rich specimen Au has been obtained from the base of the Rand Pit (Figures 3B and 4A). Gold is associated with pyrite and lesser amounts of chalcopyrite and pyrrhotite in the primary zone though there is no obvious sphalerite, galena or arsenopyrite. Some bornite has been reported from the supergene sulphide zone. The lodes are 12 m wide at Rand, 10 m at North Rand, 6 m at Triton and vary from 5 to 15 m at South Emu. Old workings reached the 14th level (300 m) at the Triton Mine, which is situated in a north-striking shear cutting pyritic metabasalt, talc-chlorite schist, albite porphyry and shale. Here, Au mineralisation occurs in both the mafic rocks and in the sheared porphyry.

Quartz veins lie both parallel to the main schistosity and cut across it. The presence of quartz and shearing appear to influence the Au grade. Quartz stockworks are found in places within the metadolerite and these carry 1-2 g/t Au but otherwise the dolerite is barren, though it is said to have an anomalous Au background of 250 ppb. The Au produced is approximately 900 fine on average (Hallberg *et al.*, 1976) which is in agreement with microprobe analysis of a single primary Au grain from the bottom of Rand Pit which is 880 fine (Robertson, 1987) and work done by Freyssinet and Butt (1988).

The mineralisation at Reedy has been classified as a shear zone and quartz vein type within mafic/ultramafic rock and intruded by porphyry (Watkins *et al.*, 1987). White (1987) suggested that the schistose mineralised rocks are weak mylonites on the basis of mineral lineations, parallel boudin elongations, intrafolial fold axes, a shear band cleavage cross cutting the schistose foliation and asymmetric quartz pods. He observed shearing had occurred at a major rheological boundary on the margins of the competent dolerite and porphyry pods which subsequently boudinaged. Campbell (1953) regarded the lode as a metasedimentary horizon and this is not inconsistent with the view of White (1987) as such a rock would be particularly susceptible to deformation.

Primary alteration (Fotios, 1985; Henderson and Hill, 1988) within the lode is dominated by quartz (Si), auriferous pyrite, minor non-auriferous pyrrhotite (S, Fe), biotite, sericite, fuchsite ($K\pm Cr$) and calcite (CO_2). Gold associated with pyrite is sub-microscopic (<20 μm), though larger grains are not uncommon and some patches of very rich, coarse, visible Au (Figure 3B) occurs in stockwork veins within the lode and in the schists of the hangingwall. Gold mineralisation is richest where shearing was most intense, adjacent to boudins and where pyrite is concentrated. The orebodies have sharp margins and no apparent extensive low-grade halo. This makes this mine area particularly amenable to a rock weathering study.

2.4 Weathering and Groundwater

The rocks of the mine sequence have been deeply weathered but the depth of weathering varies between rock types. Weathering depths range from 30-40 m in the South Emu area to 70-80 m at the North Rand deposit. The lode, basalts and dolerites are more intensely weathered than the chlorite and actinolite schists and massive intrusive porphyries (Henderson and Hill, 1988).

Groundwater is pumped from the old Triton shaft very close to the Rand Pit (Figure 2). A recent water analysis by P.W. Bamford of Analabs in Perth (N. Radford, written comm., December 1990) (Figure 2) is shown below.

This highly potable, though slightly saline, water has a similar Na:K and Na:Cl ratio to seawater. The content of SO_4 is slightly high, suggesting derivation of some of the S from the weathering of sulphides. On evaporation this water first would yield $CaCO_3$ and then NaCl.

pH	7.80	
TDS(mg/l)	1690	
	mg/l	m equiv/l
Na	265	11.5
K	9.0	0.23
Ca	36.5	1.82
Mg	36.5	3.00
Fe	<0.05	-
Cl	300	8.5
CO_3	nil	-
HCO_3	290	4.75
SO_4	110	2.29
NO_3	55	0.89

2.5 Geomorphology

The Reedy Mine is situated on a very gently sloping, stony, erosional plain, which forms a portion of a low divide between minor elements of the drainage systems for the playa lakes Austin and Annean. These plains have developed by the erosion of the deeply weathered Great Plateau of WA. They consist of low, gently-sloping, broad, flat-topped interfluves, interspersed with narrow, linear drainage floors (see Frontispiece). There are a few stony rises and low hills which expose weathered, generally ferruginised, Archaean greenstones and a few patches of lateritic duricrust. The area is drained by a dendritic system of seasonal streams occupying broad, shallow channels, filled with polymictic gravel.

Deeply-weathered country rocks form the most common substrate to a dominantly fine, gravelly, ferruginous alluvium, up to 2 m thick, much of which has been silicified to Wiluna Hardpan (Bettanay and Churchward, 1974). There are rare coatings of fine-grained carbonate along horizontal partings in the hardpan. Overlying the hardpan are shallow (<0.5 m) thick, stony to very friable, fine, sandy, red to brown, clay loams, with an acid pH. These contain gravels which, at the surface, form a ferruginous lag. Some of these lag materials are of lateritic origin, others are ferruginised lithorelics of the parent rock.

The geomorphology near the mine suggests extensive stripping of the upper parts of the regolith, which is considered to have mantled this landscape since Tertiary times. At the south end of the Rand Pit, where most of this study has been concentrated, the ferruginous, gravelly, alluvial cover forms a very thin veneer, commonly a metre or less thick, with a few small channels set in it. The mottled zone is poorly developed and appears to have been extensively stripped.

The thin layer of hardpanised alluvial cover continues along the eastern wall of the pit but, here, the mottled zone thickens considerably. A wedge of highly ferruginised lateritic material lies between the saprolitic mottled zone and the hardpanised alluvial cover.

FIGURE 4

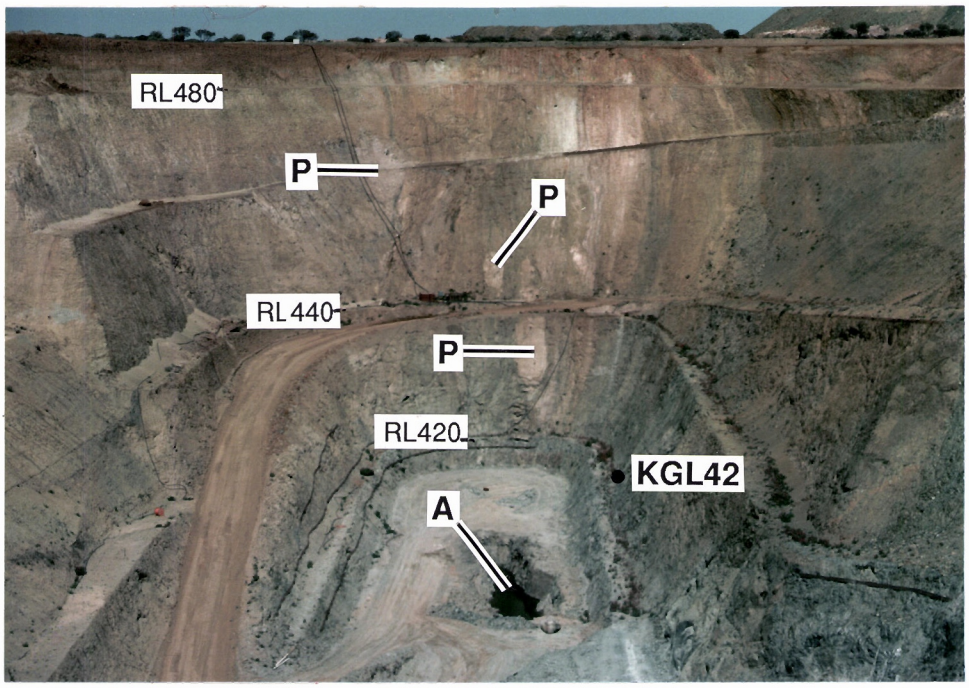

Figure 4A. The south face of the Rand Pit showing granitoid porphyry pods (P) set in interstratified mafic, ultramafic and mica schists. For details of the geology see Appendix 5. The hole in the floor of the pit at A is the location of the specimen primary Au (Figure 3B).

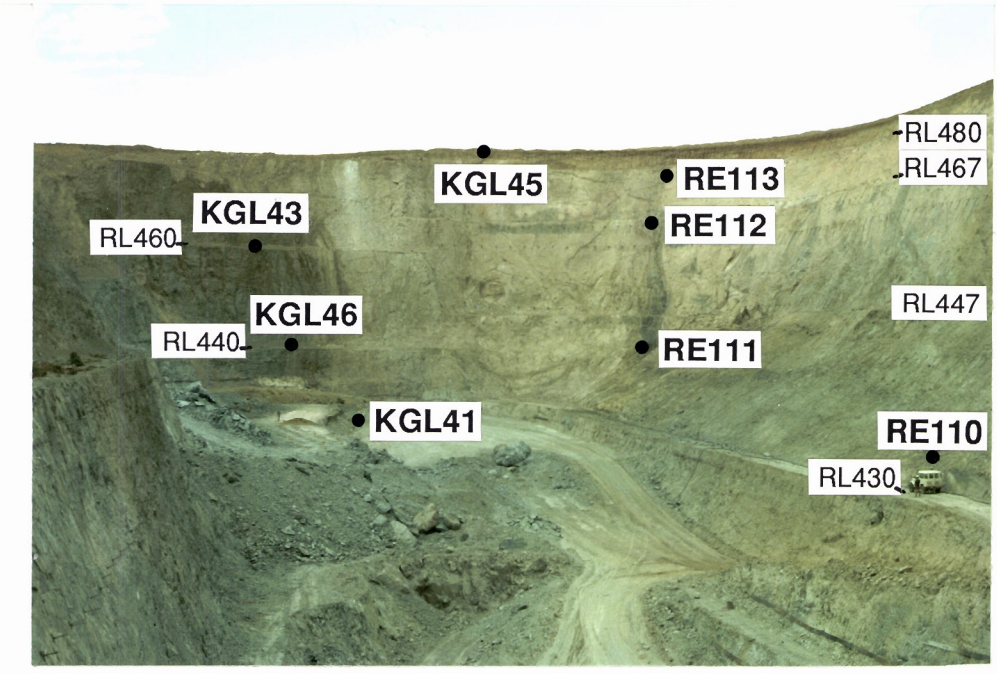

Figure 4B. The north face of the Rand Pit showing the locations of the black shale samples (RE110-113). The locations of the samples collected for Au morphology study (Freyssinet and Butt, 1988) are also shown approximately (KGL41-46) both here and on Figure 4A.

Parts of this zone are polymictic and seem to be transported but most is monomictic and is probably an eluvial material, representing nodular fragments of the mottled zone, from which the intervening clays have been washed, leading to a breccia of collapsed fragments. The underlying surface of the saprolite is very irregular in places, showing small prominences, deep cavities and even a large 'boulder' resting on the saprolite 'surface', surrounded by lateritic 'overburden'. This brecciated lateritic material is a significant Au resource.

2.6 Production

Prior to 1986 the Reedy mine has shown a production of 8406 kg of Au from 958130 tonnes of ore at an average of 8.8 g/t, with a very minor alluvial production (0.2% of total).

2.7 CSIRO Work Programme

The Reedy Mine area was selected for two studies:-

i) A descriptive study of the morphology and composition of Au particles in samples collected from various levels from the Triton and Rand pits has been completed and reported upon by Freyssinet and Butt (1988). Samples were collected from fresh rock, through the saprolite and mottled zone, to the pisolitic horizon. The primary mineralisation in the main lode consists of xenomorphic and euhedral grains containing 6-16% Ag and 300-1000 ppm Cu. All the primary Au grains are small (10-60 μm). Gold in the lateral veins is similar but coarser. Only a few residual, Ag-rich primary grains remain near the base of the saprolite and these are etched and rounded, the others are free of Ag and Cu and have secondary morphologies. All the grains in the ferruginous horizon are secondary (Ag- and Cu-free) with prismatic or flat, pseudo-hexagonal shapes and most are partly etched. Both Fe and As occur erratically distributed in many secondary grains in both the saprolite and lateritic horizon, probably as micro-inclusions. All secondary Au is remarkably pure, with no detectable Ag or Cu. The locations of the samples collected for this study are shown approximately in Figure 2 and more accurately in Figures 4A and B.

ii) The magnificent exposure left by mining, and preserved in the south face of the Rand Pit (Figure 4A), provided an excellent opportunity to study the mineralogical, fabric and geochemical changes produced by weathering of a small suite of ultramafic, mafic, felsic and metasedimentary rocks. It was hoped this would also suggest mineralogical, fabric and geochemical criteria to aid rock identification. In addition a small study of likely pathfinder elements was undertaken. A total of 109 samples were collected from the Rand Pit during visits in November 1987 and August 1988. Mineralogical work was undertaken at North Ryde (GFT), some geochemical and discriminant analysis were was done at the USGS in Denver (MAC) and the remaining geochemistry and petrography at Floreat Park (IDMR).

3.0 STUDY METHODS

3.1 Sampling and Mapping

The south face of the Rand Pit shows a sequence of near vertical, alternating, mafic and ultramafic rocks with interspersed felsic pods and bands of quartz-mica rocks and black shales. The whole has been metamorphosed to the amphibolite facies. Differentiation of the mafic from the ultramafic rocks is difficult, even near the bottom of the pit, where the rocks are almost fresh. The best distinction can be made on the presence or absence of talc as a major component. On the lower to middle benches

(420-440 m R.L.), the gross stratigraphy can be seen as alternating brownish and greenish bands, the ultramafic rocks being darker green and the felsic pods are a distinctive pale buff (Figure 4A). On the upper-mid and upper benches (467-480 m R.L.) the colours become less distinctive due to intense weathering and ferruginisation. Between the upper bench (480 m R.L.) and the surface, the colour differences are largely swamped by Fe oxide staining.

The samples were collected from approximately horizontal traverses about one metre above the floor of the pit (then at approx., 417 m R.L.) and one metre above each of four benches cut in the south face of the pit, one comprising the main access ramp. Sampling was carried out so as to obtain at least two or three samples from each lithological band at each bench level. Mineralogical and fabric changes are most evident near the surface, so an extra traverse was sampled between the topmost bench (480 m R.L.) and the surface, using a 9.4 m ladder. In addition, a prominent black shale horizon, which could not be accessed from the south face of the pit, was sampled near the floor of the pit, close to the centre of the east face, and was also accessed, higher up, from three benches on the eastern side of the north face of the pit (Figure 4B).

Representative samples of 1-2 kg were collected which were composited from two or three locations within an area of a square metre of the pit face. Steel tools were used from which all paint and Cr-plating had been removed by sand-blasting. Prior to taking the sample, surface material was chipped away as this was generally contaminated by silty material washed from above. Each sample was bagged in polythene. A sketch map of the sampling and associated geology was made during the sampling. Sample numbers were spray-painted on the face at the centre of each sample locality. These numbers were later photographed on a bench-by-bench basis and the centres of these sample numbers were later located accurately by the Mine Surveyor and the co-ordinates so obtained were added to the data file. Field numbers, beginning with 'RE' are used to locate the sample positions in Appendix 5.

The whole face was photographed and the locations of the sample points were re-plotted from the detailed photography. To this plot was added the geological information gathered while sampling and the geology of the complete face was then elucidated. The mica schists tend to be auriferous and are referred to as the S1 and S3 ore shoots (Appendix 5), the principal mafic bands are referred to as M1 and M3 and the ultramafic bands as UM2 and UM6.

3.2 Sample Preparation

Each sample was scraped and washed in tap-water to remove any remaining silty surface contaminants. The samples were then air dried at <50°C. A small representative sample was selected for reference and thin sectioning. The rest of the sample was jaw crushed in Mn steel to a nominal <12 mm and tumble mixed. A 100 g aliquot was incrementally extracted and pulped in a Ketos (Mn) steel mill to a nominal <75 μm, with a quartz wash and alcohol wipe of the mill components between samples. Sample preparation and all subsequent analysis was carried out in random order. The pulps were split into three, one to be used by CSIRO at Floreat Park for major and trace element geochemical analysis and the others sent to CSIRO at North Ryde for XRD analysis and to the USGS in Denver, USA for additional geochemical analysis.

3.3 Petrography and Mineral Analysis

Thin sections, which were not covered so as to permit EDAX SEM examination, were examined under normally transmitted light on a petrographic photomicroscope, after a few drops of water had been

introduced under a temporary glass cover-slip. When necessary, oblique reflected light was supplied using a Volpi fibre-optic source.

Information gathered by both lighting methods, one showing surface colour and fabric and the other showing birefringence and other optical properties, detailed mineralogy and fabric, are complementary.

Qualitative energy dispersive X-ray analysis of specific minerals, marked by small lead tags, on the dry, uncoated, unpolished, open, thin sections was carried out using a JEOL Geo SEM 1. The results of such analyses are shown in parentheses so as to indicate approximate relative elemental proportions, e.g. (Fe>>Si=Al). Where positive mineralogical identification was required, a small sample of the crystal or phase in question was scraped from the surface of the thin section, using a diamond-honed needle, under a binocular microscope, and the powder mounted for Debye-Scherrer diffractometry.

3.4 XRD Analysis

Qualitative Analysis

The mineralogy of each pulped sample was determined by X-ray powder diffractometry at North Ryde, using a Philips PW1050 diffractometer fitted with a graphite-crystal diffracted beam monochromator. CuKα radiation was used for both qualitative and semiquantitative analysis. For qualitative analysis, each sample was scanned over the range 4-70°2θ at a speed of 1°2θ/min and a full scale count rate of 1000 cps. Mineralogical compositions were determined by comparison with JCPDS files.

Powder diffractograms, to aid the petrography, were produced on a few grains, mounted on the end of a glass fibre with vaseline. A Philips PW1226/10 56.7 mm Debye-Scherrer powder camera was used with Ni-filtered CuKα radiation. The films were interpreted using CSIRO standards and JCPDS files.

Semi-quantitative estimation of mineral abundances

The abundance of quartz was determined from the 1.817 Å diffraction peak on the traces used for qualitative analysis. All other mineral abundances were measured from traces over the range 4-30° 2θ with the full scale count rate adjusted to bring all peaks, except for dominant quartz peaks, on scale. Estimations were made using the height above background of a selected XRD peak for each mineral (see Table 1) and the results normalised to a full scale count rate of 1000 cps. The peaks were chosen so as to avoid overlap by peaks of other minerals.

As there is a significant variation in the Fe content of the samples (1-31% Fe_2O_3), their mass absorption characteristics would distort the mineral abundances. Corrections were made for this using the method of Brindley (1980). All major elements, including Ti, were used to calculate the mass attenuation coefficient for each sample which, in turn, was used to correct the measured peak heights. The results are tabulated in Appendix 7 and graphed in Appendices 3 and 6. It must be emphasised that these results are still approximate and are influenced by the degree of crystallinity of the phases and mineral orientation as well as by abundance. They give a rough comparison of the relative abundances of *particular* minerals *between* samples; they do not indicate the relative abundances of the different minerals in each sample.

TABLE 1
DIFFRACTION PEAKS USED FOR SEMI-QUANTITATIVE MINERALOGY

Mineral	Diffraction peak (hkl)	d-Spacing (Å)
Quartz	112	1.817
Feldspar	201	4.04
Muscovite	002	9.97
Talc	002	9.34
Amphibole	110	8.40
Kaolinite	001	7.10
Chlorite	001	14.0
Smectite	001	15.0
Goethite	110	4.18
Hematite	104	2.69

3.5 Geochemical Analysis

Detection limits and methods used for the analysis of each element are given in Table 2. Neutron activation analysis was by Becquerel Laboratories on 30 g aliquots. Minor and trace elements were determined on pressed discs, using a Philips PW1220C XRF at Floreat Park, by the methods of Norrish and Chappell (1977) and Hart (1989). Iron was determined on pressed disc, for matrix correction, and these approximate results are included. Major elements and some minor elements were also determined at Floreat Park by ICP analysis on a Hilger E-100, after Li-metaborate fusion.

At the USGS in Denver, six-step semiquantitative emission spectroscopy, using the method of Grimes and Marranzino (1968) was used to determine Ag and B, atomic absorption spectroscopy, using the method of O'Leary and Meir (1984) was used to determine Hg, Te and Tl and partial sample digestion, followed by ICP analysis, using the methods of Crock *et al.,* (1987) was used as additional methods for As, Cd, and Zn. The geochemical data are tabulated in Appendix 1 and displayed graphically in Appendices 2 and 5. Frequency distribution plots are given in Appendix 4.

Values below the detection limits for most of the elements have been reported without censorship, to make the graphs more natural and to aid mathematical treatment. It must be emphasised that values in this range are of suspect precision, are estimates and should be interpreted with caution. Reference should be made to Table 2 for the detection limits.

Loss on drying was determined gravimetrically on a 1 g sample after drying in a muffle furnace at 105 $^{\circ}$C for one hour. Loss on ignition was subsequently determined on the same sample after heating to 1050 $^{\circ}$C for a minimum of two one hour periods until constant weight was achieved.

The alkalis (Na, K and Li) were determined on an aliquot of 0.2 g, which was first dissolved by digesting with HF at 150 $^{\circ}$C in teflon and taken to dryness. After three successive evaporations in c.HCl, the sample was taken up in 50 ml of 0.2 M HCl. Determination was by AAS using a Varian 875.

TABLE 2
TRACE ELEMENT
DETECTION LIMITS AND METHODS

Element	Det.Limit (ppm)	Method
Ag	5, 0.5	XRF, ES
As	2, 5	INAA, P.D.ICP
Au	0.005	INAA
B	10	ES
Ba	15, 100, 100	XRF, ICP, INAA
Be	5	ICP
Bi	5, 2	XRF, P.D.ICP
Br	2	INAA
Cd	5, 0.1	XRF, P.D.ICP
Ce	2	INAA
Co	1	INAA
Cr	5, 100	INAA, ICP
Cs	1	INAA
Cu	5, 100	XRF, ICP
Eu	1	INAA
Ga	5	XRF
Ge	3	XRF
Hf	1	INAA
In	5	XRF
Ir	0.02	INAA
La	0.5	INAA
Li	1	AAS
Lu	0.2	INAA
Mn	20, 100	XRF, ICP
Mo	5	INAA
Nb	5	XRF
Ni	10, 50	XRF, ICP
Pb	5	XRF
Rb	5, 20	XRF, INAA
Sb	0.2	INAA
Sc	0.1	INAA
Se	2, 10	XRF (lc x5), INAA
Sm	0.2	INAA
Sn	5	XRF
Sr	3	XRF
Ta	1	INAA
Te	0.005	AAS
Th	0.5	INAA
Tl	0.05	AAS
U	2	INAA
V	10, 100	XRF, ICP
W	5	INAA
Y	3, 10	XRF, ES
Yb	0.5	INAA
Zn	5, 100, 2	XRF, INAA, P.D.ICP
Zr	4, 100	XRF, ICP

INAA - Instrumental Neutron Activation Analysis - Becquerel Laboratories
XRF - X-ray Fluorescence Analysis - CSIRO, Floreat Park
ICP - Inductively Coupled Plasma Spectrometry - CSIRO, Floreat Park
lc - Long counting technique
P.D.ICP - Partial digestion ICP - USGS, Denver
ES - emission spectroscopy - USGS, Denver
AAS - Atomic absorption spectrometry, Floreat Park and USGS, Denver

3.6 Sequencing and Standards

The samples were analysed in random order and in-house weathered rock standards (STD 3, STD 6 and STD 8) were introduced into the analytical batches at a ratio of 1:10 to 1:40, to monitor both accuracy and precision. The performance of the analytical method in relation to these standards, together with their mean values and the currently accepted values for these standards are reported in Appendix 1. In general the results are satisfactory, though the values for Fe appear to be low (both ICP and XRF) and the ICP analyses show a poor precision compared to the INAA and XRF analyses.

3.7 Specific Gravity

Rock densities were determined on selected dry samples by suspending 5-30 g specimens on thin (0.1 mm dia.) copper wires. The rock specimen and wire were first weighed in air, then coated thinly in hot paraffin wax, to prevent water uptake, and reweighed. The displacement of the sample was then determined gravimetrically by suspension in water. Although account was taken of the mass and displacement of the wax, the mass (approx., 0.02 g) and displacement of the copper wire were ignored.

4.0 ROCK CLASSIFICATION

Separation of the mafic-ultramafic rock suite from the felsic rocks, the black shales and the quartz-mica schists presented little difficulty in the field except where weathering is intense. Separation of the mafic from the ultramafic rocks was more difficult as they are very similar, even where fresh. These rocks are strongly metamorphosed, so their affinities (intrusive versus extrusive, komatiite versus tholeiite suite) were not immediately apparent as all primary fabrics had been obliterated. It was considered necessary to attempt to classify the fresh igneous rocks before proceeding with a study of their weathering.

4.1 Mafic and Ultramafic Rocks

Examination of the Al_2O_3/TiO_2 ratios of the ultramafic rocks from the lower two benches (R.L. 415-420) show values mainly in the range of 20-30 (Figure 5A). The grouping in the Al_2O_3/TiO_2 ratio is fairly close in the bottom and mid benches but scatter becomes severe on and above the top bench, due to intense weathering. Where the rocks are relatively unweathered, this ratio is compatible with a chondritic value of 20.3 which suggests that the ultramafic rocks could be metamorphosed komatiites of the alumina-undepleted group of Nesbitt *et al.*, (1979). The relationships of Al, Ca, Ce, Co, Cr, Ni, Sc and Ti to Mg are similar to those described by Beswick (1982) for komatiites. The range in composition could reflect the considerable geochemical variation found, even within one flow (see Hill *et al.*, 1987).

The Jensen diagram, employing a ternary plot of the cation proportions of $FeO+ Fe_2O_3+ TiO_2$: Al_2O_3: MgO (Jensen, 1976) confirms the komatiitic affinities of the Rand ultramafic rocks (Figure 5B), as do similar plots of komatiites from the Abitibi Belt (Jensen and Pyke, 1982), Finnish greenstone belts (Auvray *et al.*, 1982) and Zimbabwe (Nisbet *et al.*, 1982). An advantage of the Jensen classification is that it ignores SiO_2 which has been introduced during metamorphism and/or mineralisation (see Section 5). Classification by this means is only viable below R.L. 445. The Jensen plot requires Mg but Mg is progressively leached above this level.

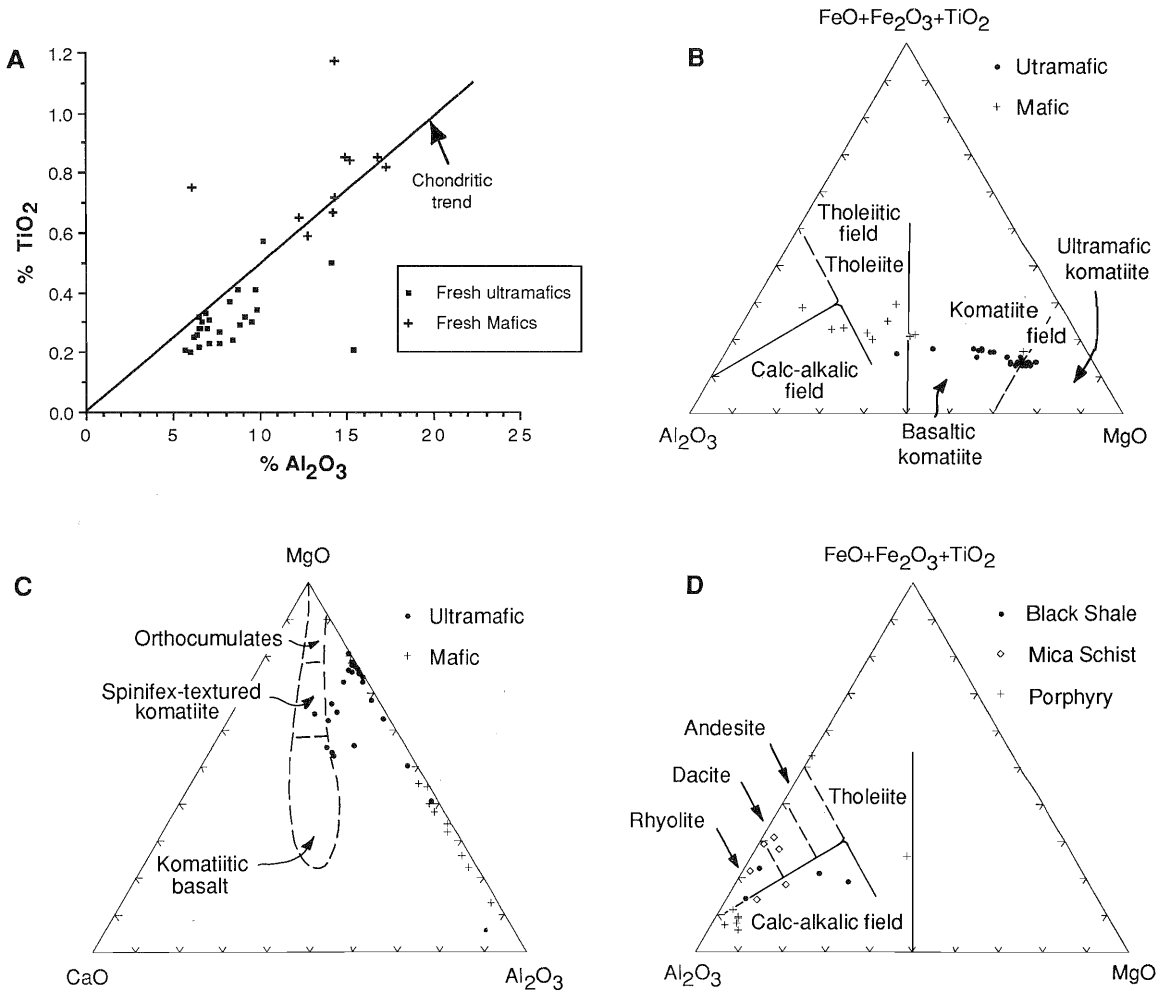

Figure 5. Rock classification plots.

The mafic rocks present a greater problem in classification. Although these rocks are richer in Al and Ti and poorer in Mg, the Al:Ti ratio is also chondritic, suggesting some relationship to the komatiites (Figure 5A). This is confirmed by the Jensen diagram where the mafic rocks form a continuation of the trend from basaltic komatiite to high Mg basalt (Figure 5B). Where these rocks are highly weathered, the degree of scatter becomes severe, due to loss of Mg and varying Fe contents.

Barnes (1985) studied the effects of alteration on komatiites in the Abitibi Greenstone Belt. She concluded that, though the alteration consisted of the separate effects of deuteric alteration, seafloor alteration and metamorphism, the effects were inseparable and resulted in disturbance in the contents of Na, K, Ca, Sr and Rb. The elements Ni, Cr, Co, Hf, Sc, Y, Zr and the rare earth elements had not been mobilised. Since olivine crystallisation dominates komatiite evolution, the CaO/Al_2O_3 ratio would be expected to remain constant and close to 1 but it is actually considerably less than 1 (Figure 5C). As the TiO_2/Al_2O_3 ratio has remained relatively constant, it is concluded that CaO has been lost. CaO was probably located in glass and augite and this was lost during serpentinisation. Thus the $MgO:CaO:Al_2O_3$ relationship indicates considerable metamorphic or seafloor loss of CaO. This is typical of talc-rich metakomatiites (R.E.T. Hill, *pers comm*, 1990).

Thus it is concluded that the mafic and ultramafic rocks are part of a komatiitic trend of intratelluric differentiated extrusives and much of the variation encountered is regarded as related to this differentiation. One rock, previously classified spatially as a mafic rock (RE 33) has an ultramafic composition. Similarly two rocks (RE 16 and RE 19), previously classified spatially as ultramafic rocks, could be better classified as mafic, though they lie on the link between the two fields. These reclassifications are used in the ensuing study.

4.2 Granitoid Porphyries

The porphyries form a tight group on the Jensen plot (Figure 5D) and are all classified as rhyolites, except for RE 9, which has been shown petrographically to be a mixture of porphyry and talc-chlorite schist. Their pod-like field relations suggest an hypabyssal origin so they are probably related to one of the several granites in the area.

4.3 Mica Schists and Black Shales

The fabric of the mica schists suggests they have absorbed a high proportion of the strain in this rock sequence but to regard them merely as shear zones or weak mylonites (White, 1987), disregards the origin of their deformed materials. If they were sheared metakomatiites, their compositions would be related to their host rocks, with additional quartz but, in fact, they contrast with them. Their ribbon-like field relationships and general appearance suggest sediments or ash beds, in which case they could represent the products of relatively slow sedimentation between volcanic events. Such materials would be incompetent, compared to the enclosing metavolcanics. Their compositions may suggest the provenance of the detritus that formed them.

Bavinton (1981) has described fine-grained sulphidic metasediments from Kambalda, invoking a mixture of local (mafic-ultramafic) and distant (felsic-granitic) detritus, some with biological carbonaceous input. To this he adds chalcophile contributions from volcanic exhalations and sea-floor leaching of underlying lava flows and proposes subsequent diagenetic and metamorphic alteration, to explain the composition of these sediments. These sediments are significantly enriched in Au (Bavinton and Keays, 1978).

The mica schists from the Rand Pit plot in the tholeiitic to calc-alkalic field on the Jensen diagram (Figure 5D) and range from dacite to rhyolite. Some show similarities with a tuff (Table 3) from the Cue area (Hallberg, 1976). The black shales follow a similar trend (Figure 5D).

TABLE 3
GEOCHEMISTRY OF METASEDIMENTS AND PORPHYRY

	Reedy Porphyry	Reedy Schist	Reedy Black Shale	Kambalda Sediment[1]	Cue Tuff[2]
SiO_2	76.12	66.99	63.9	54.85	58.6
Al_2O_3	13.88	16.63	13.75	12.35	22.3
Fe_2O_3	1.86	6.34	6.86	14.05	4.1
MgO	0.62	1.44	3.97	3.75	2.4
CaO	0.14	0.06	0.2	4.15	0.1
Na_2O	3.27	0.12	0.09	2.85	0.31
K_2O	3.59	5.26	2.67	2.05	6.06
Ti/Zr	20	52	23	-	39
n	5	3	2	-	1

[1]Bavinton (1981) [2]Hallberg (1976)

Thus the dominant mafic-ultramafic rocks seem to belong to a komatiitic suite of metavolcanics, which probably lost much of their Ca prior to weathering, and these were interstratified with micaceous and carbonaceous sediments derived in part from local materials within the volcanic pile. They were later metamorphosed and intruded with granite-related felsic lenses and inhomogeneously deformed and mineralised.

5.0 PETROGRAPHY

The objectives of the petrographic study are to trace the mineralogical and fabric changes that occur in each rock type with progressive weathering up the profile. Each specimen has been described in detail in Appendix 8, making use of the bulk XRD data, reinforced by numerous Debye-Scherrer diffractograms of selected, petrographically distinct mineral phases. A summary and interpretation of this work follows.

Fabrics seen with the petrographic microscope are shown in Figures 6 to 10. Close-up photographs were also taken of the sawn surfaces of the impregnated blocks, used for making thin sections, to illustrate the petrography further and to enhance its meaning to the field geologist. They show what would be seen on the surface of sawn drill core or RAB chips, using a binocular microscope or a good-quality hand lens. Some have been lightly varnished to simulate a wet or damp surface. Where possible these have been juxtaposed with the photomicrographs, so that direct comparisons may be made with the same or similar fabrics at different scales.

5.1 Mafic Rocks

Mafic band M3: Specimens RE 13-14, 21-23, 41, 43, 55-58, 80-83, 94-96.
Where comparatively fresh, these rocks consist of granular quartz, untwinned albite and lenticular patches of chlorite, cut by a strong foliation marked by muscovite and talc (Figure 6A). In turn, this is cut by a later, open-spaced cleavage, filled with schistose chlorite. Magnetite and ilmenite show slight weathering with release of goethite, which locally stains grain boundaries and penetrates the cleavage (Figure 6B). Some of the albite is turbid and partly altered to very fine-grained kaolinite (Figure 6B) and around R.L. 420 (70 m depth) the albite is almost completely kaolinised (Figure 6C). A few cubic goethite structures pseudomorph pyrite and sinuous quartz veins follow the cleavage. In places, these rocks are unusually coarse-grained and probably are intrusives or thick flows in the volcanic pile. These rocks are largely saprock (Butt and Zeegers, in press).

At R.L. 440 (50 m depth), the chlorite is partly altered to smectite (Figure 6C) and at R.L. 460 (30 m depth) this is complete. Some have a well-preserved schistose fabric (Figure 6E), whereas others, which contain sinuous quartz patches, now consist of very fine-grained, low birefringent kaolinite, some talc, and a kaolinite-smectite mixture with a slightly higher birefringence than the kaolinite on its own. This mixed phase occurs as patches with a sworled fabric. The rock is cut by vermiform fractures and solution channels. Most of these rocks are saprolitic, though some pedolithic fabrics occur on a small scale (Butt and Zeegers, in press).

The saprolite at R.L. 480 (10 m depth) generally consists of a very fine-grained to relatively coarse-grained, schistose mat of kaolinite and talc, with some muscovite and smectite, after a chloritic cleavage, and fine-grained granular quartz. This is cut by cleavage-associated quartz, in which the individual quartz grains are separated by a clay matrix. There are also numerous solution channels and vesicles (Figure 6F), some of which are infilled with fragments of saprolite, set in a matrix of clay. Saprolitic fabrics are preserved in these rocks as palimpsest schistosities, now consisting of clays and quartz, but pedolithic fabrics (matted clay fabrics and vesicles) become increasingly important.

Considerable reorganisation of the primary fabric is evident in other parts. Blasts of very fine-grained kaolinite have developed and these have swept remnant quartz grains into clusters (Figure 7F and similar to Figure 7C). Some saprolite has formed a breccia which comprise fragments of various round to subangular kaolinitic saprolite and vein quartz, set in a variably Fe-stained, coarser-grained matrix of flaky kaolinite and smectite.

Another reorganised saprolite variety contains two distinct clay phases: (i) an older, low birefringent kaolinite, set with quartz grains (their wide size range and strained nature suggests they are fragmented vein quartz) and vermiform books, stacks and accordion structures of recrystallised kaolinite (Figure 7A); (ii) a later, very fine-grained, pinkish yellow, very low birefringent kaolinite, containing minor smectite, which contains fragments of all the earlier components and cuts the previous clay phase. These features indicate loss of the original rock fabric and indicate the transition from saprolite to pedolith in which soil-forming processes predominate.

Mafic band M1: Specimens RE 33, 64-65, 68-69, 71-77, 101-107.
This band was not exposed to as great a depth as mafic band M3. At R.L. 440 (50 m depth) weathering is already well advanced and the rocks consist of granules of quartz and kaolinised feldspar, cut by a schistosity marked by mixed kaolinite and chlorite. These rocks are saprolitic.

At R.L. 460 (30 m depth) the mafic rocks consist of a schistose fabric of talc, chlorite and quartz, in which are set globular blasts of very fine-grained secondary pedolithic kaolinite (Figures 7C and D) which progressively destroy the original, schistose, saprolitic fabric.

FIGURE 6
MICRO- AND SEMIMICRO-FABRICS
OF SLIGHTLY-WEATHERED MAFIC SCHISTS

A. Quartz-feldspar-chlorite schist. An unweathered schistose fabric of granular quartz (QZ), untwinned albite (AB), muscovite (MU) and chlorite, cut by an open-spaced fracture cleavage marked by chlorite (CH). Specimen RE 23: R.L. 416. Mafic band M3. Compare Figure 6B. Photomicrograph with crossed polarisers.

B. A fresh, quartz-feldspar-chlorite schist. It consists of fresh, glassy quartz (QZ) and slightly turbid albite (AB), set with flakes of chlorite (CH). The strong, chloritic cleavage is parallel to x-y. Goethite stains (GO) have spread from small, partly weathered magnetite grains. Specimen RE 23: R.L. 416. Mafic band M3. Compare Figure 6A. close-up photograph of "wet" surface.

C. Quartz-chlorite schist. The albite has been completely altered to kaolinite (KA), leaving the quartz (QZ) and muscovite (MU) unaltered. The chlorite (CH) is turbid and has begun to alter to smectite. Lenses of goethite (GO) lie in the cleavage. Compare with a similar fabric in Figure 6D. Specimen RE 43: R.L. 442.0. Mafic band M3. Photomicrograph with crossed polarisers.

D. A partly kaolinised quartz-feldspar-chlorite schist. Most of the feldspar grains have been weathered to kaolinite (KA) or are very turbid. Quartz (QZ) remains glassy and black streaks of chlorite (CH) are relatively unaltered. Goethite (GO) and hematite stains have spread outward from weathered magnetite and oxidised sulphide grains, staining the surrounding silicates. Compare with a similar fabric in Figure 6C. Specimen RE 22: R.L. 416. Mafic band M3. close-up photograph of "damp" surface.

E. Quartz-kaolinite schist. A groundmass of granular quartz and kaolinite, after plagioclase (KQ), is cut by lenses of kaolinite which accurately pseudomorph two acutely intersecting schistose, previously chloritic cleavages (KL). Specimen RE 56: R.L. 467.9. Mafic band M3. Photomicrograph with crossed polarisers.

F. A deeply-weathered quartz-kaolinite-smectite schist. The kaolinite fabric, which is set with vermiform vesicles (V) has been stained brown by goethite (GO). The goethite appears to have been locally leached (L) around the solution channels and vesicles. Specimen RE 83: R.L. 481. Mafic band M3. close-up photograph of "wet" surface.

G. Kaolinite-quartz schist. A mat of slightly shard-like quartz granules (QZ) and flaky kaolinite (KA), cut by the palimpsest kaolinised remnant of a phyllosilicate cleavage (KC). Compare with Figure 6E, where this fabric is more clearly developed and with Figure 7E where the fabric has been completely overprinted by secondary kaolinite structures in the same slide. Specimen RE 76: R.L. 481.2. Mafic band M1. Photomicrograph with crossed polarisers.

H. A weathered mica schist. The muscovite has weathered extensively to kaolinite (KA) and the schistosity is now largely depicted by goethite and hematite (HM), which follow and stain the margins or quartz lenses. Specimen RE 90: R.L. 483. Mafic band M3. close-up photograph of "damp" surface.

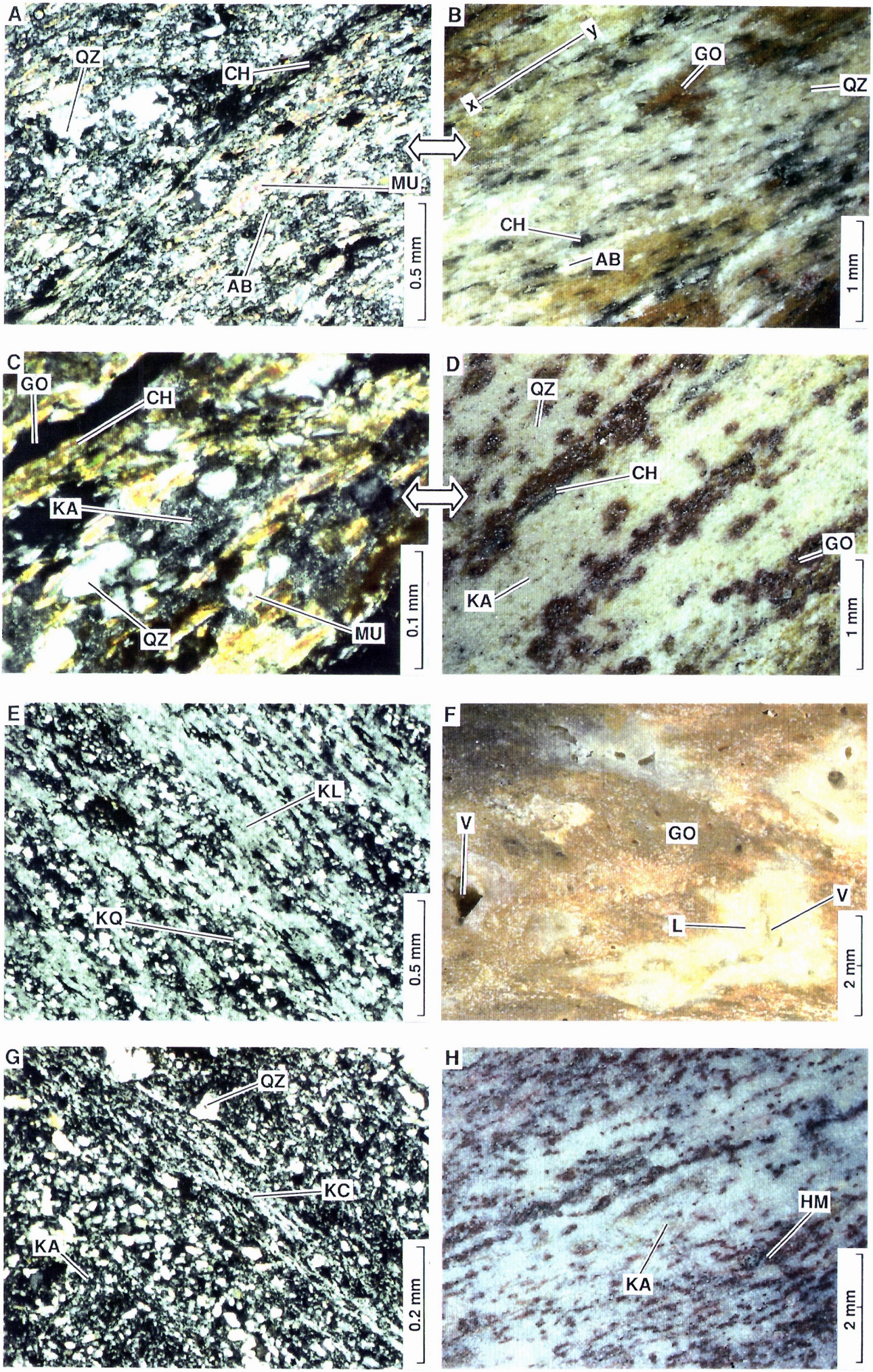
A
QZ
CH
MU
AB
0.5 mm
B
y
x
GO
QZ
CH
AB
1 mm
C
GO
CH
KA
QZ
MU
0.1 mm
D
QZ
CH
GO
KA
1 mm
E
KL
KQ
0.5 mm
F
V
GO
V
L
2 mm
G
QZ
KC
KA
0.2 mm
H
HM
KA
2 mm

FIGURE 7
MICRO- AND SEMIMICRO-FABRICS
OF INTENSELY-WEATHERED MAFIC SCHISTS

A. Quartz-kaolinite rock. Recrystallised coarse-grained vermiform books and accordions of kaolinite (AK) lie parallel in a mass of fine-grained, flaky kaolinite (KA). Specimen RE 80: R.L. 481.1. Mafic band M3. Photomicrograph with crossed polarisers.

B. A kaolinite-quartz schist. A small channelway (C), now filled with resin, and an open vesicle (V) are set in patches of fine-grained secondary kaolinite (KA) with segregations of quartz granules (QZ), possibly after a relict quartz vein. Only the slightest vestage of the original schistose fabric remains. Specimen RE 76: R.L. 481. Mafic band M1. Compare with Figures 7C-F. close-up photograph of "dry" surface.

C. Quartz-chlorite-talc-smectite schist. Globular patches of recrystallised, very fine-grained kaolinite (KA) lie in a slightly schistose mass of granular quartz and flaky chlorite, smectite and kaolinite (QC). Compare with Figures 7B, D-F, where these structures are more strongly developed. Specimen RE 65: R.L. 464.9. Mafic band M1. Photomicrograph with crossed polarisers.

D. A quartz-chlorite-talc-smectite schist. Granular quartz and the overall schistose fabric are all that remain of the original rock. The schistose fabric (SH) is being progressively destroyed by expanding patches of very fine-grained, white secondary kaolinite (KA). Compare with Figures 7B, C, E and F. Specimen RE 65: R.L. 465. Mafic band M1. close-up photograph of "dry" surface.

E. Kaolinite-quartz schist. The fabric of Figure 6G has in places been completely replaced by secondary, fine-grained kaolinite structures (KA) which form globular segregations around which the quartz (QZ) has been concentrated. Compare with similar fabrics in Figures 7B-D and F. Specimen RE 76: R.L. 481.2. Mafic band M1. Photomicrograph with crossed polarisers.

F. A mafic quartz-kaolinite rock. White patches of secondary kaolinite (KA) and segregations of quartz grains (QZ) show considerable reorganisation of the rock fabric. Small cracks, vermiform vesicles (V) and irregular cavities , some partly lined with Mn minerals (MN) are now filled with impregnating resin. Compare with similar fabrics in Figures 7B-E. Specimen RE 80: R.L. 481. Mafic band M3. close-up photograph of "wet" surface.

G. Quartz-kaolinite rock. An arcuate solution channel which is choked with fibrous, low-birefringent clay (KA). The rock consists of flaky kaolinite and quartz. Compare with Figure 7H. Specimen RE 101: R.L. 486.7. Mafic band M1. Photomicrograph with crossed polarisers.

H. A mafic quartz-kaolinite rock. Light brown patches of early kaolinite and quartz (KQ) are separated by several generations of arcuate channels, now largely filled with a lining of white kaolinite (KA) and a discontinuous grey core of mixed kaolinite and smectite (KS). These link small clay-lined vesicles (V). Compare with Figure 7G. Specimen RE 101: R.L. 487. Mafic band M1. close-up photograph of "wet" surface.

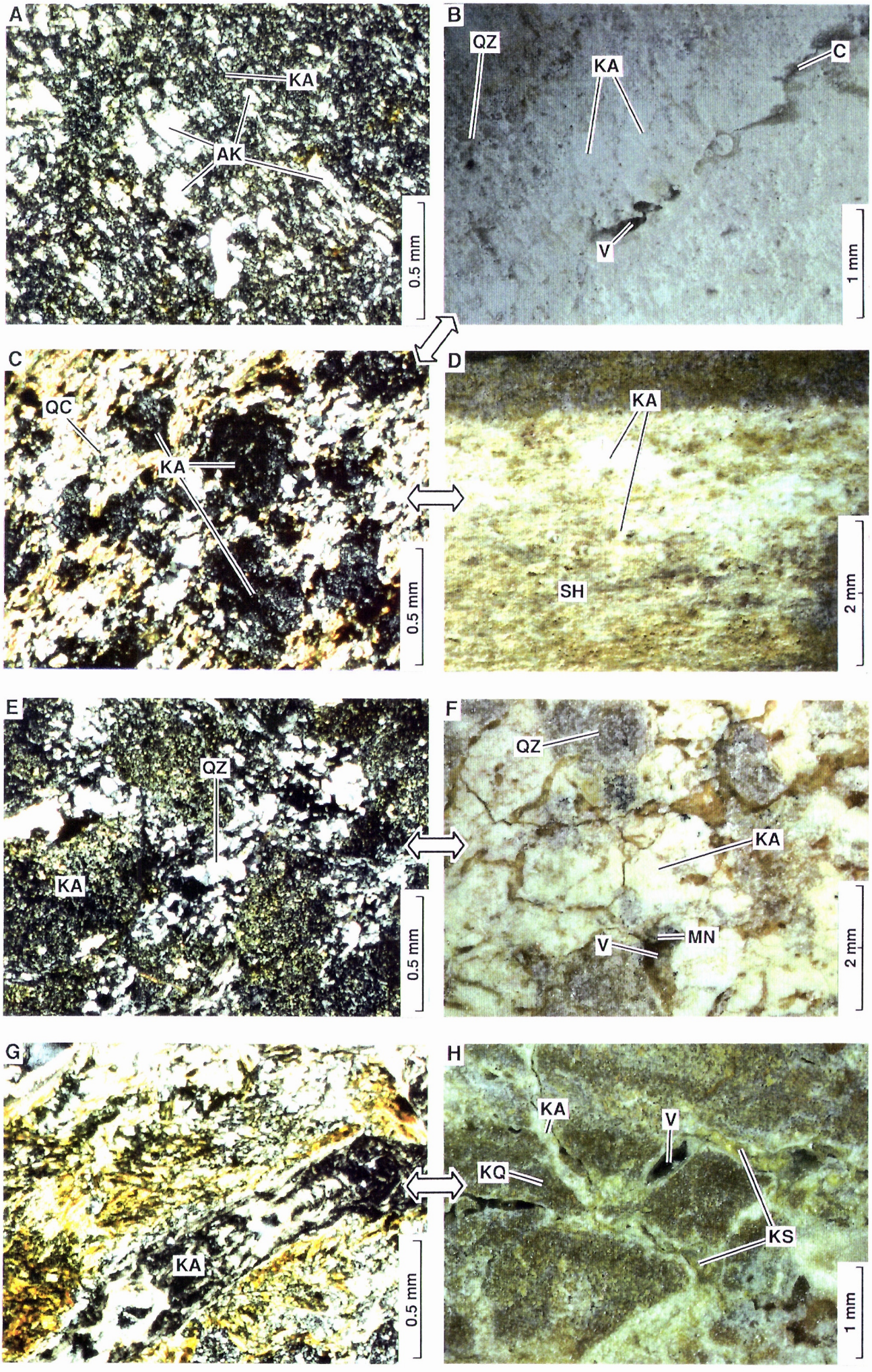
A
KA
AK
0.5 mm
B
QZ
KA
C
V
1 mm
C
QC
KA
0.5 mm
D
KA
SH
2 mm
E
QZ
KA
0.5 mm
F
QZ
KA
V
MN
2 mm
G
KA
0.5 mm
H
KA
V
KQ
KS
1 mm

FIGURE 8
MICRO- AND SEMIMICRO-FABRICS
OF SLIGHTLY-WEATHERED ULTRAMAFIC SCHISTS

A. Talc-chlorite schist. Islands of fresh matted talc (TC), with some quartz, cut by a chlorite-filled cleavage (CH). Specimen RE 29: R.L. 415.6. Ultramafic band UM2. Photomicrograph with crossed polarisers.

B. A fresh tremolite-chlorite schist. Needles and plates of fresh tremolite (TM), set in a groundmass of chlorite (CH) and tremolite. Groundwater has etched out a few small vesicles (V) into which the surrounding minerals project. Specimen RE 50: R.L. 443. Ultramafic band UM6. close-up photograph of "dry" surface.

C. Fresh talc-chlorite-tremolite schist. A mat of talc (TC), with granules of quartz (QZ), set with fresh needles of tremolite (TM). Here the tremolite is aligned with the foliation. Compare with Figure 8D. Specimen RE 31: R.L. 416.1. Ultramafic band UM2. Photomicrograph with crossed polarisers.

D. Fresh talc-chlorite-tremolite schist. Small needles of tremolite (TM) crosscut the fabric of islands of talc (TC) cleaved by chlorite (CH). Compare with Figure 8C. Manganese minerals, chiefly cryptomelane, occur in zig-zag stylolitic veins (MZ). Specimen RE 31: R.L. 416. Ultramafic band UM2. close-up photograph of "dry" surface.

E. Largely fresh talc-chlorite schist. Goethite pseudomorphs (GO) after pyrite and/or magnetite are surrounded by a goethite stain in the talc mat (TC). Ilmenite grains (IL) are unaltered. Compare to Figure 8F. Specimen RE 26: R.L. 415.6. Ultramafic band UM2. Photomicrograph with crossed polarisers.

F. Fresh talc-chlorite schist. A greenish-grey, very fine-grained mat of talc (TC) is cut by a dark green chloritic fracture cleavage (CH). Parts of this cleavage have been etched open by groundwater and goethite (GO) has been deposited. Compare to Figure 8E. Specimen RE 28: R.L. 416. Ultramafic band UM2. close-up photograph of "dry" surface.

G. Talc-chlorite-quartz schist. Large islands of relatively coarse-grained, granular quartz (QZ) and flaky talc (TC) are separated by a well-developed, discrete, open-spaced chlorite-filled cleavage (CH). Specimen RE 15: R.L. 420.5. Ultramafic band UM4. Photomicrograph with crossed polarisers.

H. A fresh talc-chlorite schist. Pale-green talc (TC), containing a small quantity of quartz and dark green chlorite (CH) form a groundmass in which are scattered small honey-brown crystals of sphene (SP). Specimen RE 29: R.L. 416. Ultramafic band UM2. close-up photograph of "damp" surface.

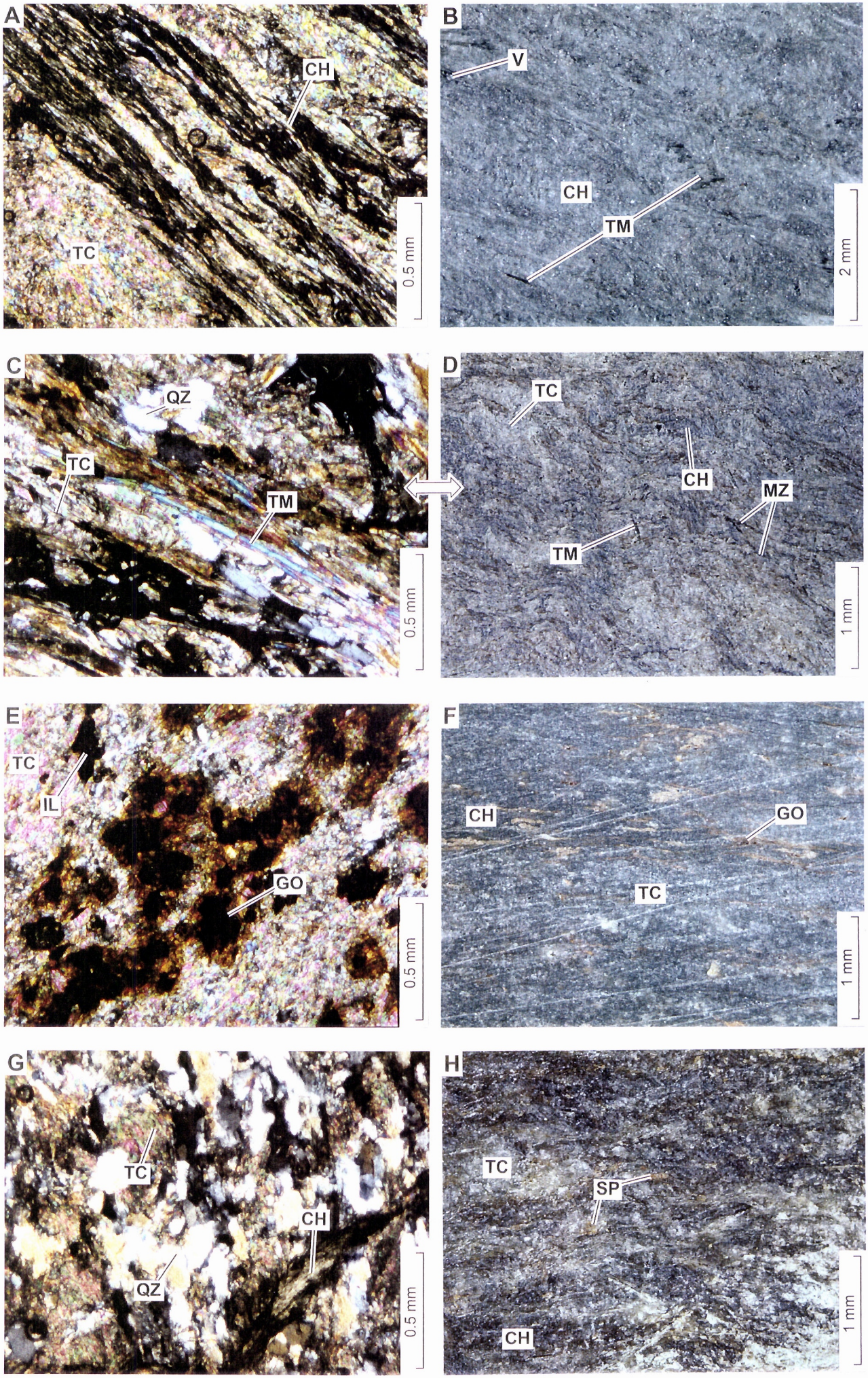
A
CH
TC
0.5 mm
B
V
CH
TM
2 mm
C
QZ
TC
TM
0.5 mm
D
TC
CH
MZ
TM
1 mm
E
TC
IL
GO
0.5 mm
F
CH
GO
TC
1 mm
G
TC
CH
QZ
0.5 mm
H
TC
SP
CH
1 mm

FIGURE 9
MICRO- AND SEMIMICRO-FABRICS
OF INTENSELY-WEATHERED ULTRAMAFIC SCHISTS

A. Partly weathered talc-chlorite schist. A brown, goethite-stained mat of talc and chlorite (TL), set with patches and granules of quartz (QZ). Pre-existing tremolite (TM) has been dissolved, leaving needle-like voids, some of which have been filled or partly filled with goethite. Specimen RE 35: R.L. 440.5. Ultramafic band UM2. Compare with Figure 9B. Photomicrograph in plain polarised light.

B. A weathered talc-chlorite schist. A schistose groundmass of talc (TC) and chlorite (CH) rich layers, which are lightly but variably stained with goethite (GO). This is set with needles of tremolite which have been largely dissolved and replaced by goethite (GT). Specimen RE 35: R.L. 440. Ultramafic band UM2. Compare with Figure 9A. close-up photograph of "dry" surface.

C. Kaolin-quartz rock. A mass of stumpy books of secondary kaolinite (KB), set in flakes of fine-grained kaolinite (KA). These are the precursors to accordion structures (compare with Figure 8D). Specimen RE 86: R.L. 482.6. Ultramafic band UM4. Compare with Figure 9D. Photomicrograph with crossed polarisers.

D. A strongly weathered ultramafic - now a kaolinite-quartz rock. It consists of patches of white, coarse-grained recrystallised kaolinite (KS), with a stumpy stack micro-fabric, set in yellowish fine-grained kaolinite (KY). The whole contains small vesicles (V) and has been variably stained pink with Fe oxides. The blue patch is quartz (QZ). Specimen RE 86: R.L. 483. Ultramafic band UM4. Compare with Figure 9C. close-up photograph of "wet" surface.

E. Saprolite-fragment breccia. A wide variety of texturally different, polymictic, round to sub-angular saprolite fragments which form a loosely clay-cemented breccia. The saprolite fragments are of matted kaolinite and some are mixed with smectite and palygorskite. Some show clay-rich skins and there are also a few goethitic granules. Specimen RE 93: R.L. 486.9. Ultramafic band UM4. Compare with Figure 9F. Photomicrograph in plain polarised light.

F. A saprolite fragment breccia. This consists of a loosely-cemented, clast-supported polymictic breccia of saprolite fragments. Most fragments consist of matted kaolinite, some containing smectite and palygorskite. Some still retain a schistose fabric (SH), others are matted (MT). They show varying stages of goethite staining from intense and largely replaced (GO) through lightly stained (LS) to unstained kaolinite (KA). Specimen RE 93: R.L. 487. Ultramafic band UM4. Compare with Figure 9E. close-up photograph of "wet" surface.

G. Talc-kaolinite-smectite schist. The phyllosilicates, which form a well-preserved schistosity, have been intensely stained with goethite, so as to be petrographically unrecognisable. Needles of ilmenite lie parallel to the cleavage. Specimen RE 88: R.L. 482.7. Photomicrograph in plain polarised light.

H. Weathered pyrite (PY), set in fresh plagioclase (PL) and quartz (QZ), of a relatively fresh granitoid porphyry. The pyrite is cavernous and has an outer and an inner lining of goethite (GO). Specimen RE 25: R.L. 415. close-up photograph of "wet" surface.

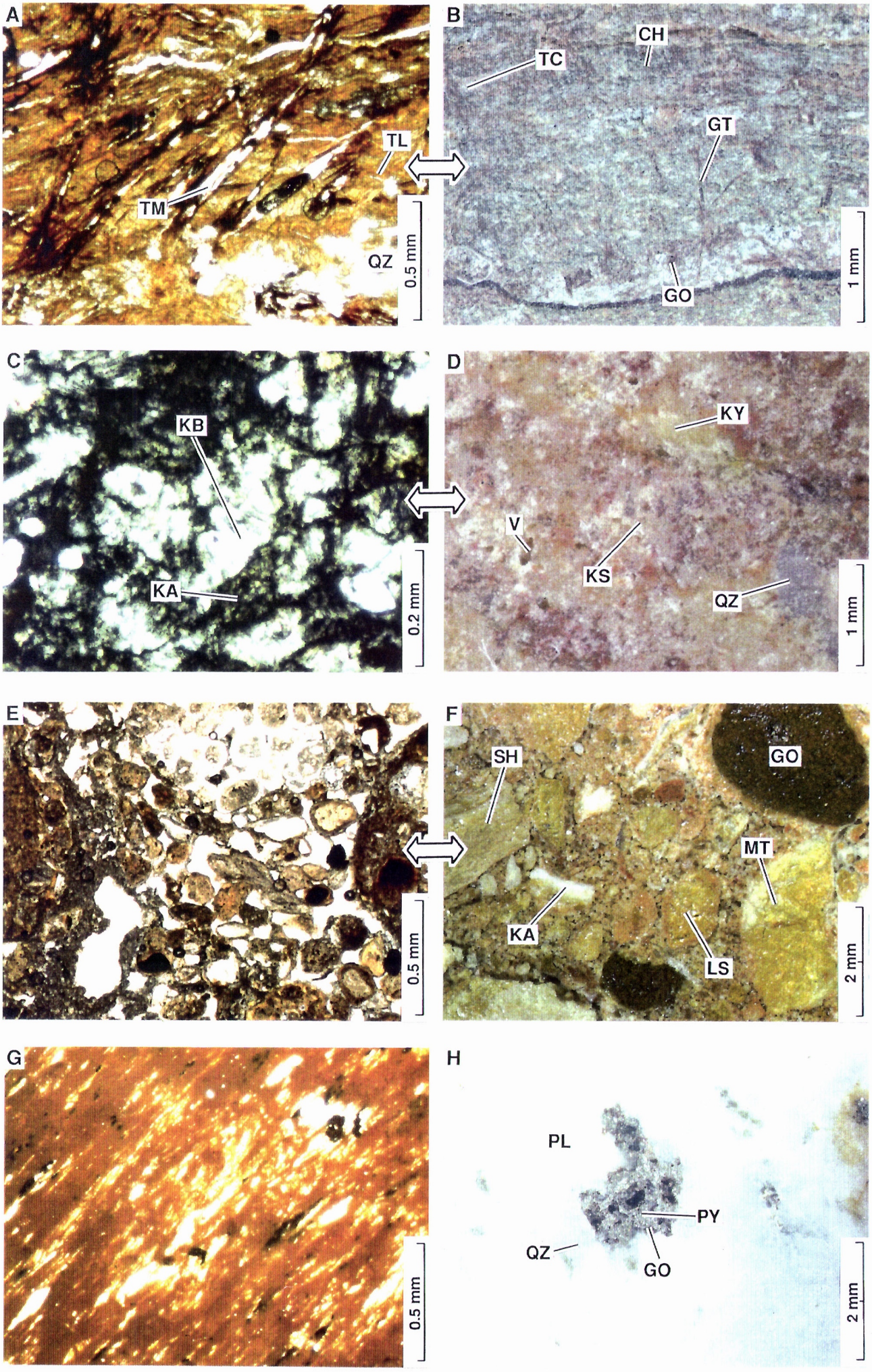
A
TL
TM
QZ
0.5 mm
B
CH
TC
GT
GO
1 mm
C
KB
KA
0.2 mm
D
KY
V
KS
QZ
1 mm
E
0.5 mm
F
SH
GO
MT
KA
LS
2 mm
G
0.5 mm
H
PL
PY
QZ
GO
2 mm

FIGURE 10
MICRO-FABRICS OF FRESH AND WEATHERED MICA SCHISTS, BLACK SHALES, PORPHYRIES AND VEIN QUARTZ

A. Quartz-mica schist. Small quartz granules (QZ), forming narrow composite lenses, and muscovite flakes (MU) with a few slightly larger flakes of chlorite and mixed chlorite and muscovite (CH) form a wavy, schistose fabric. Specimen RE 32: R.L. 440.6. Mica schist band S1. Crossed polarisers.

B. Black Shale. Schistose muscovite, kaolinite and minor graphite (MK) occur with lenticular patches of quartz (QZ) which approximate the bedding (S1). Graphite is concentrated in a later cleavage (S2). A few patches of goethite (GO) are scattered in the fabric. Specimen RE 112: R.L. 469.0. Plain polarised light.

C. Granitoid Porphyry. Granular quartz (QZ) and completely kaolinised microcline (KM) with vein quartz (QV) and cryptomelane (CY). Specimen RE 36: R.L. 441.8. Granitoid porphyry pod P2. Crossed polarisers.

D. Granitoid Porphyry. A pseudomorph of a micrographic intergrowth of quartz and microcline. The microcline is completely altered to kaolin (KA) but the quartz (QZ) remains. Specimen RE 91 R.L. 486.8. Granitoid porphyry pod P5. Crossed polarisers.

Progressive weathering of vein quartz.

E. A small quartz pod (QZ) showing interlocking granoblastic quartz veins which are virtually unweathered. Quartz-feldspar-chlorite-mica schist. Specimen RE 47. R.L. 442.1. Mafic band M5. Plain polarised light.

F. The still interlocking quartz grains (QZ) of a vein are separated by a thin layer (30 m) of kaolinite (KA). Quartz-kaolinite-smectite rock. Specimen RE 96. R.L. 486.9. Mafic band M3. Crossed polarisers.

G. Irregular quartz patch in which individual grains (QZ) are extensively corroded and separated by fine grained kaolinite (KA). The grains are no longer interlocked and the quartz has a sugary appearance in the hand specimen. Quartz-kaolinite-smectite schist. Specimen RE 83. R.L. 481.3. Mafic band M3. Plain polarised light.

H. Previously interlocking quartz grains (QZ) are now more widely separated by kaolinite (KA) and they have drifted apart. In this manner the quartz loses its integrity. Quartz-kaolinite-smectite rock. Specimen RE 96. R.L. 486.9. Mafic band M3. Crossed polarisers.

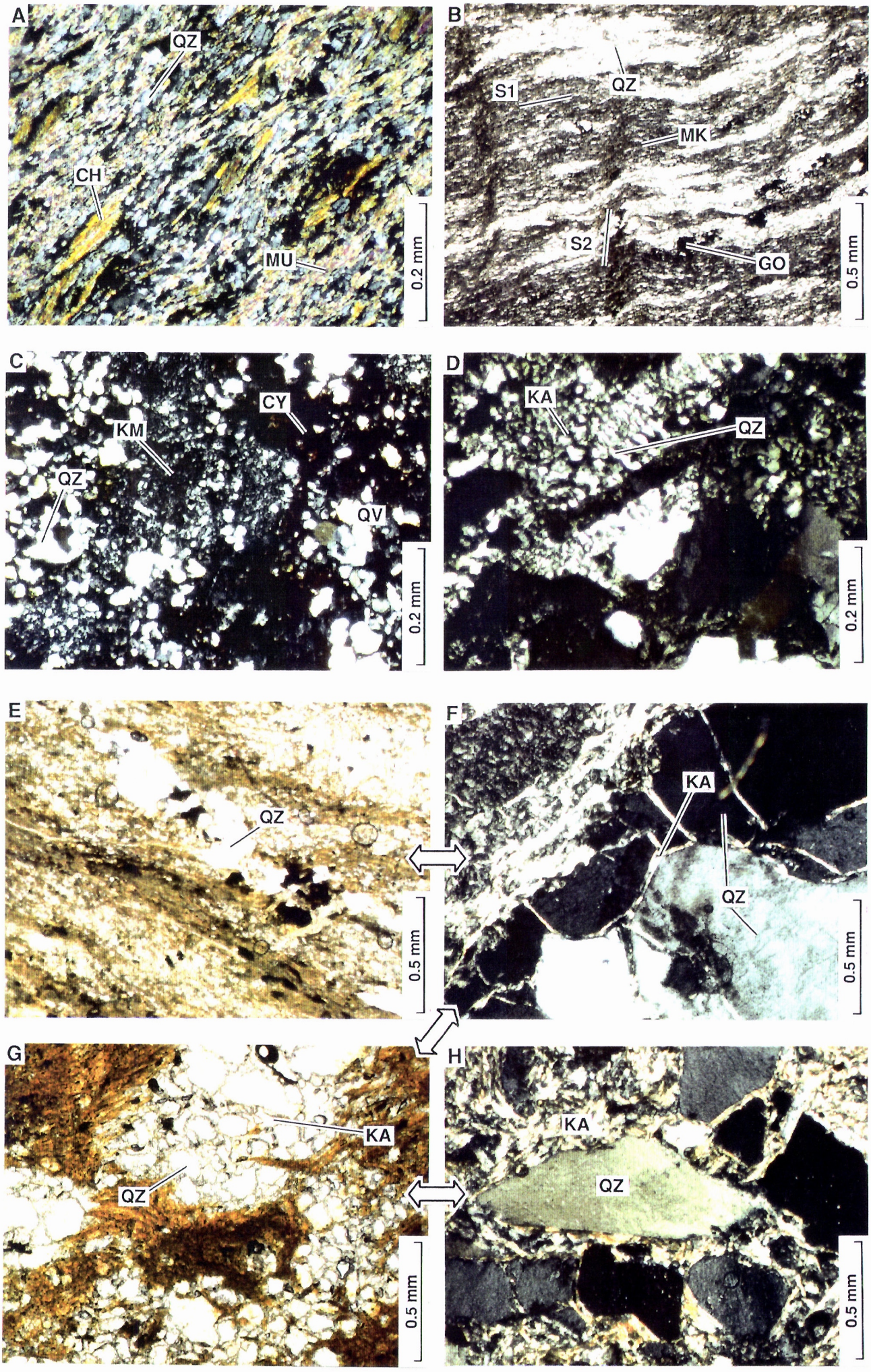
A
QZ
CH
MU
0.2 mm
B
S1
QZ
MK
S2
GO
0.5 mm
C
CY
KM
QZ
QV
0.2 mm
D
KA
QZ
0.2 mm
E
QZ
0.5 mm
F
KA
QZ
0.5 mm
G
KA
QZ
0.5 mm
H
KA
QZ
0.5 mm

These kaolinite patches are more prominent at R.L. 480 (10 m depth) (Figure 7B), where they vary from fine- to coarse-grained, and are set amongst shard-like quartz and remnants of talc, kaolinite and smectite, depicting a palimpsest cleavage (Figure 6G). Clusters of quartz granules are concentrated around the margins of these kaolinite patches (Figure 7E). There are numerous vesicles and sinuous channelways (Figure 7B), some filled with yellowish kaolinite (Figures 7G and H). The saprolitic clay fabrics have been almost completely destroyed.

5.2 Ultramafic Rocks

Ultramafic band UM2: Specimens RE 1, 2-5, 26, 28-31, 34-35, 37, 40, 59-63, 78-79, 97-100.
In the very slightly weathered state around R.L. 420 (70 m depth), these in part tremolitic talc schists are cut by a relatively open-spaced chloritic cleavage. The talc forms slightly schistose mats and islands (Figure 8A), in places set with decussate tremolite. Small amounts of graphite are found in the pre-chlorite talc schistosity. Where the cleavage is intense, the tremolite is needle like and aligned to the cleavage (Figure 8C). Where the cleavage crosses tremolite crystals, these crystals are broken. In places, groundwater has penetrated parts of the cleavage, etching it open, and has deposited small amounts of goethite (Figure 8F).

Although most of these rocks are relatively quartz-poor, introduced quartz is locally an important component and occurs as chains of grains, closely associated with the cleavage, or as clusters in pressure shadows, where it occurs with coarse talc. Accessory minerals are Fe minerals, including chromite and ilmenite, as well as hypidiomorphic sphene (Figure 8H). Ilmenite, which is generally found aligned to the cleavage, has a feathery appearance and shows early alteration to anatase and goethite. Sphene becomes semi-opaque and has a creamy colour in oblique reflected light. Goethite, from granules of magnetite or ilmenite, stains the talc (Figure 8E) and spreads along the cleavage or follows stylolitic fractures and the margins of quartz veins. In places goethite is found pseudomorphing pyrite cubes. Small amounts of cryptomelane follow stylo-fractures (Figure 8D). Most of these specimens are classified as fresh rock to saprock.

Iron staining is more apparent along the cleavage and in small fractures around R.L. 440 (50 m depth). Small amounts of graphite are still to be found in the older, talcose schistosity. Sphene is opaque here and has been altered to creamy-coloured anatase lenses in the cleavage. The cleavage-related chlorite is yellow brown, slightly opaque and dusted with yellowish smectite. Tremolite needles have been dissolved and replaced in part by goethite (Figures 9A and B).

Around R.L. 460 (30 m depth), the talc of the saprolites has remained unaltered, though weathering of chlorite to smectite is more advanced. Tremolite is represented only by goethite-coated cavities, sphene has been altered entirely to anatase, all traces of Ca have been leached and ilmenite has also been altered to anatase, though the characteristic feathery structures remain. Goethite occurs both in the talcose schistosity and in the later chloritic cleavage and penetrates quartz vein margins. Some fractures are filled with asbolane ($Mn[O,OH]_2.[Co,Ni,Ca]_x.OH_{2x}.nH_2O$) and an indeterminate secondary V mineral. Some rocks show lensoid cavities and one example (RE 59) of a blue-green talc-kaolinite rock was found which could have formed either by alteration of a talc-chlorite rock or by filling of cavities with secondary chromian kaolinite.

Kaolinite is an important component at and above R.L. 480 (10 m depth). In places it occurs as an alteration product of smectite, which was produced from largely cleavage-associated chlorite, and so it contains relict "islands" of talc; in others, it is more pervasive. Some of the talc relicts contain voids after tremolite which have been partly replaced with goethite. Unaltered chromite is still preserved.

Goethite staining is quite pervasive in some rocks and is restricted to specific parts of others. Some fractures are lined with pyrolusite and barian cryptomelane. Cryptomelane is, in places, found developed in the clay fabric. Although many saprolitic fabrics remain, pedolithic fabrics are also common.

Ultramafic band UM4: Specimens RE 15-18, 19-20, 44-46, 52-54, 84-86, 92-93.
This ultramafic band is more schistose than the UM2 band. Around R.L. 410-420 (70-80 m depth), the rocks are almost completely fresh. They consist of schistose mats of talc and quartz (Figure 8G) with varying amounts of tremolite, which occur as islands, generally cut by a chlorite-filled, crenulated fracture cleavage. The quartz content is variable. Tremolite varies from decussate in the undeformed islands to needle-like near the cleavage. Accessory minerals are wedge-shaped sphene, magnetite and ilmenite. Minor Fe-staining is restricted to the fracture cleavage and minor cryptomelane coats the interiors of small voids. Smectite, which occurs as small patches, is rare.

At and above R.L. 480 (10 m depth), kaolinite, and mixtures of smectite and kaolinite, make up most of the rock; in places, this is partly to pervasively Fe-stained. The saprolite is pockmarked with vesicles which form chains linked by solution channels. Some of the kaolinite has recrystallised to stumpy stacks and books of coarser-grained kaolinite (Figures 9C and D). Some of these rocks, typically those that occur above the upper boundary of the saprolith, where the original rock fabric has been destroyed (pedolith), are polymictic breccias, containing a variety of angular, partly Fe-stained saprolite fragments (Figures 9E and F) consisting of matted kaolinite and kaolinite mixtures. One such specimen contained palygorskite, set in a matrix of smaller, angular aggregates of kaolinite.

Ultramafic band UM6: Specimens RE 49-51, 87-89, 108-109.
These rocks, which were only exposed from R.L. 440 (50 m depth) and above, are both very schistose and rich in tremolite (Figure 8B). They consist of lenses and islands of quartz, albite and decussate tremolite cut by a very strong chloritic cleavage. At R.L. 480 (10 m depth), the talc still survives in part but most of the chlorite has altered to smectite and kaolinite. Iron staining is in part pervasive (Figure 9G), leading to mottling of the rock.

5.3 Mica Schists

Specimens RE 12, 32, 42, 66-67, 90.
These are strongly schistose rocks, composed of flakes of fine-grained muscovite and, in some, talc, and fine-grained granular quartz (Figure 10A). Variations in the proportions of phyllosilicate to quartz across the foliation suggests that this may represent a bedding.

The foliation is also followed by lenses of coarse-grained granular to sutured quartz and by small lensoid clots of chlorite or chlorite and muscovite. Weathering of the micas to kaolinite begins around R.L. 460 (30 m depth) and becomes quite intense, though incomplete, at R.L. 480 (10 m depth). Titanium minerals have altered to patches of creamy anatase. Goethite has locally stained highly strained and fractured parts that are phyllosilicate rich and has pervasively penetrated grain boundaries, where the rock is quartz rich. In places, hematite, possibly after pyrite, occurs instead of goethite.

5.4 Black Shales

Specimens RE 110-113.
These rocks consist of fine-grained quartz, muscovite and graphite, with some talc. Smectite and chlorite are present in the two deepest samples (below R.L. 450; 40 m depth) but are absent in the

upper two, which, instead, contain significant kaolinite. Minor goethite is present above R.L. 470 (20 m depth). The muscovite, quartz and talc contents appear to be unaffected by weathering. Graphite is segregated into clots in the two more weathered specimens but this appears to be a local fabric variation, unrelated to weathering. The petrography and composition of the graphite, which is responsible for the dark colour of the rock but which was not detectable by bulk XRD, indicates that these rocks were bedded carbonaceous shales with a significant organic component. They show variation in their graphite content in separate beds (Figure 10B). Goethite has variably stained the graphitic patches and penetrated intergranular boundaries, particularly along quartz veins.

The graphitic material was examined by M. Smyth (pers. comm., 1990). At R.L. 430 (60 m depth), the graphite consists of flakes 1 μm wide and up to 10 μm long, as well as round fragments 1 μm and less in diameter. These make up 5% of the rock in some layers and less in others. At R.L. 450 (40 m depth), the graphite is similar in some layers but occurs elsewhere as stringers and aggregates, commonly 5 μm wide and 20 μm long, with rarer, larger clusters. Where it is present in low concentrations, the graphite rims quartz grains; where, very rarely, it is present in high concentrations it forms bands up to 20 μm wide. At R.L. 470 (20 m depth), the graphite is similar to that at R.L. 430 (60 m depth) except that flakes are less common and fragments more so. Flakes are generally about 5 μm long but many areas of the rock contain virtually no graphite. At R.L. 481 (8 m depth), the proportion of graphite in the rock appears to be less than 1% and is very fine-grained (0.5-1.0 μm), though there are rare flakes (about 5 μm long).

The degree of metamorphism of this carbonaceous material, now largely graphite but presumably originally a kerogen, precludes determination of its origin (bacterial or algal). There appears to have been some migration of graphite, or carbon compounds, into an open-spaced crenulation cleavage and similar graphite has been found in the early talcose schistosity of the ultramafic rocks.

5.5 Granitoid Porphyry

Specimens RE 6-7, 9, 11, 25, 36, 38-39, 70, 91.
Where fresh, these felsic rocks consist of varying proportions of xenomorphic plagioclase, surrounded by granoblastic polygonal quartz. Late, generally xenomorphic microcline granules occur among the quartz or in healed fractures in the plagioclase. An anastomosing cleavage is either marked by minor chlorite or by zones of intense crystal granulation. Some porphyries contain microxenoliths of the surrounding rocks and pyrite or cube-like hematite pseudomorphs after pyrite.

Around R.L. 440 (50 m depth), the plagioclase, including that in the perthite, have been altered to kaolinite (Figure 10C) and these rocks are saprolitic. In places, the potassium feldspar has been kaolinised. Further weathering leaves a non-schistose quartz-kaolinite rock with clusters of shard-like or granular quartz, some containing a remnant micrographic fabric (Figure 10D).

6.0 MINERALOGY

The qualitative mineralogy, as determined by X-ray diffraction analysis (Section 3), has been used in the preceding section as an essential guide to the petrography. Semi-quantitative aspects of this work are discussed here and conclusions reached as to the stability of particular minerals in the weathered profile, their use in rock type identification and some mineral reactions are proposed to explain the mineralogical and fabric changes.

The abundances of each mineral have been plotted separately for each rock type against R.L. in Appendix 3. This information has been combined with the geology as a mineral distribution map of the south face of the Rand Pit in Appendix 6. The mineralogical information has been summarised in Figure 11.

6.1 Mineral Distributions

Quartz
Quartz is an important mineral in all rock types. It is an essential and primary component of the granitoid porphyries, the black shale and, probably, the mica schists. There is a very wide range of quartz content in the ultramafic rocks, suggesting that quartz has been introduced, probably during metamorphism (quartz in cleavages) and mineralisation (vein quartz). Where intense weathering has affected the mafic rocks near the very top of the profile, some appear to have become quartz depleted (Appendices 3 and 6).

Feldspar
Little feldspar survives much above R.L. 440 (50 m depth) in all lithologies, indicating early breakdown of plagioclase to kaolinite in the mafic rocks and later, similar degradation of K-feldspar in the porphyries, where this feldspar survives higher in the profile (Figure 11).

Muscovite
Mica is an important component of the black shales and particularly of the mica schists but the porphyries are mica poor. Mica is generally little affected by weathering but it degrades in part to kaolinite near the top of the profile (Figure 11).

Talc
Talc is a dominant component of the ultramafic rocks and it survives in an unweathered state almost to the surface. The presence of talc can therefore be a very useful indicator of the presence of ultramafic rocks in the near-surface environment. The talc content decreases very close to the surface and there is a complementary increase in the content of kaolinite (Figure 11).

Tremolite
Like talc, tremolite characterises the ultramafic rocks but it does not survive much above R.L. 440 (50 m depth) (Figure 11). Petrographic evidence indicates that tremolite weathers and dissolves, leaving a void which is infilled by Fe oxides (Figure 9A).

Chlorite
Chlorite is present in all the rocks and generally lies in a discrete fracture cleavage (Figure 8A). It is particularly abundant in the ultramafic rocks but its abundance decreases sharply above R.L. 475 (15 m depth), where it has been probably altered via smectite to kaolinite by intense weathering (Figures 6E and G). Although chlorite is not as abundant in the mafic rocks, the mica schists and the black shales, their chlorite contents also decrease sharply above R.L. 470 (20 m depth) (Figure 11).

Kaolinite
Kaolinite is an important weathering product in all the rocks and is abundant above R.L. 440 (50 m depth). It has been produced by the weathering of plagioclase (Figure 6C), K-feldspar (Figure 10D), chlorite (Figure 6E) and, to a limited extent, mica. In the ultramafic rocks, it becomes particularly abundant above R.L. 480 (10 m depth) where chlorite and talc degradation takes place (Figure 11). Kaolinisation is particularly evident in the mafic rocks.

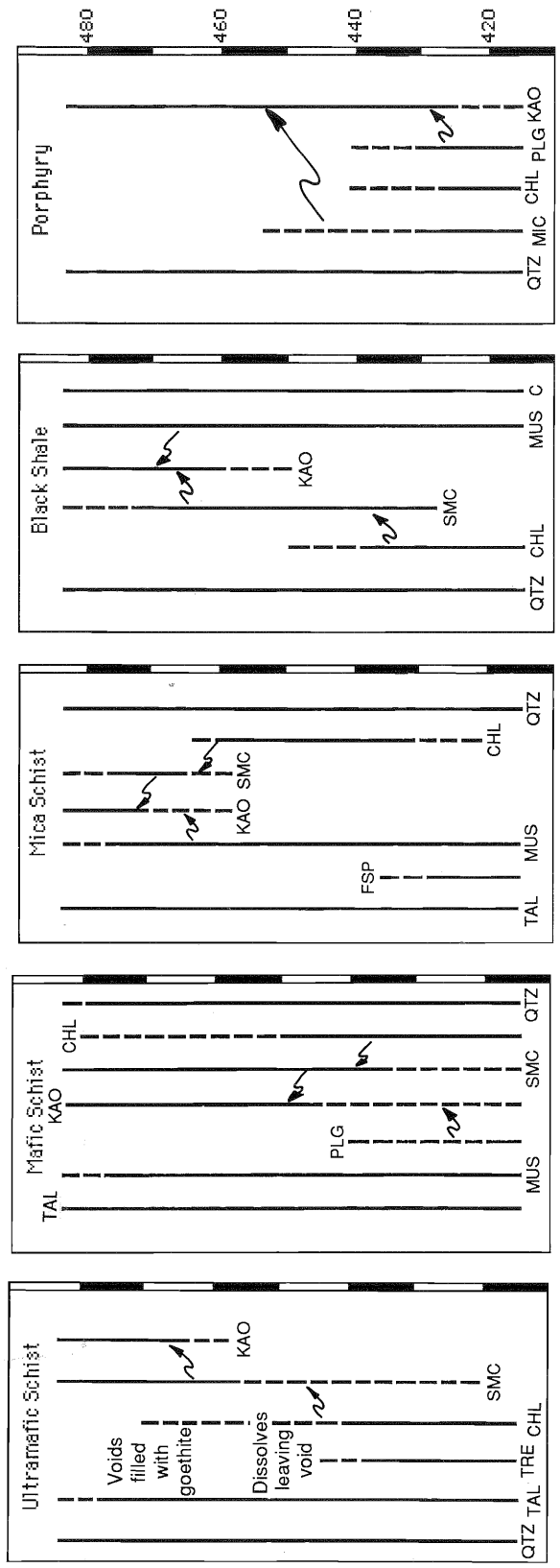

Figure 11. Distributions of minerals in each rock type with depth in regolith.

CHL = Chlorite; KAO = Kaolinite; MIC = microcline; MUS = muscovite; PLG = Plagioclase; QTZ = Quartz; SMC = Smectite; TAL = Talc; TRE= Tremolite

Smectites
These expanding clays are particularly abundant in the mafic and ultramafic rocks where they become progressively more important above R.L. 440 (50 m depth) (Figure 11). In the upper parts of the profile, smectite becomes altered to kaolinite. The smectite-rich zone is thicker in the west of the pit where smectite is more abundant near the surface (Appendix 6). It also occurs at depth, along the deeply-weathered edge of the S3 ore shoot, where alteration of chlorite has probably been promoted by the acid conditions generated by sulphide oxidation.

Goethite and Hematite
These Fe oxides are present throughout the profile at Rand because no completely unweathered rocks were reached. Breakdown of sulphides at the base of the profile has released these Fe oxides as a stain which penetrated the fretted edges of quartz veins and along discrete portions of the rock cleavage. Higher in the profile Fe oxides become more pervasive and are important mineral components in the mottled zone, particularly in weathered mafic and ultramafic rocks (Figure 9G). Hematite is more abundant than goethite at the base of the profile, the reverse being true near the surface.

Halite
Percolation of slightly saline waters into the base of the pit at Rand has deposited small quantities of halite which have become concentrated by evaporation. Halite is not regarded as an exclusive product of weathering, because much of the sodium chloride of the groundwaters in the Yilgarn Block was probably derived from a salt aerosol from the ocean.

6.2 Rock Type Identification

Ultramafic rocks may be identified by the presence of talc, the mica schists by the presence of quartz and muscovite, all of which are important primary minerals and survive to the surface or very near it. The deeply-weathered mafic rocks contain lesser quantities of talc but large proportions of kaolinite, smectite, quartz and mica. The black shales are characterised by quartz, kaolinite and mica. Carbon tends to oxidise near the surface, probably by bacterial action, and the black shales become progressively bleached. The porphyries are altered to quartz and kaolinite. Thus it requires a semi-quantitative estimation of several minerals to identify the underlying rock from its deeply-weathered saprolite.

Identification of rock types from chips and pulps of saprolite, collected from the surface or from the near-surface by RAB drilling, is notoriously difficult. Only a few minerals survive to the surface and the clay mineral weathering products of the others are very fine-grained and difficult to identify. Although talc survives even intense weathering, it is easily confused with kaolinite (both are white and have a soapy feel). X-ray analysis is too slow and costly and does not give the quick, definitive answers required for drill-spoil logging. The most useful field instrument will probably be some form of hand-held radiometer. By measuring the characteristic absorptions in the infra-red spectrum, talc, chlorite, kaolinite, muscovite, tremolite and smectite may be identified and estimated on a semi-quantitative basis. The underlying rock type may then be interpreted from this information.

6.3 Weathering Reactions

Recent research into mineral weathering has been greatly assisted by advances in electron microscopy and some very detailed studies of contiguous weathered mineral phases are now possible. Rainwater contains reactive H^+ ions which find access to the rock along open cleavages, intergranular boundaries and the margins of quartz veins. Weathering solutions penetrate minerals along twin boundaries and

lattice dislocations, where they etch out tube-like channels from which the weathering process spreads. Most weathering reactions remove components from the rock, so causing a volume loss, improving access for solutions and hence rapidly accelerating the weathering process. Weathering reactions are largely those of hydration and oxidation. Typical mineral reactions that would be expected at Rand are given below.

Feldspar
Sodic plagioclase breaks down to smectite with a volume loss of 100:87.

$$\underset{\text{plagioclase}}{4Ca_{0.5}Na_{1.5}(Si_{5.5}Al_{2.5})O_{16}} + 8H^+ + 16H_2O \rightarrow \underset{\text{montmorillonite}}{4Ca_{0.25}Al_2[Si_{3.5}Al_{0.5}]O_{10}(OH)_2} + 6Na^+ + Ca^{2+} + 8H_4SiO_4$$

Clearly smectites (which include montmorillonite) have very variable and complex formulae so their representation can only be schematic. Montmorillonite then breaks down further, with a volume loss of 100:79.

$$\underset{\text{montmorillonite}}{4Ca_{0.25}Al_2[Si_{3.5}Al_{0.5}]O_{10}(OH)_2} + 2H^+ + 13H_2O \rightarrow \underset{\text{kaolinite}}{5Al_2Si_2O_5(OH)_4} + 4H_4SiO_4 + Ca(OH)_2$$

The overall volume loss is 100:69. Further hydration of kaolinite to halloysite also occurs but the hydration leads to a slight volume increase of 100:127.

$$\underset{\text{kaolinite}}{Al_2Si_2O_5(OH)_4} + 2H_2O \rightarrow \underset{\text{halloysite}}{Al_2Si_2O_5(OH)_4.(2H_2O)}$$

Thus plagioclase hydrates to kaolinite and even to halloysite via intermediate montmorillonite. If the feldspar is potassic the intermediate stage is illite (which may also be expressed as a smectite with interlayered K). Plagioclase is weathered more readily than microcline. Details of the microscopic aspects of these mechanisms are given by Eggleton and Busek (1980), Robertson (1990b) and Robertson and Eggleton (1991).

Chlorite
Weathering of chlorite to smectite requires a source of soluble silica (readily available from other weathering reactions) and results in leaching of soluble alkali and alkaline earth elements, in particular Mg, and precipitates Fe oxyhydroxides which stain the phyllosilicates. This reaction results in a volume loss of about 100:87 and requires a source of H^+ (acid pH).

Smectite occurs to considerable depth in the envelope of the S3 ore shoot, probably due to the weathering of chlorite in the acid conditions generated by weathering of sulphides.

$$\underset{\text{chlorite}}{(Mg_3\ Fe^{2+}{}_2\ Al)(Si_3\ Al)O_{10}(OH)_8} + 0.5O_2 + 0.5H_4SiO_4 + 4.6H^+ \rightarrow$$
$$\underset{\text{oxidising, acid conditions}}{}$$

$$\underset{\text{smectite}}{Mg_{0.4}(Al_{1.5}Mg_{0.3}Fe^{3+}{}_{0.2})(Si_{3.5}Al_{0.5})O_{10}(OH)_2} + 2.3Mg^{2+} + \underset{\text{iron oxyhydroxide}}{1.8Fe(OH)_3} + 3.6H_2O$$

The stability of smectites produced by weathering of feldspars and chlorites is dependant on the concentration of Si in the groundwater. At high Si contents, smectite and amorphous silica are stable, at intermediate Si contents, kaolinite is stable and at very low Si contents (extreme leaching), kaolinite loses Si and converts to gibbsite.

Muscovite and Kaolinite

Electron microscopic studies indicate that, on weathering, first the mica loses some of its K and becomes hydrated (illite) as an intermediate stage before kaolinisation begins (Robertson and Eggleton, 1991). The illite then loses a Si tetrahedral layer from one side and a 10Å layer converts to a 7Å layer. The implications of this are that, instead of two molecules of muscovite converting directly to three molecules of kaolinite, two molecules of muscovite convert first to two of kaolinite and the third kaolinite molecule is precipitated elsewhere. The result is a localised volume decrease of 100:71 but, taking into account the later kaolinite precipitation, there is an overall slight increase in volume in the saprolite of 100:104 as a result of this reaction. Biotite, which is less stable than muscovite, alters to a mixture of kaolinite and goethite, probably via intermediate vermiculite or smectite. Thus first muscovite is weathered and some Al and Si are removed:-

$$\underset{\text{Muscovite}}{2KAl_3Si_3O_{10}(OH)_2} + 8H^+ + 2H_2O \rightarrow \underset{\text{kaolinite}}{2Al_2Si_2O_5(OH)_4} + 2K^+ + 2Al^{3+} + 2H_4SiO_4$$

Then, elsewhere, kaolinite precipitation occurs:-

$$2Al^{3+} + 2H_4SiO_4 \rightarrow \underset{\text{kaolinite}}{Al_2Si_2O_5(OH)_4} + 2H_2O$$

Precipitation of kaolinite from solution is likely to occur where there is space available. This reaction is probably only significant very close to the surface, under conditions of the most severe weathering. Kaolinite may also be dissolved and reprecipitated (congruent dissolution), so providing a means to move kaolinite within the saprolite.

Talc

Talc appears to be a stable mineral that does not seem to be affected by weathering except in the very top few metres of the profile. There appears to be a complementary increase in kaolinite where all other minerals show a decrease.

$$\underset{\text{talc}}{Mg_6Si_8O_{20}(OH)_4} + 8Al^{3+} + 12H^+ \rightarrow \underset{\text{kaolinite}}{4Al_2Si_2O_5(OH)_4} + 6Mg^{2+}$$

The source of Al^{3+} could be provided from the localised decomposition of micas, which also takes place close to the surface, or from the downward migration of Al^{3+} from the overlying duricrust, which has since been stripped away.

Tremolite

Most amphiboles weather via smectite to kaolinite but, because tremolite does not contain appreciable Al, neither smectite nor kaolinite can form. Hence, tremolite probably dissolves directly and the volume loss is total. The result is a void which is readily filled by migrating Fe oxides.

$$\underset{\text{tremolite}}{Ca_2Mg_5Si_8O_{22}(OH)_2} + 14H^+ + 8H_2O \rightarrow 2Ca^{2+} + 5Mg^{2+} + 8H_4SiO_4$$

Sphene

The accessory minerals in the saprolite have also been altered by hydration and oxidation. Sphene is altered to anatase, releasing Ca and Si to the groundwater with a volume loss of 100:34.

$$\underset{\text{sphene}}{CaTiSiO_4(OH)_2} + 2H^+ \rightarrow \underset{\text{anatase}}{TiO_2} + H_4SiO_4 + Ca^{2+}$$

Ilmenite

The alteration of ilmenite appears to take place via pseudo-rutile (a variety of TiO_2), to a mixture of anatase and goethite. This reaction produces a volume increase of 100:131 but, as ilmenite is an accessory mineral, this would be more than compensated for by dominant deflationary reactions.

$$\underset{\text{ilmenite}}{4FeTiO_3} + 2H_2O + O_2 \text{ --> } \underset{\text{anatase}}{4TiO_2} + \underset{\text{goethite}}{4FeO.OH}$$

This is a mixture of hydration and oxidation.

Magnetite

This is a simple oxidation to hematite which results in a slight gain in volume of 100:102.

$$\underset{\text{Magnetite}}{4Fe_3O_4} + O_2 \text{ --> } \underset{\text{hematite or goethite}}{6Fe_2O_3}$$

Pyrite

This oxidation takes place near the base of weathering where the sulphuric acid produced is readily buffered by carbonates and other minerals.

$$\underset{\text{Pyrite}}{4FeS_2} + 15O_2 + 8H_2O \text{ --> } \underset{\text{hematite}}{2Fe_2O_3} + 16H^+ + 8SO_4^{2-}$$

The H_2SO_4 produced is very reactive and promotes further very intense alteration in the immediate vicinity of oxidising sulphides. Generally the reaction occurs in two stages: firstly soluble Fe^{2+} is released and secondly, higher in the profile where oxygen is more abundant, Fe^{2+} is then oxidised to insoluble Fe^{3+} and Fe oxyhydroxides are precipitated. The overall volume loss is 100:63.

These mineral reactions serve to illustrate the type of weathering processes that are postulated to have taken place at Rand. In general the initial reactions remove alkalis and alkaline earth elements and the later, more intense, weathering reactions remove silica. The groundwater becomes enriched in Na, K and Ca salts and dissolved Si which are flushed from the system. These weathering reactions leave a saprolite of lower volume than the fresh rock. If the overall fabric of the rock is preserved then this volume loss must be reflected in an enhanced porosity. This is observed to be the case, both on the micron and millimetre scales, and is reflected in decreased bulk densities. Vesicles and solution channels abound in the upper parts of the saprolite. Kaolinite has been dissolved and deposited in purely secondary fabrics (illuviation) as blastic patches and accordion structures. Smectites occur in the upper third of the profile but not at the very top where more severe leaching has occurred, altering them to kaolinite.

7.0 GEOCHEMISTRY

Histograms for the ignition losses, specific gravity and each element have been plotted (Appendix 4). Although a few distributions approach normality (Si, LOI, Ir), many show positively skewed distributions that are nearly lognormal. Many variables, especially the major elements and S.G., show a weak bimodality or polymodality (Al, Fe, Mg, Ti, S.G., Br, Co, Cr, Cu, Ga, Li, Mo, Ni, Sc, Se, U, V, Yb and Zr). This deviation from unimodality is thought to be due to three factors; different rock types, mineralisation and differing degrees of weathering.

7.1 Dispersion

Geochemical maps of the south face of Rand Pit have been included (Appendix 5) for 53 elements as well as for specific gravity and ignition loss. Where elements have been analysed by two or more methods, the method regarded as being the most reliable has been used. For seven elements (Bi, Ge, In, Mo, Se, Sn and U) an appreciable proportion of the data are below the detection limit, so interpretation should be considered with care. The Be and Ir data, though reported for completeness in Appendix 1, were not plotted. In addition, plots have been constructed separately for each rock type of element abundances against R.L. to demonstrate both the variance within each rock type and the effects of weathering (Appendix 2).

The maps in Appendix 5 show class intervals for individual samples as different symbols. These class intervals were determined somewhat subjectively by using both the frequency and spatial distributions of the data. Interpretations have been added as shaded areas to the maps. The interpretations are interpolations between adjacent sample points with extrapolation within lithological boundaries. Thus both fact and interpretation are shown together. These maps in Appendix 5 should be referred to in the ensuing discussion of the geochemistry.

7.2 Depth of Weathering

None of the rocks collected for this study, even from the base of the Rand Pit (to 75 m depth), may be regarded as completely fresh. Even the freshest samples show signs of Fe staining along cleavages and parts of quartz veins have been fretted out. The boundary between fresh rock and saprolite is the weathering front but the accurate location of this boundary can, in many instances, be severely limited by scale. At the top of the profile, weathering is intense and a zone of low bulk density (<2.0) forms a layer 10-20 m thick. In addition to this overall deeply weathered layer, a few narrow, nearly vertical zones of low specific gravity, 10 m wide, extend to 50 m. These narrow zones in part surround zones enriched in Au (>100 ppb) which previously may have been pyritic. The decay of pyrite and the resultant acid conditions would promote localised deep weathering.

7.3 Element Groups and Geochemical Zonation

The geochemical behaviour of most elements varies with depth. There appears to be a natural geochemical subdivision of the profile into deep and shallow zones. The boundary between the two varies but generally lies at about 10-15 m below the surface and roughly corresponds to the zone of low bulk densities (<2.0). In the deep part of the profile, the distributions of most elements are ore- or lithology-related. Elements in the shallow zone have been affected by very intense weathering (which has considerably modified some rock fabrics) with some elements having been enriched, some depleted and a few having remained relatively stable. A few elements (e.g. Al and Fe) have been enriched and depleted in different places. A small number of those elements that have been shown to be ore related at depth have retained their usefulness as pathfinder elements in the shallow part of the profile.

7.4 Deep Profile: Ore-related Elements

The sampling pattern employed at Rand was designed to investigate weathering processes rather than to carry out a dispersion study. The sampling was carried out after the pit had been completed, so any mineralisation extending into the pit face would be expected to be sub-economic.

The extent of the primary dispersion of Au, and other, ore-related elements in the wallrocks could not be determined confidently without a detailed study of the fresh rocks below the Rand Pit, which is beyond the scope of this project. Nevertheless, it was considered necessary to determine, as far as was possible, which elements were ore related so that they could be excluded from any rock-identifying statistical processes.

Gold, which defines the mineralisation, is concentrated in and around two sub-economic ore shoots on the south face of the Rand Pit that roughly conform to the S1 and S3 mica schist zones (see Appendix 5). The Au concentration was plotted against its approximate horizontal distance from the nearest mica schist zone. Samples from above R.L. 480 (10 m depth), which are likely to have suffered enrichment or depletion in the upper part of the laterite profile, were excluded. In a vein system, the maximum Au concentrations would be expected to lie close to the ore shoots, where the concentration of mineralised veinlets is greatest. The concentration of veinlets, and with it Au, would decrease exponentially with distance from the ore shoot. Some samples, collected close to the vein system but, by chance, not including any vein material, would have locally low values. Thus a considerable range in Au may be expected close to the vein system but this range, or envelope, would decrease towards background further from the vein system. The Au plot (Figure 12) shows just such an exponential distribution.

Similar plots have been constructed for other elements to test the hypothesis that they are ore related. A selection of these plots is shown in Figure 12. Similar exponential distributions can be seen for As, Cu, Pb, Sb, Sn, W and Zn which can thus be considered to be ore related elements. Other elements, which are probably also ore related (Ag, Mo, Se, Te and Tl), did not show such clear distributions, mainly because most of their abundances are near or below their respective detection limits.

Only Sn, W, Ag, Mo and Se show weak, though significant, correlation with Au; the more overtly ore-associated elements do not. This is to be expected where elements may be concentrated sporadically in a vein system and, though spatially associated, may not be co-located. Other elements, that correlate well with Au, and reflect the association of Au with the mica schists, include Bi, U, the REE (Ce, Eu, La, Lu, Sm, Y, Yb), K, Ba and Rb. Bismuth may be ore related but its concentrations are too close to the detection limit to be certain.

There is a concentration of Au near the base of the profile, reflecting proximity to the very rich patch of Au mined in the floor of the pit (Figures 3B and 4A). Here, Ag has been shown to be a significant component of this primary Au (Hallberg *et al.*, 1976; Robertson, 1987; Freyssinet and Butt, 1988). Background levels for Au, away from the ore shoots, approach average crustal abundances. Tungsten, Te and Tl are enriched both in the ore shoots and in the porphyry lenses. Together with Au, As and Sb, these are among the better halo elements but, at Rand, W, Te and Tl have very low background abundances so that anomalies in these elements are only present close to the ore shoots. These elements are poorly correlated. The distributions of both Cu and Sn are erratic. Zinc probably occurs as Zn sulphide inclusions in pyrite and Cu probably is from the ore-associated chalcopyrite and bornite reported by Henderson and Hill (1988).

7.5 Deep Profile: Lithology-related Elements

Some elements, such as Ga, Hf, Zr, Sc, Ta, Nb, Cd, Ti, U, Y and Yb, are clearly related to lithology. A selection of these (Ga, Hf and Zr) has been plotted against distance from the mica schists (Figure 12) to compare their distributions with those of the ore-related elements. They show linear (in contrast to exponential) decrease away from the mica schists. This relationship is particularly true if mafic schist samples RE57 and RE58, which are very rich in Ga, Zr, Hf and Nb, are ignored (Figure 12). Other elements, such as B, Ba, Lu and V, are of uncertain affinity. Vanadium, however, shows an

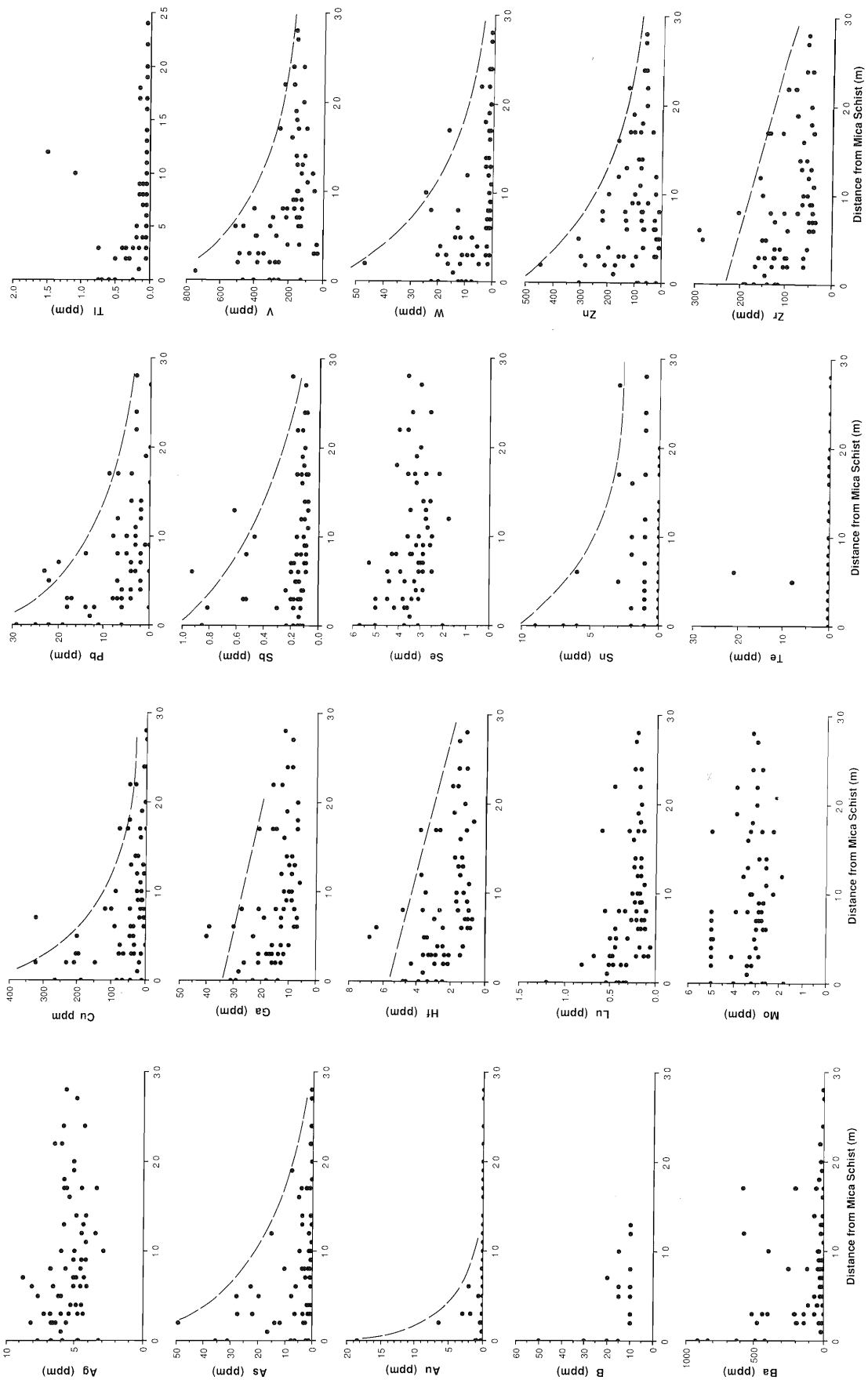

Figure 12. Distributions of ore-related and lithology-related elements with distance from the nearest mica schist band.

exponential distribution that most probably reflects the presence of white mica, which is particularly abundant in the mica schist, is less so in the adjacent mafic rocks and is very scarce in the more distant ultramafic rocks.

The mica schists, the porphyry pods and the mafic units, where they are adjacent to the ore shoots, are locally Si rich (>70% SiO_2). Although quartz veins are associated with some of the primary Au mineralisation at Rand, no obvious silicification halo was seen around known areas of quartz veining. However, quartz has clearly been introduced into these rocks during metamorphism and mineralisation as sinuous quartz lenses that follow the cleavage (see Section 5).

Aluminium and Ga differentiate the mafic and mica schist units and the porphyry pods from the ultramafic rocks. The Ga/Al ratio is relatively constant for the mafic and ultramafic rocks and the granitoid porphyries but Ga is enriched in the sedimentary rocks (black shale and mica schist) relative to Al (Figure 14B). Gallium and Al correlate with Hf, Nb, Sb, Sc, Se, Te, Th, Ti, U, V, Yb and Zr (Appendix 9).

Although the majority of the ultramafic rocks are Hf poor (<2 ppm), this rock type has the widest range in Hf concentration (0.79-11.7 ppm). The higher average Hf values (>3 ppm) are concentrated in the mafic and mica schists. Low concentrations of Fe (<6.0%) mark the mica schist, black shales and porphyry units. Some of the highest Fe values (9-20% Fe_2O_3)occur at depth in the M3 zone and may have been related to the distribution of hydrothermally-associated pyrite.

Boron and Ba are concentrated in the mica schists and in the porphyry; they are thus probably useful lithological indicators for these rock types at depth. Strontium and Ca are commonly associated in minerals; however, though abundant Sr characterises the porphyry pods and the mafic rocks, Ca does not show this relationship.

Bromine seems to be concentrated in the mica schist, in some of the mafic units and in the porphyry bodies. It also occurs in lower concentrations (<1 ppm) in the ultramafic rocks. However the groundwater at Rand is slightly saline. It is suspected that much of the Br has been deposited from seeping groundwaters that have penetrated the deeply-weathered aureole around the ore shoots, hence the association of Br with the mica schist and mafic rocks.

The mafic and mica schists are comparatively rich in Nb, Th and V (>5, >5, >250 ppm respectively); the porphyry pods also carry Th but are low in V (<100 ppm). Ta is enriched in the mafic rocks but the data are close to the INAA detection limit of 1 ppm.

7.6 Shallow Profile: Pathfinder Elements

There is a zone of lateral Au dispersion with Au abundances of >10 ppb that in many places reaches >30 ppb in the top 5-15 m of the profile. Strongly anomalous Au only extends to the surface over the S3 ore shoot, where one sample contained over 120 ppb. Two samples over the S1 ore shoot contained over 300 ppb at 5 m depth but they are all overlain by samples assaying <60 ppb. This pattern suggests a zone of weak Au enrichment (>100 ppb) at about 5-10 m, overlain by a zone of Au depletion (<<50 ppm).

Arsenic near the surface is mostly at background abundances (1-5 ppm), suggesting extensive leaching, even though there is a weakly anomalous sample (>10 ppm) above each oreshoot. At a depth of 20 m, at the top of the saprolite, As appears to have been slightly enriched (10-30 ppm), though, again, most of these enrichments (30-50 ppm) lie proximal to the ore shoots.

Although the distribution of As in the shallow part of the profile is erratic, the highest As concentrations (18-57 ppm) are found over the mineralised zones; thus As is probably one of the best pathfinders, particularly below about 10 m depth, but its abundance is very low.

Copper is anomalous in the upper 10-15 m of the profile. There is a lack of continuity between Cu anomalies in the upper part of the S3 zone and those at the surface, which suggests either that the Cu is not related to the primary Au or that the Cu has been depleted between depths of 15 and 30 m; the latter explanation is preferred. The anomaly around the S1 ore shoot reaches the surface, where it joins a broad horizon of enrichment (100-400 ppm).

Antimony shows a locally erratic enrichment (0.4-0.8 ppm) in the upper 10-20 m of the profile and is particularly abundant at a shallow depth around the S1 ore shoot. However, the data from this study do not indicate that Sb would be of much value as a near-surface pathfinder.

Although much of the Sn data lie close to or below the XRF detection limit, Sn still seems to be weakly enriched (2-8 ppm) locally in the upper 10 to 20 m of the profile. Even though Sn seems to be related to the primary Au mineralisation, the erratic nature of its anomalies in the upper part of the profile suggests that Sn would not be a good pathfinder. Perhaps Sn analysis by a more sensitive analytical method (ICP/MS) would provide a clearer picture.

Although the subcrops of the ore shoots are marked by high W abundances (>10 ppm), the top 5 m of most of the profile also shows elevated W concentrations (3 ppm) where the underlying background is 1-2 ppm. This effect is particularly apparent in the ultramafic schists. This overall pattern would suggest some limited dispersion of W in the upper horizons of the profile (see also Robertson, 1990a). Although the detection limit (5 ppm) may be too high to confidently exploit the potential of W as a pathfinder element, experience has shown that this INAA detection limit is probably slightly high. Thus, even at low concentration levels, W may still have some potential as a pathfinder element.

Silver was determined by three methods. Optical emission spectrometry, which has the lowest detection limit (0.5 ppm), is thought to be the most reliable. The data, which are strongly positively skewed, indicate that Ag has been largely removed from the top 10 m of the profile. Silver is readily separated from Au during weathering in a chloride-rich environment (Liversidge, 1893; Mann, 1984; Gray, 1989) and the presence of halite in the rocks at the base of the profile shows that the groundwaters contain chloride. Silver does not seem to be a good pathfinder element in the shallow part of the profile, though its usefulness improves below depths of about 20-30 m.

Although all the Mo data lie at or below the 5 ppm detection limit, this detection limit is probably higher than necessary. Some apparent weak Mo concentrations occur above the S1 and S3 ore shoots at 20 m depth, where Mo appears to be slightly enriched (3-4 ppm) over a broad zone between the two ore shoots. The top 5 m appears to be slightly depleted (<3 ppm) in Mo. Thus this element may possibly be a useful pathfinder at shallow to moderate depth, particularly if a more sensitive analytical method is used. As the Mo data stand they must be interpreted with some caution.

Lead occurs in low concentrations (20-40 ppm) around the ore shoots and is generally depleted (<8 ppm) in the top 10 m of the profile; it is not a useful near-surface pathfinder.

Selenium, a strongly chalcophile element with a detection limit of 2 ppm, appears to be weakly enriched at concentrations of >3.5 ppm in a horizon in the upper 15 m of the profile between the S1 and the S3 ore shoots. On oxidation of sulphides, Se also would be readily oxidised and the resultant Se ions are almost completely adsorbed by Fe oxyhydroxides (Leutwein, 1978a), suggesting that Se may be a useful pathfinder, particularly if a more sensitive analytical method is used.

Tellurium is strongly enriched (0.04-2.0 ppm; detection limit 0.005 ppm) near much of the present surface and this enrichment extends to depths of about 20 m. In spite of this, the highest Te abundances (8-21 ppm) tend to overlie the S3 ore shoot, indicating a potential for Te as a surface or near-surface pathfinder element.

High Tl values (0.1-0.5 ppm; detection limit 0.05 ppm) overlie both ore shoots and are also present as a dispersion to the west of the S3 ore shoot in the top 5 m of the profile. A discontinuity in the Tl anomaly at depths of 20-30 m in the S3 zone seems to be related to leaching. Thallium tends to disperse during oxidation of sulphide ores but it is readily precipitated with Mn oxides and jarosite. Because it seems to delineate both ore and the porphyry pods, this element could be a useful pathfinder.

Zinc, which follows the ore shoots at depth, is depleted (<50 ppm) from the surface to a depth of 15 m but appears to be slightly enriched (>200 ppm) between 15-30 m depths. No Zn anomalies overlie the ore shoots near the surface so Zn has little use as a pathfinder in the upper part of the profile.

7.7 Shallow Profile: Stable Elements

A group of seven elements, Cr, Ti, K, Cs, Rb, Zr and Hf have distributions that are primarily related to specific lithologies and show only minor changes caused by weathering.

Chromium shows distinct concentration differences between the mafic (and mica schist), ultramafic, and porphyry units that generally extend from the base of the pit to the surface. The mobility of Cr on weathering depends upon its mineralogical form in the fresh rock. Chromites tend to survive weathering and the Cr in them concentrates as a residual element. On weathering, Cr in pyroxenes, amphiboles, micas and ilmenite is generally released as the soluble Cr^{2-} ion, which tends to be taken up by clays (Shiraki, 1978). In a few localities, at the top of the profile, Cr shows a reduced abundance for a given lithology, probably due to weathering of silicate-hosted Cr. This weatherable Cr has probably been redeposited as blue-green chromian clays, e.g. in the vicinity of Sample RE59. In general, Cr concentrations in surface and near-surface samples should be a good lithological indicator.

Titanium is present in ilmenite, sphene, rutile, biotite and amphibole. On weathering it converts to stable anatase or may be taken up by clays (Correns, 1978) and Fe oxides. At Rand Ti seems to be a useful element for separating some lithologies. This element has distinctly higher concentrations (>0.65%) in the mafic and in the mica schist units and much lower concentrations (<0.65%) in the ultramafic and porphyry units. Some parts of the upper profile (<20 m), particularly overlying the ultramafic rocks of UM4, show Ti enrichment, possibly due to residual concentration during weathering.

The alkalis, K, Cs, and Rb have similar distribution patterns. At Rand, they all show only relatively limited areas of high concentrations (>1.0%, >1 ppm, >20 ppm respectively) in the felsic rocks and the mica schists that are related to their concentrations in micas. At depth, their concentrations are related to their K-feldspar host minerals. Weathering of K-feldspar deeper in the profile and of mica further up would release these elements which are then readily taken up by smectites, in the order Cs > Rb > K (Heier, 1978). The porphyry pods above 30 m depth are all alkali depleted; otherwise there seems to have been only very local abundance changes in these elements near the surface. This pattern is to be expected where mica is dominant, as this mineral is not readily destroyed by weathering and tends to survive near to the surface.

The higher Zr concentrations (>120 ppm) in the mafic and mica schists persist through the entire profile. A significant, residual increase in the Zr content of the mafic and ultramafic rocks occurs in the top 10-15 m of the profile. The majority of the ultramafic rocks are Hf poor and higher Hf values (>3 ppm) are concentrated in the mafic and mica schists. Two very high Hf values (>10 ppm) occur near the top of the profile (<10 m). Because Hf commonly occurs with Zr in zircon, the Zr/Hf ratio was investigated. Despite some very high Hf concentrations (11 ppm) near the top of the profile, the Zr/Hf ratio remained relatively constant (Figure 14C), indicating that zircon has remained stable throughout the profile and that it may have been sporadically concentrated by residual processes near the surface (or that, when it is dissolved, both Zr and Hf behave similarly).

7.8 Shallow Profile: Enriched Elements

The upper part of the profile is generally enriched in the major elements Si and Al and sporadically enriched in Fe. The strongest Si enrichment is caused by an increased quartz content and overlies the mafic M1 unit, the ultramafic UM2 and possibly the UM6 unit. Some localities overlying the mafic M3 unit show localised Si depletion (<60% SiO_2). Both the mafic and the ultramafic units show relative enrichments in Al. Areas with >20% Al_2O_36
occur in the upper 10-20 m of the profile. Some of this Al enrichment may be due to deposition of kaolinite that was leached from the previously overlying (now stripped) duricrust and redeposited in the upper saprolite. These enrichments are the result of intense leaching of Na and the alkaline earth elements that followed the destruction of feldspars, chlorites and amphiboles and the formation of the clays during lateritic weathering. Iron is generally leached but, in places, it is locally enriched at the base of the sporadically-developed mottled zone.

The upper part of the profile also shows enrichments in B, Ba, Ga and, to a lesser extent, Nb, Sr, Ta, Th and V. Boron, Ba and V are dispersed in the upper 10-20 m of the profile where they were probably released during the progressive breakdown of micas to kaolinite. Secondary Ba probably occurs as barite, though a variety of carbonates, phosphates and manganese minerals containing Ba are also possible. Strontium is concentrated sporadically across the uppermost part of the profile but it seems to have been leached at depths between 10 and 25 m in the mafic M3 unit. This depletion in Sr (to <30 ppm) between 10 and 25 m is probably linked to feldspar breakdown which is thought to be a gradational process with plagioclase breakdown occurring deep in the profile and progressively greater K-feldspar degradation higher up. Strontium is less mobile than Ca and is very readily taken up by near-surface carbonates and also adsorbed by clays.

A residual enrichment in Ga (>25 ppm) near the top of the profile is thought to be related to the Al enrichment of intense weathering, particularly where the Ga enrichment overprints the inherently Ga-poor weathered ultramafic rocks of the UM2, UM4 and UM6 units to depths of about 15-30 m. This Ga enrichment is similar to and related to that of Al.

Both Nb and Th appear to be enriched (both >15 ppm) in the upper 10 to 20 m of the profile. For near-surface geochemical sampling, Nb and Th may have some value in defining lithologies that are favourable hosts for Au mineralisation, even though they are not ore-related themselves. In contrast, Ta is erratically distributed in the upper 10-20 m of the profile and thus shows no strong relationship to lithology.

7.9 Shallow Profile: Depleted Elements

Nineteen elements (Ag, Al, Ca, Cd, Ce, Co, Eu, Fe, Ge, La, Li, Lu, Mg, Mn, Na, Ni, Sm, Y and Zn) show depletions in the top, low-density part of the profile.

Silver contents of all samples in the top 10 m are below the emission spectrometry detection limit of 0.5 ppm; thus the Ag dispersion that occurs around the S3 ore shoot at depth is blind. Although Cd and Ge, as well as the rare earth elements Ce, Eu, La, Lu, Sm and Y are relatively abundant in the rocks surrounding the S1 and S3 ore shoots, all of these elements are strongly depleted in the top 10-20 m overlying these shoots. Like Zn, Cd has been strongly leached from the upper part of the profile, though possibly less so than Zn. The heaviest rare-earth element, Lu, shows the least depletion. Burkov and Podporina (1967) reported a significant decrease in the lighter lanthanides (including Y) in the kaolinite zone overlying granitic rocks. They ascribed this decrease to leaching and lanthanide mobility under acid conditions.

Cobalt and Ni are abundant in the ultramafic rocks except in the top 15 m of the profile, where Co is strongly depleted (to <50 ppm) and Ni slightly depleted (to <400 ppm). Although Fe was concentrated in the mafic units around the ore shoots, it is strongly depleted (to <6% Fe_2O_3) in the top 10-15 m of the profile, except for a few places where it has been concentrated (to >20% Fe_2O_3). The ultramafic rocks also show Fe depletion at the top of the profile, though to a lesser extent than for Co and Ni. Magnesium and Mn are both strongly depleted (to <5% MgO) in the upper part of the profile overlying the mafic and, to a lesser extent, the ultramafic rocks, though the range of Mn concentrations becomes very broad in both rock types near the surface, indicating both depletion and concentration.

Of all the elements studied, Ca and Na are probably the two most strongly depleted (to <0.2 and <0.06 oxide% respectively). Plagioclase feldspars (Na- and Ca-rich) have been weathered completely very deep in the profile. Approximately 50% of the Na and 80% of the Ca have been leached from the mafic and ultramafic rocks to depths of 40 m. Lithium is only slightly leached as it is not associated with feldspars but probably with more stable chlorite. At shallower depths, this chlorite is in turn destroyed.

8.0 ROCK TYPE IDENTIFICATION

The purpose of this study of the Rand Pit was to determine whether the five main lithologies (ultramafic, mafic, porphyry, mica schist, and black shale) could be identified on the basis of their overall chemistry, regardless of their state of hydrothermal alteration or weathering. During the course of the geochemical investigation, a number of elements emerged as potential rock-type identifiers. These were investigated at first singly, then in pairs, in threes and finally in n-dimensional space by discriminant analysis.

8.1 Univariate Analysis

The chief of these discriminant elements is Cr, which very clearly identifies the majority of the rocks of ultramafic composition. Less effective are Ni, Mg and Co, the effectiveness of which is obscured by weathering and resultant leaching at the top of the weathered profile. The ultramafic rocks are also poor in Ga and Al. This discrimination is illustrated in Figures 13C and D where the Cr frequency distribution of the ultramafic suite (Figure 13C) is compared with that of the other rock types (Figure 13D). There is considerable overlap in the 0-2000 ppm range. The other rock types are more difficult to separate. The most useful elements for the non-ultramafic rocks are those elements associated with the micas that resist weathering (K, Rb, Cs and Ba). This is illustrated in Figures 13A and B, which shows the distribution of Rb in the combined mafic and ultramafic suite (Figure 13A) compared with that of the combined mica schists and black shales (Figure 13B). Again there is significant overlap in the 30-80 ppm range.

Clearly, though univariate analysis may distinguish some of the ultramafic and metasedimentary rocks, the degree of uncertainty is high and the suite of rocks that this technique can distinguish is limited.

8.2 Bivariate Analysis

All the element pairs in the correlation matrix (Appendix 9) were plotted (not shown), using different colours to identify rock types. These confirmed the value of Cr and to a lesser extent those of Ni, Mg, Co and Ga in identifying the ultramafic rocks. Again the mica-associated elements Ba, K, Rb and Cs delineated the mica schists, the black shales and some porphyries. They also showed the expected high correlations between the alkalis, the rare-earth elements and coherent element pairs such as Al-Ga and Zr-Hf. Some of these relationships are shown in Figure 14.

The Ti/Zr relationship (Figure 14A; Hallberg, 1976) has been used to classify weathered igneous rocks but this ratio is not as high in the mafic-ultramafic suite as would be expected. The reason for this is not clear. The Al/Ga relationship (Figure 14B) is fairly constant for the mafic and ultramafic rocks and the porphyries but Ga is enriched relative to Al in the mica schists and black shales. This ratio could be used to distinguish igneous from metasedimentary material. Although the black shales fall into a tight group in the Rb/Si diagram (Figure 14D), the fields of the mica schists and the porphyries overlap considerably.

The Rb-Nb, Rb-Sc and Rb-Li plots (Figures 14E-G) distinguish the mafic-ultramafic suite from the other rock types moderately well and show some separation of the porphyries and the black shales; however there is still a large amount of overlap of these fields with that of the mica schists. Similar results may be obtained using other alkalis (K and Cs) instead of Rb.

Although a bivariate study improves discrimination of the rock types, the amount of overlap still remains unacceptable for a scheme of geochemical rock classification, so it is necessary to add more elements to improve the discrimination (multivariate analysis).

8.3 Trivariate Analysis

Some three-dimensional plots of three elements were constructed. These produced 'clouds' of data points. The plots were rotated so as to maximise the separation of the rock types in the plane normal to the viewing axis. Examples of these are provided in Figures 15A-D. These stereopairs should be viewed using a small lens stereoscope (as used for air photographs in the field).

Some quite acceptable discriminations of the fields occupied by the ultramafic, mafic, porphyry and combined mica schists and black shales are achieved on the Cr-Ti-Rb and the Cr-Rb-Ga plots and most of the porphyries form a tight group on the Cr-Ti-Zr plot. These trivariate plots thus provide both a visual impression of the improvements gained by adding an extra element and form an introduction to discriminant analysis, which is an extension of this three-dimensional study into n dimensions.

8.4 Discriminant Analysis

Discriminant analysis is a mathematical technique that is used to classify samples into groups by attempting to maximise the differences between these groups. Samples have been initially grouped according to known *(a priori)* geological classes. Geochemical data, determined for the samples, are then evaluated mathematically, to confirm or reject this original classification. Further details of the technique are given by Davis (1973).

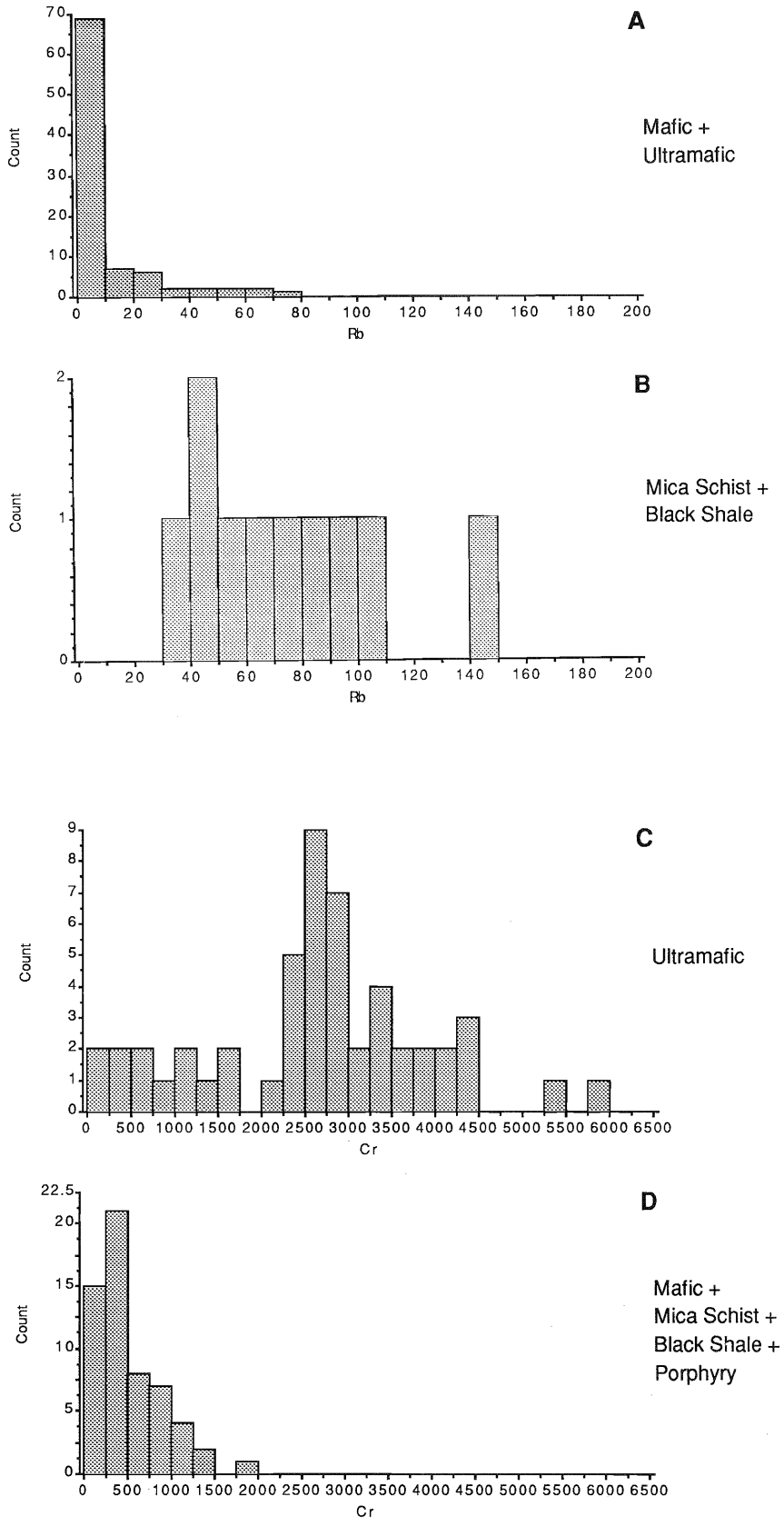

Figure 13. Frequency distributions for Rb in the mafic and ultramafic rocks (A) and the combined mica schists and black slates (B). Frequency distributions for Cr in the ultramafic rocks (C) and all other rocks (D).

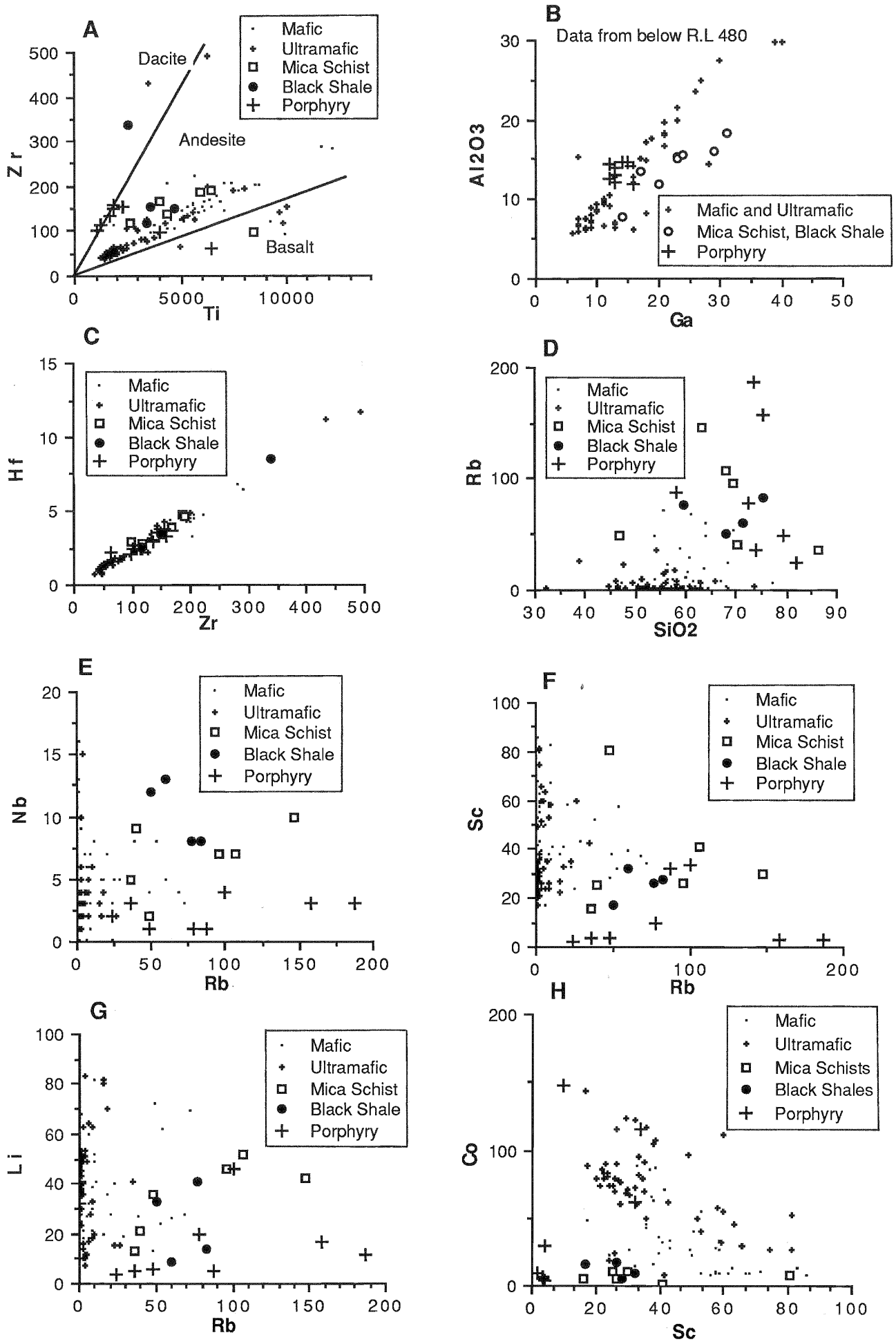
A
Mafic
Ultramafic
Mica Schist
Black Shale
Porphyry
Dacite
Andesite
Basalt
Zr
Ti
B
Data from below R.L 480
Mafic and Ultramafic
Mica Schist, Black Shale
Porphyry
Al2O3
Ga
C
Hf
Zr
D
Rb
SiO2
E
Nb
Rb
F
Sc
Rb
G
Li
Rb
H
Mafic
Ultramafic
Mica Schists
Black Shales
Porphyry
Co
Sc

Figure 14.

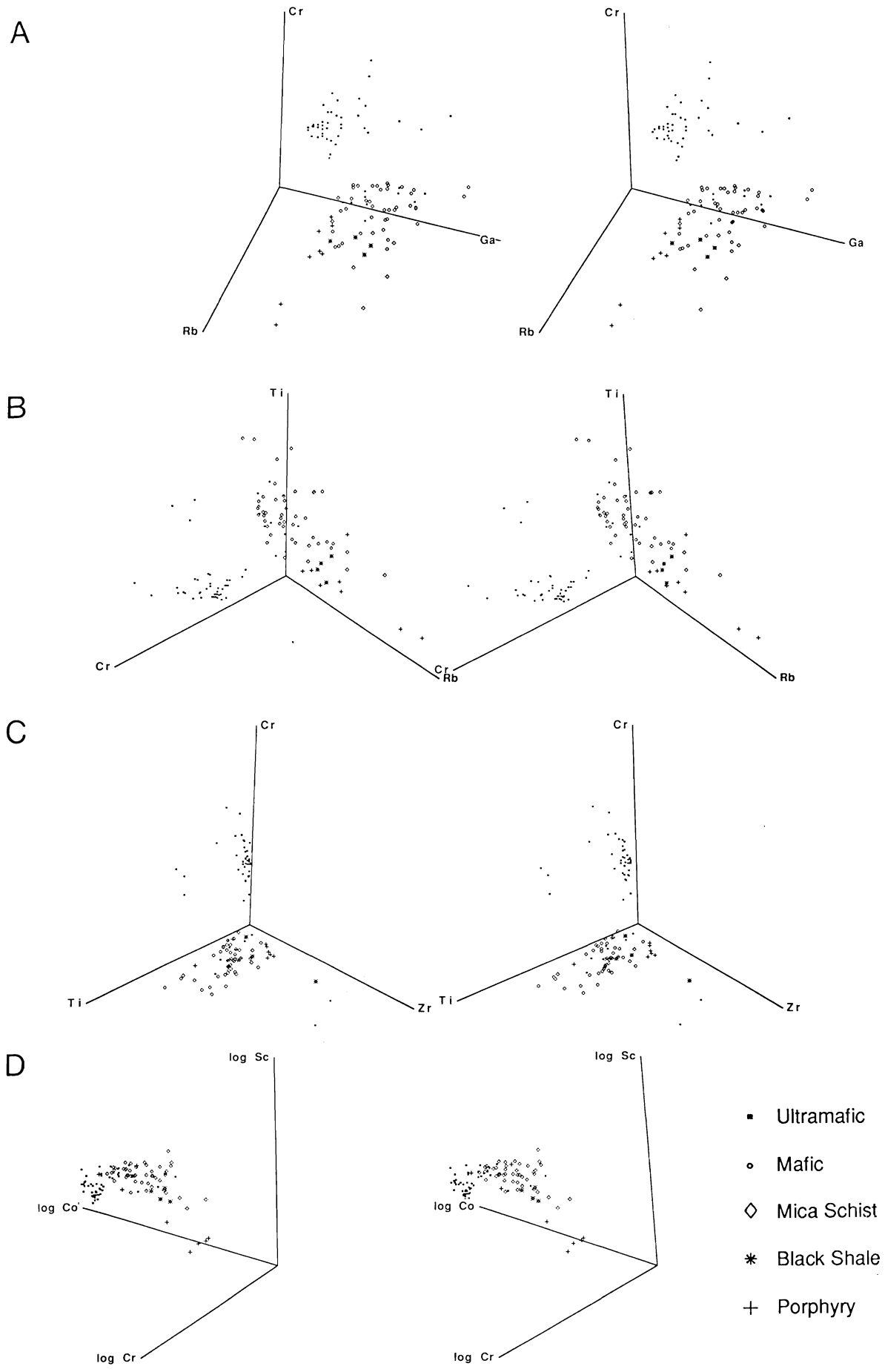

Figure 15. Three dimension plots of groups of three elements. View using a lens stereoscope.

More than one horizon or locality for most of the five lithologies, identified for this study, have been mapped and sampled. For this evaluation the assumption has been made that all samples identified, for example, as "ultramafic" have similar chemical characteristics and can be considered as a group. The results suggest that this assumption is largely correct.

Limitations

To be an effective technique, discriminant analysis imposes certain requirements on a data set. For geological data, some of these requirements are difficult to attain.

i) The number of samples in a data set (in this case a data subset consisting of one lithological unit) should exceed the number of elements by a factor of at least 3, with a value of 10 highly recommended (Le Maitre, 1982; Howarth, 1983). Factors greater than three are often not possible to obtain for geological data and were not achieved for these data subsets, particularly for samples of the mica schist and black shale units.

ii) The analyses for a given sample should not sum to a constant value (Miesch, 1969). This restriction can be a problem with whole-rock analyses but it is not important for the present study, which is based largely on trace element geochemistry.

iii) Discriminant analysis works best where no extreme values are present. Extreme values are common among geochemical data and these extreme values are not normally discarded. At least some of this effect may be overcome by transformation of the raw data, as described below.

iv) Discriminant analysis assumes normal data distribution, which is rarely encountered in natural geochemical data. As noted previously, the frequency distributions for the Rand Pit samples (Appendix 4) show that very few elements approximate a normal distribution. It has been commonly accepted that most geochemical data are lognormally distributed (Ahrens, 1954; Shaw, 1961). In detail this assumption is not always true (Howarth and Earle, 1979). The best approach to producing normal distributions for all variables is to use a power transform (Howarth and Earle, 1979).

Data and Method

A raw data set, a log-transformed data set, and a power-transformed data set were prepared. Each of these were investigated using the BMDP forward and backward stepwise discriminant analysis program P7M (Jennrich and Sampson, 1981), a version of which has been modified for use in the U.S. Geological Survey's STATPAC[1] program (VanTrump and Miesch, 1977). In this method one variable is entered or removed from the analysis at each step, according to an "F-to-enter" value set by the user[2].

---

[1] There are numerous other statistical packages, containing routines for Discriminant Analysis, such as SPSS, QGAS, IMSL, SAS, NAG and SYSTAT. These operate in a number of environments, ranging from IBM PC, VAX, Sun, HP , Macintosh and mainframe computers.

[2] The "F" value represents a test of the significance of the ability of a variable to distinguish between two groups.

The original data set was reduced to 35 elements (Si, Al, Fe, Mg, Ca, Na, K, Ti, B, Ba, Br, Ce, Co, Cr, Cs, Eu, Ga, Hf, La, Lu, Mn, Nb, Ni, Rb, Sc, Sm, Sr, Ta, Th, Tl, U, V, Y, Yb, and Zr). Elements removed included those thought to be related to mineralisation as well as several which were highly censored because their lower limits of determination were well above their background ranges.

Results

The models generated by the analysis for each of the three data sets are summarized in a plot showing the proportion of samples correctly classified at each step (Figure 16). This plot shows that, for essentially all steps, the raw or untransformed data set is the poorest for correctly classifying the data. This would be expected for a method that assumes normally-distributed data. Canonical variate scatter plots of the data sets, a spatial means of evaluating each data set, also produced the poorest results for the raw data (not shown). This evaluation confirmed that only data transformed to approach normality were valid for separating the five lithologies. Figure 16 shows that discriminant analysis of log-transformed data correctly classifies about 85-89% of the samples. Discriminant analysis of the power-transformed data correctly classifies as much as 93% of the samples.

Discriminant analyses of the log- and the power-transformed data sets indicate that the cumulative proportion of the total dispersion at each step level (a measure of the percent of variance explained at each step level) requires only four variables to explain 100% of the variance. Figure 16 indicates that correct classification of the samples reaches a maximum at about seven steps. From this preliminary evaluation, it is concluded that a 6-step model (with elements in order of entry: Cr, Sc, Co, K, Br, and Nb; "F-to-enter", 4.0) was best for the log-transformed data set and a 7-step model (with variables in order of entry: Cr, Nb, Co, Sc, Lu, Hf, and Ba; "F-to-enter", 4.5) was best for the power-transformed data set. For the former data set, 85% of the samples are correctly classified and for the latter 91%.

Tables 4 and 5 list the samples in their *a priori* lithological groups for the log- and power-transformed data sets, respectively. The tables also show which samples in each subset are misclassified by this mathematical treatment. In view of the highly altered nature of the samples collected for the study, the small data subsets for some of the lithologies and the complex interplay of metamorphism, hydrothermal alteration, mineralisation and weathering, a number of misclassified samples is to be expected. The number of samples correctly classified is, however, highly satisfactory.

Misclassification could be attributed to several causes, such as inaccurate analyses (probably not significant), petrographic misidentification (possible, due to the intensely weathered nature of many samples), and hybrid chemistry (e.g. outward movement of elements from the intrusive porphyry bodies and ore shoots into contact aureoles). This last cause is probably the most significant.

Canonical scatter plots for the log- and power-transformed data sets, respectively are shown in Figures 17A and B. These plots spatially represent the information given in Tables 4 and 5. The plots show the calculated locations for each sample, based on its chemistry, and for the mean values for each *a priori* sample group. The classifications in the sample classification tables are determined by comparing the location of a given sample relative to those of the different group means. If the sample is located anywhere between the mean for its group and the mid-point of the distance to any other group mean, then the sample is classified in the first group even though it may contain a component for one or more other groups. Put another way, classifications in the classification table are made assuming that a straight-line boundary exists equidistant between any two group means and orthogonal to a line drawn between these means.

Curved rather than straight boundaries between lithologically similar samples *(a priori)* may alternatively be drawn on the canonical plot for classification. These curved boundaries improve the classification of outlying samples when compared with the straight-line boundaries.

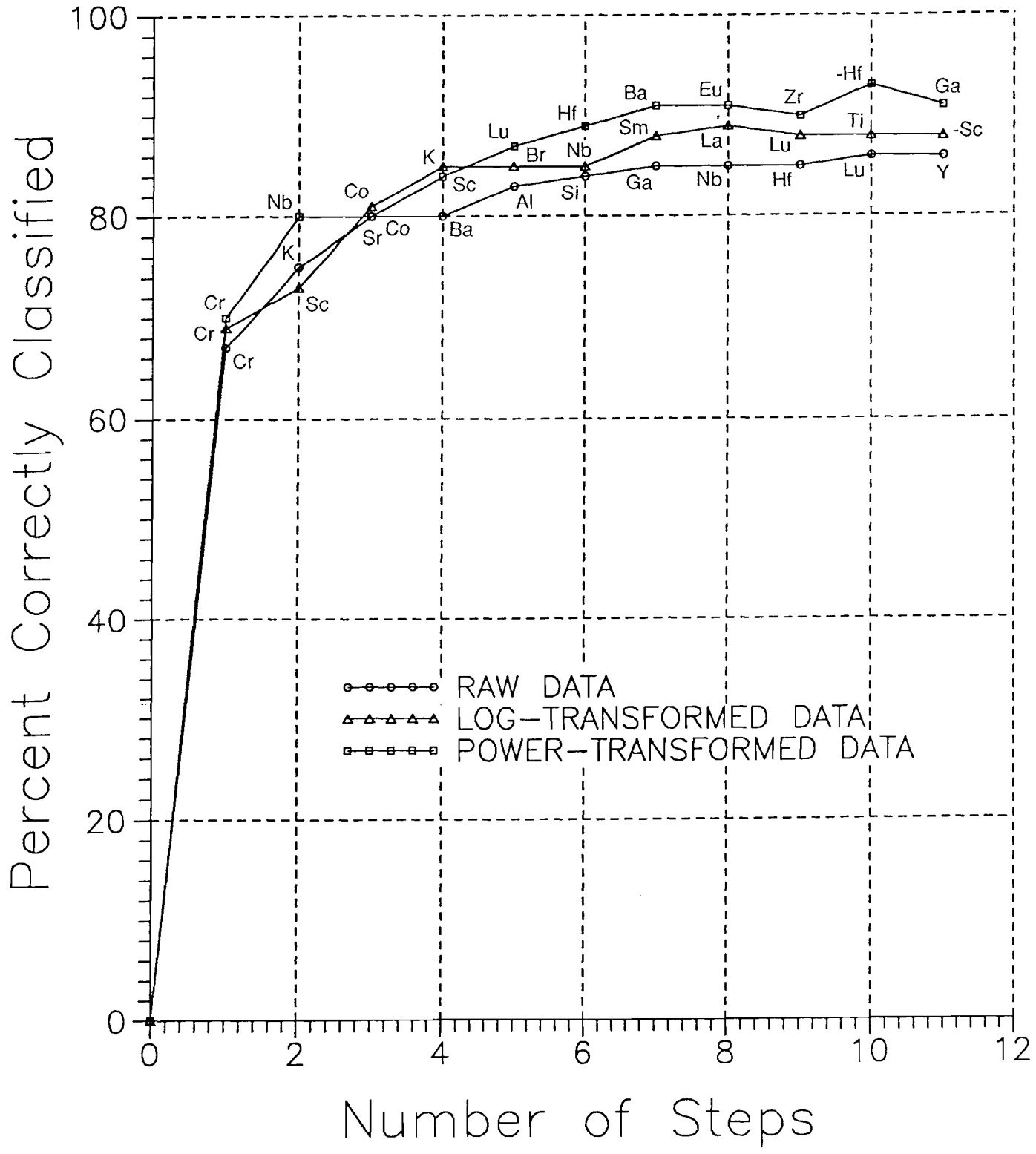

Figure 16. Summary of discriminant analysis.

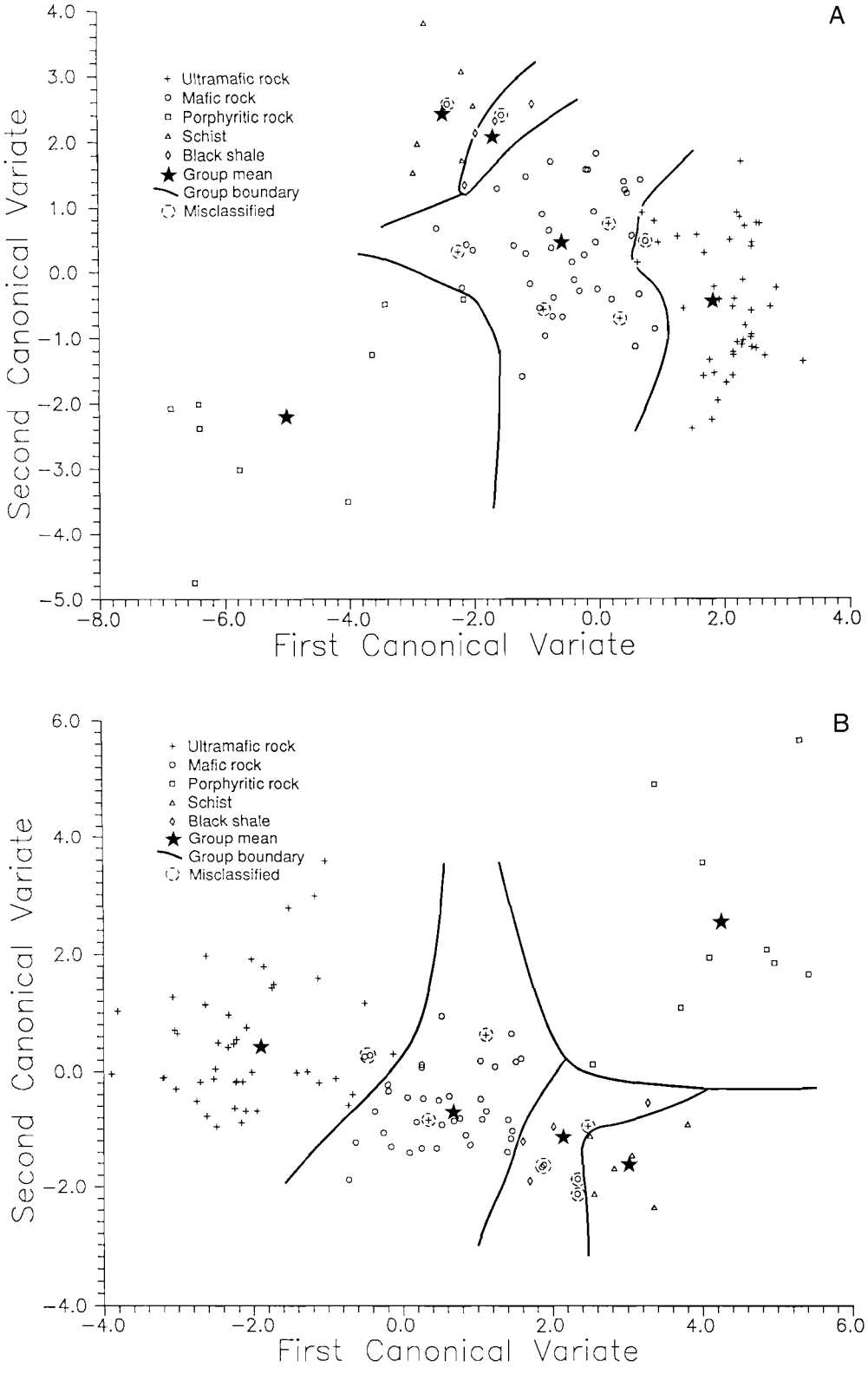

Figure 17. Canonical variate plots using log-transformed data (A) and power transformed data (B) with curved boundaries between rock type groups.

TABLE 4

DISCRIMINANT ANALYSIS CLASSIFICATION OF LOG-TRANSFORMED DATA

ULTRAMAFIC (Um) GROUP

Sample No	Group with largest probability	Square of Distance from Group Mean (Mb) Posterior Probability for Assigned Group (Pr)									
		Ultramafic		Mafic		Porphyry		Mica Schist		Black Shale	
		Mb	Pr	Mb	Pr	Mb	Pr	Mb	Pr	Mb	Pr
RE001	Um	7.527	0.997	18.932	0.003	51.286	0.000	36.886	0.000	36.047	0.000
RE002	Um	5.971	0.996	17.301	0.003	66.067	0.000	28.028	0.000	20.156	0.001
RE003	Um	2.892	0.998	15.017	0.002	58.914	0.000	40.994	0.000	31.703	0.000
RE004	Um	6.589	0.994	17.788	0.004	66.270	0.000	28.423	0.000	18.440	0.003
RE005	Um	4.271	0.996	15.369	0.004	61.031	0.000	27.122	0.000	19.277	0.001
RE015	Um	3.001	0.993	13.044	0.007	58.936	0.000	39.635	0.000	29.430	0.000
RE017	Um	1.446	0.958	7.722	0.042	52.069	0.000	24.638	0.000	16.719	0.000
RE018	Um	1.761	0.995	12.326	0.005	56.279	0.000	39.138	0.000	28.637	0.000
RE019	Um	3.634	0.997	15.502	0.003	52.110	0.000	39.421	0.000	33.965	0.000
RE020	Um	1.751	0.996	12.799	0.004	55.663	0.000	38.179	0.000	29.840	0.000
RE026	Um	2.515	0.995	13.258	0.005	55.529	0.000	39.216	0.000	27.582	0.000
RE028	Um	3.481	0.998	15.739	0.002	64.531	0.000	29.960	0.000	22.610	0.000
RE029	Um	7.604	0.997	19.426	0.003	53.533	0.000	36.216	0.000	34.936	0.000
RE030	Um	3.481	0.997	15.060	0.003	68.127	0.000	41.909	0.000	28.478	0.000
RE031	Um	9.093	0.993	19.117	0.007	51.990	0.000	28.190	0.000	28.222	0.000
RE034	Um	2.509	0.993	12.354	0.007	48.888	0.000	37.803	0.000	28.954	0.000
RE035	Um	6.366	0.998	18.861	0.002	57.643	0.000	42.839	0.000	29.317	0.000
RE037	Um	5.458	0.996	16.495	0.004	66.973	0.000	34.558	0.000	21.837	0.000
RE040	Um	4.502	0.998	17.435	0.002	54.691	0.000	39.888	0.000	34.322	0.000
RE044	Um	8.473	0.998	21.012	0.002	54.115	0.000	42.694	0.000	40.758	0.000
RE045	Um	9.026	0.999	22.151	0.001	52.174	0.000	43.849	0.000	41.069	0.000
RE046	Um	2.198	0.945	7.948	0.053	52.276	0.000	22.649	0.000	14.694	0.002
RE049	Um	0.763	0.985	9.147	0.015	54.928	0.000	34.051	0.000	24.652	0.000
RE050	Um	1.052	0.989	10.118	0.011	55.998	0.000	33.243	0.000	24.049	0.000
RE051	Um	0.465	0.984	8.710	0.016	52.009	0.000	30.401	0.000	21.326	0.000
RE052	Um	2.261	0.994	12.327	0.006	53.894	0.000	39.642	0.000	28.407	0.000
RE053	Mf	8.064	0.057	2.462	0.937	39.851	0.000	19.403	0.000	12.674	0.006
RE054	Um	2.075	0.997	14.006	0.003	60.613	0.000	44.015	0.000	33.934	0.000
RE059	Um	4.754	0.988	13.627	0.012	69.358	0.000	32.697	0.000	27.311	0.000
RE060	Um	1.742	0.998	14.101	0.002	58.621	0.000	40.777	0.000	30.980	0.000
RE061	Um	0.647	0.997	12.450	0.003	57.244	0.000	37.485	0.000	28.354	0.000
RE062	Um	2.563	0.997	14.323	0.003	58.931	0.000	38.254	0.000	33.032	0.000
RE063	Um	9.601	1.000	26.282	0.000	75.797	0.000	58.371	0.000	40.151	0.000
RE078	Um	1.978	0.996	12.994	0.004	59.577	0.000	32.452	0.000	22.334	0.000
RE079	Um	5.834	0.992	15.498	0.008	66.748	0.000	31.479	0.000	23.086	0.000
RE084	Mf	9.041	0.152	5.610	0.847	50.740	0.000	31.404	0.000	21.171	0.000
RE085	Mf	6.072	0.140	2.447	0.859	45.795	0.000	20.140	0.000	15.766	0.001
RE086	Mf	30.269	0.000	10.609	0.997	27.693	0.000	25.727	0.001	22.735	0.002
RE087	Um	2.958	0.996	13.966	0.004	65.415	0.000	42.381	0.000	30.080	0.000
RE088	Um	5.412	0.996	16.285	0.004	63.411	0.000	40.491	0.000	31.578	0.000
RE089	Um	5.490	0.980	13.256	0.020	69.405	0.000	35.331	0.000	25.171	0.000
RE092	Mf	3.085	0.435	2.577	0.560	44.749	0.000	18.465	0.000	12.082	0.005
RE093	Mf	4.483	0.356	3.303	0.643	33.454	0.000	24.922	0.000	16.164	0.001
RE097	Mf	7.014	0.289	5.218	0.709	42.775	0.000	25.606	0.000	16.466	0.003
RE098	Mf	8.288	0.078	3.431	0.885	20.792	0.000	14.456	0.004	10.019	0.033
RE099	Um	5.485	0.981	13.551	0.017	69.144	0.000	23.747	0.000	18.114	0.002
RE100	Um	5.243	0.897	9.583	0.102	50.972	0.000	20.871	0.000	19.606	0.001
RE108	Um	16.307	0.998	28.720	0.002	54.538	0.000	49.178	0.000	45.273	0.000
RE109	Um	5.651	0.974	12.887	0.026	56.775	0.000	34.115	0.000	24.890	0.000

TABLE 4 (contd)

MAFIC (Mf) GROUP

Sample No	Group with largest probability	Square of Distance from Group Mean (Mb) Posterior Probability for Assigned Group (Pr)									
		Ultramafic		Mafic		Porphyry		Mica Schist		Black Shale	
		Mb	Pr	Mb	Pr	Mb	Pr	Mb	Pr	Mb	Pr
RE009	Mf	13.031	0.298	12.549	0.379	53.666	0.000	22.192	0.003	12.890	0.320
RE013	Mf	13.629	0.021	5.977	0.955	31.359	0.000	16.767	0.004	13.775	0.019
RE014	Mf	26.241	0.000	6.764	0.932	20.042	0.001	14.518	0.019	12.699	0.048
RE016	Mf	8.431	0.074	3.517	0.862	37.512	0.000	14.715	0.003	8.831	0.061
RE021	Mf	24.515	0.000	7.559	0.976	24.070	0.000	18.866	0.003	15.297	0.020
RE022	Mf	22.777	0.000	7.063	0.979	18.953	0.003	20.207	0.001	15.249	0.016
RE023	Mf	14.622	0.014	6.336	0.912	32.811	0.000	16.824	0.005	11.512	0.069
RE033	Mf	9.420	0.022	1.816	0.974	21.439	0.000	16.857	0.001	13.033	0.004
RE041	Mf	6.860	0.342	5.555	0.658	43.082	0.000	34.582	0.000	27.759	0.000
RE043	Mf	6.371	0.379	5.383	0.621	37.228	0.000	31.382	0.000	26.162	0.000
RE047	Mf	8.838	0.068	3.624	0.918	33.477	0.000	18.235	0.001	12.099	0.013
RE048	Um	2.758	0.506	2.811	0.493	37.147	0.000	22.417	0.000	16.296	0.001
RE055	Sh	29.890	0.000	9.129	0.180	32.926	0.000	6.647	0.623	8.949	0.197
RE056	Mf	13.267	0.046	7.221	0.952	34.515	0.000	22.390	0.000	21.114	0.001
RE057	Mf	10.539	0.086	5.840	0.900	47.935	0.000	18.518	0.002	14.317	0.013
RE058	Mf	12.387	0.102	8.066	0.885	49.531	0.000	21.297	0.001	16.749	0.012
RE064	Mf	18.871	0.001	5.496	0.998	30.481	0.000	27.583	0.000	21.699	0.000
RE065	Mf	13.386	0.008	3.729	0.992	28.042	0.000	27.667	0.000	19.405	0.000
RE068	Mf	4.030	0.294	2.281	0.705	42.847	0.000	20.084	0.000	16.166	0.001
RE069	Mf	4.420	0.219	1.891	0.776	40.454	0.000	18.820	0.000	12.247	0.004
RE071	Mf	13.283	0.011	4.294	0.988	29.146	0.000	24.074	0.000	19.007	0.001
RE072	Bs	12.573	0.006	3.904	0.448	34.833	0.000	7.266	0.083	3.843	0.462
RE073	Mf	5.594	0.191	2.705	0.808	33.835	0.000	23.443	0.000	15.929	0.001
RE074	Mf	11.120	0.008	2.161	0.709	20.556	0.000	7.963	0.039	4.295	0.244
RE075	Mf	10.333	0.022	2.708	0.977	22.029	0.000	22.379	0.000	16.805	0.001
RE076	Mf	19.690	0.001	4.903	0.904	29.106	0.000	9.764	0.080	13.047	0.015
RE077	Mf	20.129	0.001	5.514	0.956	20.693	0.000	12.370	0.031	14.306	0.012
RE080	Mf	13.682	0.020	5.918	0.976	17.988	0.002	26.182	0.000	19.092	0.001
RE081	Mf	10.500	0.056	5.571	0.661	43.296	0.000	9.430	0.096	8.093	0.187
RE082	Mf	16.911	0.001	2.596	0.974	33.367	0.000	12.893	0.006	10.389	0.020
RE083	Mf	10.794	0.038	4.340	0.961	36.712	0.000	28.762	0.000	18.896	0.001
RE094	Mf	5.522	0.158	2.217	0.823	42.863	0.000	14.247	0.002	9.908	0.018
RE095	Sh	19.877	0.000	5.603	0.167	33.985	0.000	3.432	0.494	4.187	0.339
RE096	Mf	10.278	0.095	5.774	0.898	26.722	0.000	21.173	0.000	15.613	0.007
RE101	Mf	11.740	0.031	5.047	0.893	41.954	0.000	12.300	0.024	10.748	0.052
RE102	Mf	11.592	0.014	3.133	0.986	33.656	0.000	26.111	0.000	21.615	0.000
RE103	Mf	8.526	0.030	1.568	0.960	30.157	0.000	18.315	0.000	10.616	0.010
RE104	Mf	9.381	0.015	1.428	0.806	26.933	0.000	6.920	0.052	5.124	0.127
RE105	Mf	8.375	0.084	3.606	0.911	36.266	0.000	16.976	0.001	14.471	0.004
RE106	Mf	9.685	0.029	2.924	0.855	39.366	0.000	10.340	0.021	7.312	0.095
RE107	Mf	19.430	0.002	6.774	0.997	31.701	0.000	20.291	0.001	23.385	0.000

TABLE 4 (contd)

PORPHYRY (Py) GROUP

Sample No	Group with largest probability	Square of Distance from Group Mean (Mb) Posterior Probability for Assigned Group (Pr)									
		Ultramafic		Mafic		Porphyry		Mica Schist		Black Shale	
		Mb	Pr	Mb	Pr	Mb	Pr	Mb	Pr	Mb	Pr
RE006	Py	74.158	0.000	54.654	0.000	10.485	1.000	48.319	0.000	49.482	0.000
RE007	Py	75.783	0.000	50.234	0.000	6.914	1.000	38.929	0.000	43.431	0.000
RE011	Py	41.923	0.000	21.470	0.031	14.592	0.968	29.725	0.001	33.435	0.000
RE025	Py	89.132	0.000	65.124	0.000	9.582	1.000	70.315	0.000	71.516	0.000
RE036	Py	51.793	0.000	34.079	0.000	10.862	1.000	50.715	0.000	47.166	0.000
RE038	Py	85.060	0.000	59.412	0.000	9.549	1.000	43.787	0.000	46.932	0.000
RE039	Py	82.195	0.000	60.175	0.000	11.736	1.000	46.114	0.000	47.400	0.000
RE070	Mf	53.496	0.000	29.366	0.812	32.384	0.180	38.606	0.008	51.331	0.000
RE091	Mf	24.961	0.000	8.740	0.985	20.894	0.002	25.350	0.000	17.475	0.012

MICA SCHIST (Sh) GROUP

Sample No	Group with largest probability	Square of Distance from Group Mean (Mb) Posterior Probability for Assigned Group (Pr)									
		Ultramafic		Mafic		Porphyry		Mica Schist		Black Shale	
		Mb	Pr	Mb	Pr	Mb	Pr	Mb	Pr	Mb	Pr
RE012	Bs	25.690	0.000	12.311	0.002	33.655	0.000	3.016	0.236	0.673	0.762
RE032	Sh	31.617	0.000	18.053	0.000	39.012	0.000	1.479	0.793	4.170	0.207
RE042	Sh	51.038	0.000	36.100	0.000	52.544	0.000	7.421	0.986	15.926	0.014
RE066	Bs	21.486	0.000	7.438	0.025	24.290	0.000	2.911	0.243	0.706	0.732
RE067	Sh	35.002	0.000	19.159	0.001	28.713	0.000	5.212	0.891	9.431	0.108
RE090	Sh	38.164	0.000	18.834	0.023	29.783	0.000	11.384	0.970	21.501	0.006

BLACK SHALE (Bs) GROUP

Sample No	Group with largest probability	Square of Distance from Group Mean (Mb) Posterior Probability for Assigned Group (Pr)									
		Ultramafic		Mafic		Porphyry		Mica Schist		Black Shale	
		Mb	Pr	Mb	Pr	Mb	Pr	Mb	Pr	Mb	Pr
RE110	Bs	20.193	0.000	10.907	0.011	41.203	0.000	5.697	0.144	2.165	0.845
RE111	Bs	23.078	0.000	9.212	0.037	25.072	0.000	8.809	0.045	2.777	0.918
RE112	Bs	27.008	0.000	18.894	0.000	38.791	0.000	5.157	0.413	4.454	0.587
RE113	Bs	22.817	0.000	8.941	0.014	30.035	0.000	4.464	0.133	0.740	0.853

TABLE 5

DISCRIMINANT ANALYSIS CLASSIFICATION OF POWER-TRANSFORMED DATA

ULTRAMAFIC (Um) GROUP

Sample No	Group with largest probability	Square of Distance from Group Mean (Mb) Posterior Probability for Assigned Group (Pr)									
		Ultramafic		Mafic		Porphyry		Mica Schist		Black Shale	
		Mb	Pr	Mb	Pr	Mb	Pr	Mb	Pr	Mb	Pr
RE001	Um	3.716	0.997	15.119	0.003	40.244	0.000	35.928	0.000	27.972	0.000
RE002	Um	9.181	0.996	20.401	0.004	65.519	0.000	37.120	0.000	29.616	0.000
RE003	Um	1.169	0.998	13.840	0.002	46.635	0.000	39.478	0.000	26.928	0.000
RE004	Um	3.474	0.997	15.024	0.003	53.197	0.000	32.973	0.000	22.600	0.000
RE005	Um	3.022	0.998	15.349	0.002	50.142	0.000	36.614	0.000	25.632	0.000
RE015	Um	2.145	0.994	12.263	0.006	49.590	0.000	40.478	0.000	27.730	0.000
RE017	Um	1.056	0.931	6.270	0.069	39.258	0.000	26.998	0.000	17.792	0.000
RE018	Um	22.037	0.994	32.423	0.006	81.263	0.000	71.156	0.000	58.159	0.000
RE019	Um	14.775	0.998	27.529	0.002	33.338	0.000	47.398	0.000	41.411	0.000
RE020	Um	0.851	0.997	12.272	0.003	46.931	0.000	35.622	0.000	24.918	0.000
RE026	Um	4.032	0.997	15.474	0.003	56.638	0.000	39.447	0.000	28.044	0.000
RE028	Um	6.271	0.997	18.129	0.003	58.652	0.000	31.102	0.000	24.375	0.000
RE029	Um	2.381	0.997	14.190	0.003	38.469	0.000	34.053	0.000	25.509	0.000
RE030	Um	12.811	0.999	26.707	0.001	80.304	0.000	70.500	0.000	53.029	0.000
RE031	Um	3.530	0.994	13.655	0.006	32.266	0.000	27.936	0.000	20.773	0.000
RE034	Um	0.763	0.997	12.668	0.003	44.543	0.000	33.945	0.000	23.395	0.000
RE035	Um	4.140	1.000	21.059	0.000	57.383	0.000	52.154	0.000	35.918	0.000
RE037	Um	3.457	0.997	14.908	0.003	54.914	0.000	40.476	0.000	26.477	0.000
RE040	Um	24.252	0.997	36.213	0.003	51.814	0.000	60.313	0.000	55.566	0.000
RE044	Um	3.357	0.999	16.969	0.001	41.061	0.000	41.185	0.000	30.437	0.000
RE045	Um	3.323	0.998	16.220	0.002	39.677	0.000	38.347	0.000	28.251	0.000
RE046	Um	1.152	0.929	6.301	0.071	37.769	0.000	24.755	0.000	15.731	0.001
RE049	Um	1.358	0.982	9.397	0.018	49.078	0.000	34.581	0.000	24.375	0.000
RE050	Um	1.434	0.986	9.960	0.014	47.100	0.000	32.964	0.000	22.877	0.000
RE051	Um	3.618	0.972	10.705	0.028	51.459	0.000	30.766	0.000	22.374	0.000
RE052	Um	4.815	0.992	14.462	0.008	56.815	0.000	29.886	0.000	22.639	0.000
RE053	Mf	11.214	0.014	2.678	0.984	30.397	0.000	21.105	0.000	14.836	0.002
RE054	Um	2.905	0.998	15.271	0.002	58.009	0.000	39.212	0.000	28.928	0.000
RE059	Um	8.562	0.998	21.044	0.002	65.838	0.000	42.197	0.000	34.956	0.000
RE060	Um	1.995	1.000	17.798	0.000	57.305	0.000	44.894	0.000	32.606	0.000
RE061	Um	1.102	0.999	14.535	0.001	50.658	0.000	36.632	0.000	26.037	0.000
RE062	Um	17.118	0.998	30.035	0.002	40.232	0.000	46.766	0.000	43.027	0.000
RE063	Um	9.780	1.000	29.899	0.000	73.143	0.000	65.253	0.000	44.860	0.000
RE078	Um	3.874	0.999	17.188	0.001	54.388	0.000	30.216	0.000	21.273	0.000
RE079	Um	9.108	0.999	22.791	0.001	66.686	0.000	36.712	0.000	29.432	0.000
RE084	Mf	12.192	0.187	9.249	0.813	42.781	0.000	42.681	0.000	27.957	0.000
RE085	Mf	9.857	0.124	5.944	0.876	39.072	0.000	34.052	0.000	25.301	0.000
RE086	Mf	35.834	0.000	16.149	0.816	29.226	0.001	25.431	0.008	19.235	0.174
RE087	Um	3.779	0.999	17.739	0.001	64.434	0.000	47.679	0.000	34.951	0.000
RE088	Um	8.232	1.000	23.677	0.000	63.538	0.000	52.539	0.000	40.826	0.000
RE089	Um	8.591	0.997	20.006	0.003	67.441	0.000	51.545	0.000	39.555	0.000
RE092	Um	9.390	0.627	10.436	0.372	30.723	0.000	35.633	0.000	23.567	0.001
RE093	Mf	6.137	0.308	4.544	0.683	26.861	0.000	22.661	0.000	13.213	0.009
RE097	Mf	11.643	0.364	10.531	0.634	43.308	0.000	31.454	0.000	21.943	0.002
RE098	Bs	14.159	0.037	9.624	0.362	19.182	0.003	15.511	0.019	8.683	0.579
RE099	Um	8.306	0.995	19.190	0.004	59.046	0.000	31.770	0.000	25.053	0.000
RE100	Um	6.687	0.938	12.169	0.061	42.818	0.000	24.066	0.000	20.473	0.001
RE108	Um	3.727	1.000	19.984	0.000	52.767	0.000	41.933	0.000	33.191	0.000
RE109	Um	13.440	0.999	27.279	0.001	57.400	0.000	63.702	0.000	46.937	0.000

TABLE 5 (contd)

MAFIC (Mf) GROUP

Sample No	Group with largest probability	Square of Distance from Group Mean (Mb) Posterior Probability for Assigned Group (Pr)									
		Ultramafic		Mafic		Porphyry		Mica Schist		Black Shale	
		Mb	Pr	Mb	Pr	Mb	Pr	Mb	Pr	Mb	Pr
RE009	Mf	11.682	0.238	9.369	0.756	45.161	0.000	26.303	0.000	18.958	0.006
RE013	Mf	17.691	0.004	6.900	0.978	28.505	0.000	17.392	0.005	15.581	0.013
RE014	Mf	28.871	0.000	8.494	0.712	29.482	0.000	11.375	0.169	12.064	0.119
RE016	Mf	8.370	0.027	1.237	0.960	24.845	0.000	16.329	0.001	9.996	0.012
RE021	Mf	25.560	0.000	7.565	0.965	29.241	0.000	16.433	0.011	14.982	0.024
RE022	Mf	21.948	0.000	6.167	0.994	28.697	0.000	21.118	0.001	16.717	0.005
RE023	Mf	14.592	0.011	5.687	0.985	28.637	0.000	23.422	0.000	16.837	0.004
RE033	Mf	12.602	0.005	2.191	0.963	22.204	0.000	12.068	0.007	9.477	0.025
RE041	Mf	7.906	0.101	3.531	0.899	35.321	0.000	24.831	0.000	18.750	0.000
RE043	Mf	8.794	0.104	4.492	0.895	32.116	0.000	25.832	0.000	19.930	0.000
RE047	Mf	9.940	0.045	3.829	0.953	26.277	0.000	24.872	0.000	16.543	0.002
RE048	Mf	4.326	0.365	3.216	0.635	29.453	0.000	26.323	0.000	17.145	0.001
RE055	Mf	25.643	0.000	4.600	0.925	24.716	0.000	11.348	0.032	10.710	0.044
RE056	Mf	12.358	0.025	5.042	0.965	35.383	0.000	17.310	0.002	14.632	0.008
RE057	Mf	12.111	0.062	6.712	0.928	39.983	0.000	22.601	0.000	15.819	0.010
RE058	Mf	14.065	0.095	9.561	0.903	51.066	0.000	28.722	0.000	22.343	0.002
RE064	Mf	21.294	0.001	6.526	0.999	34.435	0.000	30.346	0.000	23.993	0.000
RE065	Mf	14.038	0.004	2.954	0.995	30.879	0.000	24.650	0.000	16.927	0.001
RE068	Mf	8.446	0.100	4.071	0.895	30.047	0.000	19.104	0.000	14.703	0.004
RE069	Mf	7.946	0.063	2.688	0.874	33.780	0.000	12.563	0.006	8.148	0.057
RE071	Mf	14.266	0.004	3.381	0.913	15.197	0.002	15.141	0.003	8.303	0.078
RE072	Bs	14.222	0.001	3.678	0.260	21.825	0.000	5.981	0.082	1.826	0.656
RE073	Mf	6.276	0.244	4.021	0.755	30.147	0.000	29.531	0.000	18.411	0.001
RE074	Mf	13.650	0.005	4.213	0.599	14.104	0.004	11.348	0.017	5.154	0.374
RE075	Mf	11.284	0.035	4.678	0.963	20.268	0.000	29.404	0.000	18.934	0.001
RE076	Mf	21.420	0.001	7.877	0.998	24.837	0.000	30.204	0.000	24.130	0.000
RE077	Mf	21.314	0.000	4.881	0.845	25.976	0.000	9.091	0.103	10.443	0.052
RE080	Mf	13.471	0.009	4.331	0.873	13.281	0.010	16.569	0.002	8.551	0.106
RE081	Mf	11.791	0.039	5.941	0.721	33.125	0.000	10.896	0.061	8.718	0.180
RE082	Mf	17.767	0.000	1.857	0.993	26.131	0.000	16.010	0.001	12.299	0.005
RE083	Mf	10.346	0.025	3.019	0.975	37.415	0.000	28.411	0.000	18.206	0.000
RE094	Mf	6.594	0.079	1.735	0.894	25.894	0.000	14.805	0.001	8.784	0.026
RE095	Mf	17.046	0.001	3.601	0.969	23.317	0.000	15.847	0.002	10.732	0.027
RE096	Mf	7.787	0.069	2.650	0.900	30.011	0.000	14.740	0.002	9.558	0.028
RE101	Mf	10.940	0.024	3.931	0.795	27.070	0.000	12.247	0.012	7.034	0.168
RE102	Mf	12.294	0.003	0.921	0.981	26.759	0.000	12.888	0.002	9.494	0.013
RE103	Mf	10.250	0.049	4.311	0.947	26.400	0.000	26.233	0.000	14.939	0.005
RE104	Mf	10.707	0.019	2.937	0.921	17.603	0.001	14.829	0.002	8.494	0.057
RE105	Mf	8.604	0.118	4.584	0.881	32.525	0.000	24.699	0.000	17.595	0.001
RE106	Mf	9.870	0.011	1.118	0.890	19.792	0.000	10.274	0.009	5.712	0.090
RE107	Mf	22.611	0.001	9.423	0.999	35.648	0.000	31.726	0.000	28.215	0.000

TABLE 5 (contd)

PORPHYRY (Py) GROUP

Sample No	Group with largest probability	Square of Distance from Group Mean (Mb) Posterior Probability for Assigned Group (Pr)									
		Ultramafic		Mafic		Porphyry		Mica Schist		Black Shale	
		Mb	Pr	Mb	Pr	Mb	Pr	Mb	Pr	Mb	Pr
RE006	Py	56.311	0.000	40.269	0.000	12.154	1.000	47.535	0.000	38.511	0.000
RE007	Py	52.760	0.000	31.869	0.000	5.477	1.000	24.278	0.000	21.361	0.000
RE011	Py	50.243	0.000	31.150	0.000	12.249	1.000	28.035	0.000	34.669	0.000
RE025	Py	80.174	0.000	63.059	0.000	11.474	1.000	63.634	0.000	61.628	0.000
RE036	Py	61.738	0.000	50.168	0.000	19.066	1.000	65.724	0.000	59.655	0.000
RE038	Py	59.198	0.000	37.103	0.000	7.711	0.993	18.982	0.004	19.048	0.003
RE039	Py	53.246	0.000	33.523	0.000	6.362	0.995	19.171	0.002	17.667	0.003
RE070	Py	62.894	0.000	38.392	0.030	31.474	0.969	48.154	0.000	58.052	0.000
RE091	Bs	35.053	0.000	19.166	0.256	23.689	0.027	26.488	0.007	17.121	0.711

MICA SCHIST (Sh) GROUP

Sample No	Group with largest probability	Square of Distance from Group Mean (Mb) Posterior Probability for Assigned Group (Pr)									
		Ultramafic		Mafic		Porphyry		Mica Schist		Black Shale	
		Mb	Pr	Mb	Pr	Mb	Pr	Mb	Pr	Mb	Pr
RE012	Bs	24.678	0.000	10.617	0.005	20.542	0.000	2.809	0.235	0.456	0.761
RE032	Sh	33.883	0.000	18.501	0.000	25.137	0.000	0.685	0.765	3.049	0.235
RE042	Sh	52.976	0.000	37.036	0.000	45.364	0.000	7.240	0.983	15.413	0.017
RE066	Sh	29.945	0.000	13.655	0.001	24.530	0.000	1.192	0.539	1.508	0.460
RE067	Sh	40.640	0.000	22.477	0.000	20.371	0.000	2.501	0.841	5.834	0.159
RE090	Sh	37.773	0.000	16.472	0.395	35.709	0.000	15.664	0.592	23.249	0.013

BLACK SHALE (Bs) GROUP

Sample No	Group with largest probability	Square of Distance from Group Mean (Mb) Posterior Probability for Assigned Group (Pr)									
		Ultramafic		Mafic		Porphyry		Mica Schist		Black Shale	
		Mb	Pr	Mb	Pr	Mb	Pr	Mb	Pr	Mb	Pr
RE110	Bs	20.811	0.000	9.660	0.011	22.019	0.000	4.269	0.164	1.033	0.825
RE111	Bs	42.862	0.000	26.351	0.001	26.857	0.001	16.111	0.148	12.613	0.850
RE112	Bs	22.405	0.000	14.681	0.003	30.330	0.000	5.381	0.287	3.569	0.710
RE113	Bs	21.003	0.000	7.146	0.120	29.401	0.000	7.767	0.088	3.368	0.792

Thus, for the log-normalised data set, the classification table (Table 4) indicates that 16 samples are misclassified. By drawing curved boundaries on the canonical plot (Figure 17A), the number of misclassified samples is reduced to 7.

Similarly, for the power-transformed data set the classification table (Table 5) shows 10 samples misclassified, while the canonical plot (Figure 17B) shows 9 samples misclassified. The effectiveness of this multivariate rock classification may be compared with that shown by the first three elements (Cr-Co-Sc) of the discriminant analysis on their own (Figure 15D) and the second and third elements (Co-Sc) in Figure 14H.

8.5 Use and Improvement of Discriminant Analysis

Discriminant analysis is an effective way to separate the five lithologies exposed on the south face of the Rand Pit, despite the small number of samples and the effects of variable mineralisation and deep lateritic weathering. Although power-transformation of the analytical data produced the closest approximation to normal distributions for all of the variables, and thus is the best way to transform the raw data used in discriminant analysis, a logarithmic transformation is nearly as good. Logarithmic transformations are more readily available in statistical software.

Depending on the type of data transformation chosen, the five lithologies exposed at Rand can be optimally discriminated by between six and seven elements and certainly by no more than nine elements (Cr, Nb, Co, Sc, Lu, Hf, Ba, K, and Br). Chromium alone explains about 70% of the variation for both log- and power-transformed data (step 1, Figure 16). This element has already been shown to be a good preliminary discriminant screen for classifying new samples. In view of the very close Zr-Hf correlation, it is likely that Hf could be replaced by Zr with little degradation of the discrimination.

The intensity of weathering in the Reedy area varies markedly with depth and lithology. The five lithologies studied here could be better separated using discriminant analysis if samples that had suffered a similar degree of weathering were analysed. By far the greatest fabric, mineralogical and geochemical changes occur in the top 5-15 m so sampling below this depth may well yield better results. The results of this study are based on data from a relatively limited number of samples. Discrimination of the five lithologies at the Rand Pit could be improved by adding analyses for new, documented samples to the existing database, particularly samples of the porphyry, mica schist, and black shale units, and re-running the discriminant analysis.

The value of this discriminant analysis study is to demonstrate that the method is effective and to encourage its use. No discriminant functions are provided as they would have only local application. Each group of lithologies and possibly each area will need individual treatment. After a number of such studies have been completed, a short list of the most effective elements should emerge. This should reduce the need for analysis for large numbers of elements and focus resources on larger sample sets, so improving the statistical base.

9.0 CONCLUSIONS

9.1 Geology, Mapping and Optimum Mapping Conditions

Mapping and sampling of the pit face showed there to be a sequence of near vertical, alternating, mafic and ultramafic rocks, interspersed with bands of quartz-mica schist and black shale, all intruded by pods of granitoid porphyry.

The mafic and ultramafic rocks are quite variable, even in the relatively fresh state, and appear to be part of a komatiitic suite of metavolcanics which have lost much of their Ca prior to weathering. The gross stratigraphy is visible on the lower benches of the pit but, towards the surface, the distinctions become less clear with the onset of kaolinisation and particularly intense weathering.

A freshly cut, dust covered pit face, seen in the stark noon light of summer will yield the least geological information. Strong sunlight, falling on the pit face at an acute angle, throws shadows which accentuate irregularities in the surface of the pit face. These are governed more by the means of excavation than by geology. Three years of washing and etching by rainwater of the south face of the Rand Pit greatly increased the observable structural, fabric and field relation detail. While mapping of pits cannot be delayed, minor preparation of the pit face, by hosing down, and mapping the pit face while in shadow or when the day is overcast, will increase the yield of geological information.

9.2 Petrography and Mineralogy

The objective of the petrographic study was to trace the detailed mineralogical and fabric changes that occur in each rock type with progressive weathering up the profile and so to aid rock identification. This has been illustrated with photomicrographs and close-up photographs (Figures 6-10).

Ultramafic Rocks
In the unweathered state these rocks are talc-chlorite±tremolite schists. They consist of matted to schistose fine-grained talc, some with blades and needles of decussate tremolite and variable quantities of quartz. This is cut by a later chlorite-filled fracture cleavage. The first sign of weathering is Fe staining along some cleavage planes. Progressively, the chlorite becomes opaque and is altered to smectite and tremolite dissolves to leave needle-like voids, which become infilled with goethite. Sphene and ilmenite alter to anatase.

Around R.L. 460 (30 m depth) and particularly above R.L. 480 (10 m depth), kaolinite is abundant and contains relict islands of talc as the rock changes from saprolite to pedolith (10 m depth). Some of the kaolinite has recrystallised to stumpy stacks and booklets. Fractures are lined with pyrolusite and cryptomelane (±Ba). The rocks at this depth are pockmarked with solution channels and vesicles. In places these rocks are Fe-stained, polymictic saprolite breccias, set in kaolinite, where most of the gross saprolite fabric has been destroyed.

Mafic Rocks
Where fresh, these rocks consist of granulated lenses of untwinned albite and quartz, cut by a strong foliation marked by muscovite and talc and by a later, more open-spaced chloritic cleavage. Deep in the saprolite profile, albite becomes turbid and alters to kaolinite and this is largely complete at R.L. 420 (70 m depth).

Around R.L. 440 (50 m depth) and above it, chlorite alters to smectite, kaolinite becomes abundant and vesicles and solution channels develop. The schistose saprolitic fabric is progressively lost and is replaced by blastic patches of kaolinite of the pedolith, surrounded by patches of granular quartz. In places some of the kaolinite has recrystallised to accordion structures and books. Some are saprolite breccias.

Mica Schists and Black Shales
The mica of the fine-grained quartz-muscovite±talc schists begin to weather to kaolinite above R.L. 460 (60 m depth) and this alteration is intense though incomplete at R.L. 480 (10 m depth). The black shales have a similar mineralogy and fabric but with additional carbonaceous material. The carbonaceous material (now largely graphite) shows evidence of migration into a crenulation cleavage.

Granitoid Porphyry
Fresh porphyries consist of plagioclase, quartz and granular microcline and are intensely fractured and cleaved, some with chlorite. Weathering kaolinises the plagioclase and, higher in the profile, the microcline as well, leaving a non-schistose rock in which only a trace of relict micrographic quartz remains.

Mineral Weathering Parageneses
As weathering proceeds, most component minerals alter to varying extents. Many of these reactions result in considerable volume loss which makes the rock porous and promotes the formation of vesicles and channelways. This porosity increases access of weathering solutions and leaves spaces which may be filled with secondary clays that progressively destroy the saprolite fabric.

Plagioclase weathers readily to kaolinite at depth (>R.L. 440 ;<50 m depth) but kaolinisation of *microcline* occurs higher in the profile. This reaction probably takes place with smectite and illite as intermediate phases. *Talc* is generally unchanged and is found from fresh rock almost to the surface, where it is partly altered to kaolinite. Kaolinisation of talc requires a supply of Al^{3+} and acid conditions. *Muscovite* alters to kaolinite only in part at the top of the profile but, in so doing, releases Al^{3+} which is deposited as kaolinite nearby or assists in kaolinisation of talc. *Chlorite* alters to smectite under oxidising, acid conditions, particularly above R.L. 475, where it is extensively stained with goethite that was probably released by this clay-forming reaction. Ultimately this smectite is further altered to kaolinite.

Smectite is abundant in the mafic and ultramafic rocks above R.L. 440 (50 m depth) but, near the top of the profile, it is extensively altered to kaolinite under acid conditions. Smectites penetrate to depth along the edge of the S3 ore shoot, where alteration of chlorite probably has been promoted by acidic solutions generated by pyrite weathering. *Tremolite* is dissolved and leaves needle-like voids, some of which are filled with migrating Fe oxyhydroxides. *Sphene* is progressively altered to anatase and Ca is leached out. *Magnetite and ilmenite* are altered to goethite and mixed goethite and anatase. *Chromite* remains unaltered.

Fine-grained, granular *quartz* is an important primary component of most of the lithologies, except for the ultramafic rocks. Slightly coarser-grained, granoblastic quartz grains occur in small, lensoid patches and segregations, which lie parallel to the foliation. These appear to be metamorphic segregations, though some may be related to mineralisation. Even coarser-grained quartz, with a strained fabric, forms small veinlets which cross-cut the foliation at acute angles. This last type of quartz has probably been introduced and is related to mineralisation. There is evidence for some quartz depletion near the very top of the weathered profile. This variability in quartz content dictates that the Si content be excluded as a determining factor in any intended rock classification.

Weathering of Vein Quartz
As a quartz vein weathers, the tightly locked, granoblastic polygonal to sutured margins of quartz grains (Figure 10E) become separated by fine-grained clay (Figure 10F) or Fe oxides. As the secondary minerals penetrate a vein, the quartz grains separate and appear corroded and overall the quartz takes on a stained, sugary appearance. The quartz grains of the vein progressively lose their coherence (Figure 10G) and finally the vein loses its shape, leaving a mass of angular or corroded quartz fragments set in secondary saprolitic minerals (Figure 10H). Only the strained nature of the quartz indicates its origin.

Vesicles and Solution Channels
Small fractures in the deep saprolite are common. Some fractures represent joints and many are cemented with goethite or, in the ultramafic rocks, with cryptomelane and pyrolusite.

Higher in the saprolite, around R.L. 480 (10 m depth), lenticular, vermiform and globular vesicles are common. Most are open, but many are filled or lined with either goethite or poorly crystalline, yellow-stained kaolinite and mixed kaolinite and smectite. Some vesicles form chains, linked by a stylolitic fracture which may be fretted out so that the vesicles coalesce into a channelway. These channelways greatly increase the access of water to the saprolite and clays have been deposited onto their walls. Although some are completely plugged with secondary clays, others form open cavities, partly filled with subrounded to subangular saprolitic particles, partly cemented by coarse-grained, flaky kaolinite.

Migration of Carbon
Migration of some carbonaceous material from the bedding planes to the cleavage has been demonstrated in the black shales and small quantities of graphitic material have been found in the schistosity of some ultramafics. Migration of carbon compounds could have occurred at any stage from initial dewatering of the volcano-sedimentary pile (by liquid hydrocarbon migration (Alterman, 1973; Robertson and Taylor, 1987)) to metamorphism (by precipitation of graphite by limited oxidation of permeating methane).

9.3 Geochemical Dispersion

The weathered profile may be naturally subdivided into deep and shallow zones. The shallow zone is an horizon of weathered rock with low specific gravities (<2.0) extending to 10-15 m depth, in which considerable leaching and element dispersion has taken place. Below this zone, dispersions largely depend on variations in rock type and mineralisation.

Some elements in the deeper part of the profile may be regarded as ore-related (Ag, Au, As, Cu, Mo, Pb, Sb, Se, Sn, Te, Tl, W and Zn); the more abundant of these show an exponential relationship between the variance of their concentrations and distance from the major ore shoots.

Others are lithology-related (Cd, Ga, Hf, Nb, Sc, Ta, Ti, U, V, Y, Yb and Zr). Aluminium and Ga differentiate the mafic and mica schists and the porphyry pods from the ultramafic rocks. Low Fe concentrations mark the mica schist, black shales and porphyries, though some high Fe concentrations that occur at depth in the M3 mafic band, probably are related to hydrothermal pyrite from the adjacent ore shoot. High B and Ba abundances characterise the mica schists and porphyries.

Useful pathfinder elements in the shallow weathered profile proved to be As, Au, Cu, (possibly Mo), Se, Te, Tl and W. The ore-associated elements Ag, Pb, Sb, Sn and Zn were less useful because of intense leaching and/or erratic enrichment. Chromium, Ti, K, Cs, Rb, Zr and Hf are relatively unaffected by weathering. The alkalis (K, Rb and Cs) are probably related to unweathered or partly-weathered micas. The Zr/Hf ratio is relatively constant, indicating that zircon has remained stable. The Cr and Ti abundances are useful lithological indicators, despite some localised leaching of Cr and residual concentration of Ti. The low density, near surface zone of the profile contains enrichments of Al, B, Ba, Fe, Ga, Nb, Si, Sr, Ta, Th and V, as well as depletions (some local) of Ag, Al, Ca, Cd, Ce, Co, Eu, Fe, Ge, La, Li, Lu, Mg, Mn, Na, Ni, Sm, Y and Zn.

9.4 Discriminant Analysis

Discriminant analysis is an effective way to separate the five lithologies at Rand, despite the small number of samples used and the overprinting of metamorphism, mineralisation and weathering.

Power-transformation of the geochemical data, prior to discriminant analysis, produced the closest approximation to normal element distributions and the best discrimination. However the more readily available logarithmic transformation is nearly as effective.

The five lithologies at Rand may be effectively discriminated using between six and nine elements. The element list varies according to the type of data transformation used. For power transformation, Cr, Nb, Co, Sc, Lu, Hf and Ba should be used, for log transformation Cr, Sc, Co, K, Br, Nb, Sm and La. Chromium alone explains about 70% of the variation for both log- and power-transformed data (step 1 in Figure 16), so the concentration of this element is a good preliminary discriminator.

The intensity of weathering at Rand varies markedly with lithology and also with depth. The top 5-15 m contain the greatest geochemical changes. The effectiveness of discriminant analysis probably would be greatly improved by using samples from below this depth.

This discriminant analysis study has been made to demonstrate the effectiveness of the technique. No discriminant functions have been given as they probably would have only local application. Each group of lithologies and each area would need individual treatment. A short list of useful elements may emerge from a number of such studies that would focus resources on larger sample sets and so improve the statistical base.

9.5 Implications for Exploration

* In the deeper parts of the saprolite, the mineralisation at Rand is characterised by As, Au, Cu, Pb, Sb, Sn, W and Zn; the elements Ag, Mo, Se, Te, and Tl may contribute to this signature but their abundances are very close to their detection limits, so improved analytical methods are required.

* In the shallower part of the weathered profile, As, Au, Cu, Se and W show promise as pathfinder elements.

* High Cr and talc abundances are useful indicators of ultramafic rocks. These abundances persist to the surface, or nearly so. The metasedimentary rocks are distinguished by high mica abundances, which are related to high K, Rb and Cs.

* Discriminant analysis best separates the five rock types found at Rand (mafic volcanic, ultramafic volcanic, mica schist, black shale and granitoid porphyry), using Cr, Nb, K, Co, Br, Se, Lu, Sm, Hf, Ba, and La. Power transformation of the data prior to discriminant analysis is marginally better than log transformation and the suite of elements is slightly different. A rate of 90-95% correct classification is achievable using a 7-9 step analysis. Further improvements may be made by using curved boundaries on the canonical plots.

* The petrographic study has revealed a number of primary and secondary fabrics in the mafic and ultramafic rocks which are visible and recognisable without using a petrographic microscope. Reference to the petrographic section and to Figures 6-10 should assist those engaged in logging percussion drill cuttings and intensely weathered rocks in pits.

* Where the rocks carry even small quantities of sulphides, weathering has penetrated deeply. The acid conditions, produced by sulphide oxidation, are particularly conducive to the degradation of feldspar, chlorite, tremolite, and sphene.

Thus, the envelopes of ore shoots tend to be unusually deeply weathered and produce saprolites of low density and high porosity. Although the sulphides may be too sparse or too deep for detection by geophysical methods, any method that can detect these deeply-penetrating rocks of low density and high porosity may be useful, particularly if these low density rocks are coupled with a geochemical response.

10.0 ACKNOWLEDGEMENTS

Sample preparation was by R.J. Bilz, G.D. Longman and M.J. Lintern. The XRF geochemical analyses were performed by M.K.W. Hart, and the ICP analyses by J.E. Wildman and M. Richardson. INAA analysis was by Becquerel Laboratories and the majority of this work was provided free, as part of an introductory package. Emission spectrographic analysis, some AAS and partial digestion ICP analyses were performed by R.H. Hill and S.J. Sutley of the U.S. Geological Survey Laboratories in Denver, Colorado. XRD data were collected by A. Horne and thin sections were prepared by G.W. Hansen, both at North Ryde. Determinations of Na, K, Li, and ignition losses were by K.A. Howe. Assistance on the SEM was ably given by B.W. Robinson, G. Burkhalter and R.B.W. Vigers. M. Smyth made a detailed examination of the carbonaceous material of the black shales. E.C. Grunsky and R.E.T. Hill advised on mafic-ultramafic rock classification. H.M. Churchward provided geomorphological input. Drafting and artwork was by A.D. Vartesi. D.J. Gray, C.R.M. Butt and E.C. Grunsky assisted with computing. The plots in Appendix 5 were generated using a demonstration copy of the BRGM's GDM package. G.A Love and J.J. Porter formatted the final document. M. Palmer provided the xy plots of the correlation matrix and J.L. Perdrix kindly provided access to the HP 7580B plotter. Metana Minerals N.L., assisted with accommodation and logistics while at the Reedy Mine. All this is acknowledged with appreciation. Especial thanks goes to W.H. Waldeck, who surveyed the sample locations; to L.M. Lawrance, who assisted with collection of samples along the top bench using the 9.4 m ladder; to E.H. Nickel, who exposed and processed over 50 Debye-Scherrer diffractograms, which were essential to understanding the petrography; to R. Henderson, for his assistance while at Reedy and to C.R.M. Butt, who provided critical comment on the manuscript.

11.0 REFERENCES

Ahrens, L.H., 1954. The lognormal distribution of the elements. Geochim. et Cosmochim. Acta, part 1, 5, pp. 49-73; part 2, 6, pp. 121-131.

Alterman, I.B. 1973. Rotation and dewatering during slaty cleavage formation: Some new evidence and interpretations. Geology, 1. 33-36.

Arnold, J. M. 1963. Climate of the Wiluna-Meekatharra Area. in J.A. Mabbutt *et al.* General report on lands of the Wiluna-Meekatharra Area, Western Australia, 1958. CSIRO Land Research Series 7. 73-92.

Auvray, B., Blais, S., Jahn, B.M. and Piquet, D. 1982. Komatiites and the komatiitic series of the Finnish greenstone belts. In N.T. Arndt and E.G. Nisbet (eds). Komatiites. George Allen and Unwin Lond. 131-146.

Barnes, S-J. 1985. The petrography and geochemistry of komatiite flows from the Abatibi greenstone belt and a model for their formation. Lithos. 18, 241-270.

Bavinton, O.A. 1981. The nature of sulfidic metasediments at Kambalda and their broad relationships with associated ultramafic rocks and nickel ores. Econ. Geol. 76, 1606-1628.

Bavinton, O.A., and Keays, R.R. 1978. Precious metal values from interflow sedimentary rocks from the komatiite sequence at Kambalda, Western Australia. Geochimica et Cosmochimica Acta. 42. 1151-1163.

Bettanay, E. and Churchward, H.M. 1974. Morphology and stratigraphic relationships of the Wiluna Hardpan in arid Western Australia. J. Geol. Soc. Aust. 21, 73-80.

Beswick, A.E. 1982. Some geochemical aspects of alteration, and genetic relations in komatiitic suites. In N.T. Arndt and E.G. Nisbet (eds). Komatiites. George Allen and Unwin Lond. 283-308.

Brindley, G.W. 1980. Quantitative X-ray mineral analysis of clays in G.W. Brindley and G. Brown (eds). Crystal structures of clay minerals and their X-ray identification. Mineralogical Society Monograph No 5. 411-438.

Burkov, V.V., and Podporina, Y.K. 1967. Rare earths in granitoid residuum. Dokl. Acad. Sci. USSR, Earth Sci. Sect. 177, 214-216.

Butt, C.R.M., and Zeegers, H. (in press) Profile terminology and glossary of terms. in C.R.M. Butt and H. Zeegers. Handbook of exploration geochemistry. Regolith geochemistry in mineral exploration of humid and arid tropically weathered terrains. Appendix 3.

Campbell, J.D. 1953. The Triton gold mine, Reedy, WA. in A.B. Edwards (ed). Geology of Australian Ore Deposits Vol. 1. 195-207.

Correns, C.W. 1978. Titanium. in K.H. Wedepohl (ed). Handbook of Geochemistry. Springer-Verlag. New York.

Crock, J.G., Briggs, P.H., Jackson, L.L. and Lichte, F.E. 1987. Analytical methods for analysis of stream sediments and rocks from wilderness study areas. U.S. Geological Survey Open-File Report No 87-84, 35 pp.

Davis, J.C. 1973. Statistics and data analysis in geology. New York, John Wiley and Sons, 549 pp.

Eggleton, R.A., and Busek, P.R. 1980. High resolution electron microscopy of feldspar weathering. Clays and Clay Minerals. 28, 173-178.

Fotios, M.G. 1985. Geological report on diamond drill holes HM1-5, Rand area, Reedy's Project. Homestake Australia Ltd. Report No 1985/12.

Freyssinet, P. and Butt, C.R.M. 1988. Morphology and geochemistry of gold in a lateritic profile, Reedy Mine, Western Australia. CSIRO/AMIRA Project 241. Exploration Geoscience Restricted Report MG58R. 15 pp.

Frondel, C. 1978. Scandium. in K.H. Wedepohl (ed). Handbook of Geochemistry. Springer-Verlag. New York.

Fuge, R. 1978. Bromine. in K.H. Wedepohl (ed). Handbook of Geochemistry. Springer-Verlag. New York.

Gray, D.J. 1989. The aqueous chemistry of gold in the weathering environment. CSIRO/AMIRA Projects 240/241. Exploration Geoscience Restricted Report EG4R. 91 pp.

Grimes, D.J., and Marranzino, A.P. 1968. Direct-current arc and alternating-current spark emission spectrographic field methods of the semiquantitative analysis of geologic materials. U.S. Geological Survey Circular 591, 6 pp.

Hallberg, J.A., Maniw, J.G. and Bryan, S.G. 1976. Precious and base metal occurrence and production in a portion of the Western Yilgarn Block. CSIRO Report No FP.13.

Hallberg, J.A. 1976. A petrochemical study of a portion of the western Yilgarn Block. CSIRO Report No FP.13. 35 pp.

Hart, M.K.W. 1989. Analysis for total iron, chromium, vanadium and titanium in varying matrix geological samples by XRF, using pressed powder samples. Standards in X-ray analysis. Australian X-ray Analytical Association (WA Branch) Fifth State Conference. 117-129.

Heier, K.S. 1978. Cesium. in K.H. Wedepohl (ed). Handbook of Geochemistry. Springer-Verlag. New York.

Henderson, R.G. and Hill, L.V. 1988. Geology and gold mineralisation of the Reedy Gold Mine, Western Australia. Metana Minerals N.L. Technical Files.

Hill, R.E.T., Gole, M.J. and Barnes, S.J. 1987. Physical vulcanology of komatiites. Geol. Soc. Aust. Excursion guide book No 1. 74 pp.

Howarth, R.J. (ed.) 1983. Statistics and data analysis in geochemical prospecting. Handbook of Exploration Geochemistry, 2. Amsterdam, Elsevier Scientific Publishing Company, 437 pp.

Howarth, R.J. and Earle, S.A.M. 1979. Application of a generalized power transformation to geochemical data. Mathematical Geology. 11, 45-57.

Jennrich, R. and Sampson, P. 1981. Stepwise discriminant analysis, in Dixon, W.J., ed., BMDP statistical software 1981. Berkeley, University of California Press, 726 pp.

Jensen, L.S. 1976. A new cation plot for classifying subalkalic volcanic rocks. Ontario Division of Mines. Misc. Paper 66. 22 pp.

Jensen, L.S. and Pyke, D.R. 1982. Komatiites in the Ontario portion of the Abatibi belt. In N.T. Arndt and E.G. Nisbet (eds). Komatiites. George Allen and Unwin, Lond. 147-157.

Le Maitre, R.W. 1982. Numerical petrology. New York, Elsevier Scientific Publishing Company, 281 pp.

Leutwein, F. 1978a. Selenium. in K.H. Wedepohl (ed). Handbook of Geochemistry. Springer - Verlag. New York.

Leutwein, F. 1978b. Tellurium. in K.H. Wedepohl (ed). Handbook of Geochemistry. Springer - Verlag. New York.

Liversidge, A. 1893. On the crystallization of gold in hexagonal forms. J. R. Soc. N. S. W. 27. 343 - 346.

Mann, A.W. 1984. Mobility of gold and silver in lateritic weathering profiles: some observations from Western Australia. Econ. Geol., 79. 38-49.

Miesch, A.T. 1969. The constant sum problem in geochemistry, pp. 161-176, in Merriam, D.F., ed. Computer applications in the earth sciences: An international symposium. New York, Plenum Press, 281 pp.

Nesbitt, R.W., Sun, S. S. and Purvis, A. C. 1979. Komatiites: geochemistry and genesis. Can. Mineral. 17, 165-186.

Nisbet, E.G., Bickle, M.J, Martin, A., Orpen, J.L. and Wilson, J.F. 1982. Komatiites in Zimbabwe. In N.T. Arndt and E.G. Nisbet (eds). Komatiites. George Allen and Unwin Lond. 97-104.

Norrish, K. and Chappell, B.W. 1977. X-ray fluorescence spectrometry. in J. Zussman (ed). Physical methods in determinative mineralogy. Academic Press, London. 201-272.

O'Leary, R.M., and Meier, A.L. 1984. Analytical methods used in geochemical exploration, 1984. U.S. Geological Survey Circular 948, 120 pp.

Robertson, I.D.M. and Taylor, G.F. 1987. Depletion haloes in fresh rocks surrounding the Cobar orebodies, N.S.W., Australia: Implications for exploration and ore genesis. J. Geochem. Explor., 27. 77-101.

Robertson, I.D.M. 1987. Probe analyses on "Reedy Gold". CSIRO Division of Minerals and Geochemistry. Unpublished letter to R. Henderson, Metana Minerals N.L.

Robertson, I.D.M. 1990a. Mineralogy and geochemistry of soils overlying the Beasley Creek Gold Mine - Laverton, W.A. CSIRO Division of Exploration Geoscience Report 105R. 160 pp.

Robertson, I.D.M. 1990b. Weathering at the Trial Hill Tin Mine - Queensland. Centre for Australian Regolith Studies Occasional Publication No. 1. 48 pp.

Robertson, I.D.M., and Eggleton, R.A. 1991 . The weathering of granitic muscovite to kaolinite and halloysite and plagioclase-derived kaolinite to halloysite. Clays and Clay Minerals. 39. 113-126.

Shaw, D.M. 1961. Element distribution laws in geochemistry. Geochim. et Cosmochim Acta. 23, 116-134.

Shiraki, K. 1978. Chromium. in K.H. Wedepohl (ed). Handbook of Geochemistry. Springer-Verlag. New York.

Stueber, A.M. 1978 Strontium. in K.H. Wedepohl (ed). Handbook of Geochemistry. Springer-Verlag. New York.

VanTrump, G. Jr., and Miesch, A.T. 1977. The U.S. Geological Survey RASS-STATPAC system for management and statistical reduction of geochemical data. Computer and Geosciences. 3, 475-488.

Watkins, K.P., Tyler, I.M. and Hickman, A.H. 1987. Explanatory notes on the Cue geological sheet (Second Edition). Geological Survey of Western Australia. 31 pp.

White, S. 1987. Reedy's - notes on a visit 18/8/87. Metana Minerals N.L. Technical Files.

Wedepohl, K.H. 1978. Strontium. in K.H. Wedepohl (ed). Handbook of Geochemistry. Springer - Verlag. New York.